Numerička simulacija strujanja i prijelaza topline sustava hlađenja motora kamiona Ford Otosan

Iličić, Dominik

University of Zagreb
Faculty of Mechanical Engineering and
Naval Architecture

MASTER'S THESIS

Dominik Iličić

Zagreb, 2019

University of Zagreb
Faculty of Mechanical Engineering and
Naval Architecture

MASTER'S THESIS

CFD study of thermal management of the Ford Otosan truck underhood

Mentor:

Prof. dr. sc. Hrvoje Jasak

Student:

Dominik Iličić

Zagreb, 2019

I hereby declare that this thesis is entirely the result of my own work except where otherwise indicated. I have fully cited all used sources and I have only used the ones given in the list of references.

I extend gratitude to my professor Hrvoje Jasak for the mentorship he provided, contributing to my knowledge by invaluable advisement and guidance.

Work on this thesis has been a pleasant experience with the assist from Vanja Škurić, his willingness to help never faded.

Help from other members of the 8th floor CFD group is wholeheartedly acknowledged.

Thank you, my love Ivana, for you made this thesis possible. You never stopped believing in me, and I never stopped believing you.

SVEUČILIŠTE U ZAGREBU
FAKULTET STROJARSTVA I BRODOGRADNJE
Središnje povjerenstvo za završne i diplomske ispite
Povjerenstvo za diplomske ispite studija strojarstva za smjerove:
procesno-energetski, konstrukcijski, brodostrojarski i inženjersko modeliranje i računalne simulacije

Sveučilište u Zagrebu Fakultet strojarstva i brodogradnje	
Datum	Prilog
Klasa:	
Ur. broj:	

DIPLOMSKI ZADATAK

Student: **Dominik Iličić** Mat. br.: 0035197698

Naslov rada na hrvatskom jeziku: **Numerička simulacija strujanja i prijelaza topline sustava hlađenja motora kamiona Ford Otosan**

Naslov rada na engleskom jeziku: **CFD study of thermal management of the Ford Otosan truck underhood**

Opis zadatka:

Underhood thermal management of heavy-duty vehicles, such as trucks, includes identification of critical hot spots which can lead to system failure and an accurate control of cooling efficiency through thermal modelling and integrated heat exchanger and fan models.

In this project, Computational Fluid Dynamics (CFD) shall be used to simulate the flow and heat transfer conditions in a Ford Otosan truck underhood.
The candidate shall perform the following tasks within this project:

- Perform a literature survey of integral heat exchanger models appropriate for truck underhood thermal management simulations;
- Compare heat exchanger models from literature to models already implemented in OpenFOAM, and, if necessary, add features for this project;
- Choose a simple test case to verify and compare the heat exchanger models;
- Simplify the geometry of the Ford Otosan truck by removing the unimportant details;
- Create unstructured computational mesh of the simplified geometry;
- Perform a simulation of the flow and heat transfer in the underhood of the Ford Otosan truck, using an incompressible buoyant multiple-reference frame solver and an integral heat exchanger model;
- Present the result of simulations in an appropriate form, including integral heat transfer parameters and flow field visualisation.

The Thesis shall list the bibliography and any assistance received during this study.

Zadatak zadan:	Datum predaje rada:	Predviđeni datum obrane:
2. svibnja 2019.	4. srpnja 2019.	10., 11. i 12. srpnja 2019.

Zadatak zadao: Predsjednica Povjerenstva:

Prof. dr. sc. Hrvoje Jasak

12.

Prof. dr. sc. Tanja Jurčević Lulić

Contents

List of Figures

List of Tables

Nomenclature

Latin Characters

c	Specific heat capacity
c_p	Specific heat capacity at constant pressure
$\mathbf{D}$	Darcy-Forchheimer coefficient
e	Total specific energy
e_M	Specific kinetic energy
$\mathbf{F}$	Darcy-Forchheimer coefficient
$\mathbf{g}$	Gravitational acceleration
$\mathbf{I}$	Identity tensor
L	Length
m	Mass flow
P	Pressure
p	Kinematic pressure
Pr	Prandtl number
$\mathbf{q}$	Heat flux
Q	Volume energy source
q	Heat rejection
$\mathbf{r}$	Position vector
Ra	Rayleigh number
Re	Reynolds number
t	Time
T	Temperature
u	Specific internal energy
U	Overall heat transfer coefficient
$\mathbf{U}$	Velocity
$\mathbf{U}_R$	Relative velocity

Greek Characters

ϵ	Heat exchanger effectiveness
κ	Thermal diffusivity
λ	Thermal conductivity
μ	Dynamic viscosity
ν	Kinematic viscosity
ρ	Density
σ	Stress tensor
ω	Angular velocity

Superscripts

q^T	Transpose

Subscripts

q_{air}	Value for air
q_{aux}	Value for auxiliary fluid
q_c	Value for cold fluid
$q_{c,i}$	Value for cold fluid's inlet
q_h	Value for hot fluid
$q_{h,i}$	Value for hot fluid's inlet
$q_{\max}$	Maximum value
$q_{\min}$	Minimum value

Abbreviations

CFD - Computational Fluid Dynamics

MRF - Multiple Rotating Frame

NTU - Number of Transfer Units

CM - Control Mass

CV - Control Volume

SRF - Single Rotating Frame

CAD - Computer-aided design

NURBS - Non-uniform rational basis spline

HX - Heat exchanger

CS - Cross section

Abstract

Underhood thermal management is a crucial task in the design of new heavy-duty vehicles. Results of performing thermal analysis are used for stress analysis, *i.e.* it is one of the first steps in an integrated process of dimensioning parts related to thermal conditions. This only emphasises its importance in prototype design.

In the CFD simulation, geometry of the underhood parts is rather complex and there is a need for engineer's decision on removing redundant parts to reduce computational time and resource. Advanced meshing algorithms help in this process, but it still requires the largest amount of time. Due to the compact heat exchanger's geometry, that requires millions of cells, there is a need for accurate models that represent this feature. In industry, every heat exchanger is experimentally tested. This can be used to model pressure drop and heat effectiveness, ultimately gaining an accurate model for CFD simulations.

A new heat exchanger model was developed in `foam-extend` [1] for purpose of simulating automotive compact micro-channel heat exchanger with one pass. This model was successfully validated through testing on each individual exchanger from a truck's geometry, and their simultaneous work has been analysed.

Truck's fan was modelled as the Multiple Rotating Frame (MRF) zone, while the heat exchangers were modelled as porous zones with Darcy's law. Pre-processing of the truck's geometry was performed in ANSA [2]. Simulations were done in two steps: First, the cold flow simulation was performed, after which the temperature field was solved separately including both streams. Both simulations showed stable convergence.

Results are presented in the last chapter in the form of figures and total heat rejection of each heat exchanger for one operational condition. Lastly, in this study the heat exchanger's effectiveness was assumed to be constant, with experimental data this approach can be broader in terms of implementing effectiveness dependency on Number of Transfer Units (NTU) [3].

Key words: *CFD*, *OpenFOAM*, *foam-extend*, *underhood thermal management*, heat transfer, *heat exchanger*, *ANSA*, *MRF*, *porous media*

Sažetak

Vođenje sustava hlađenja motora jedna je od ključnih zadaća prilikom konstruiranja novih teških vozila. Rezultati provođenja termalne analize koriste se za analizu opterećenja, tj. termalna analiza jedan je od prvih koraka u integriranom procesu dimenzioniranja toplinski opterećenih dijelova. Time naglašava svoju važnost u dizajniranju prototipa.

Geometrija motora vrlo je kompleksa za računalnu analizu te zahtjeva inženjersku procjenu o izostavljanju nepotrebnih dijelova kako bi smanjili vrijeme i resurse računanja. Kroz napredne algoritme kreiranja mreže proces simulacije je donekle automatiziran, ali još uvijek zahtjeva najviše vremena. S obzirom na prirodu geometrije kompaktnih izmjenjivača topline koji zahtijevaju milijune elemenata, potrebni su precizni modeli koji bi zamijenili ovu potrebu. U industriji, svaki je izmjenjivač topline ispitan. Ovo znanje se može iskoristiti za modeliranje pada tlaka i toplinske efektivnosti kako bi dobili točan model za simulaciju.

U svrhu simuliranja kamionskog kompaktnog izmjenjivača topline s mikro kanalima s jednim prolazom, razvijen je novi model izmjenjivača topline u softverskom paketu `foam-extend`. Model je uspješno provjeren putem testiranja pojedinačnog izmjenjivača topline kamiona, kao i putem njihovog zajedničkog rada.

Ventilator je modeliran kao zona rotacije (*engl. Multiple Rotating Frame*), dok su izmjenjivači topline modelirani kao porozne zone preko Darcyjevog zakona. Priprema geometrije i mreže odrađena je u ANSA-i. Simulacije su se odradile kroz dva koraka: prvo je simuliran hladni tok, dok je nakon toga simulirana energetska jednadžba kroz dobiveno polje strujanja. Obje simulacije su pokazale stabilnu konvergenciju.

Rezultati su prezentirani u zadnjem poglavlju u obliku slika i predane topline pojedinog izmjenjivača topline. U radu se toplinska efektivnost pretpostavila konstantnom. Eksperimentalnim testiranjem ova pretpostavka se može dodatno modelirati s implementiranjem ovisnosti o broju jedinica prijenosa (*engl. Number of Transfer Units*).

Ključne riječi: *računalna dinamika fluida*, *OpenFOAM*, *foam-extend*, *sustav hlađenja motora*, *prijenos topline*, *izmjenjivač topline*, *ANSA*, *zona rotacije*, *porozni medij*

Prošireni sažetak

Otkrivanje toplinski opterećenih dijelova teških motornih vozila bitno je zbog mogućeg trajnog oštećenja. Uz eksperimentalno ispitivanje toplinskog opterećenja, računalna dinamika fluida (*engl. Computational Fluid Dynamics*) predstavlja primjenjiv alat u svrhu analize toplinskog opterećenja. Prijašnje metode koristile su jednostavne, jednodimenzionalne analize te su se uzdale isključivo u rezultate eksperimenta. Računalna dinamika fluida ne može u potpunosti zamijeniti eksperimentalnu analizu, ali može dati moć odlučivanja tijekom ranih stadija razvoja novih vozila.

U ovom radu, unutar softverskog paketa `foam-extend` implementiran je dvostrujni model izmenjivača topline. `Foam-extend` je OpenFOAM-ova inačica koju razvija zajednica.

Priprema geometrije i izrada računalne mreže kamiona provedena je u softverskom paketu ANSA.

Matematički model

Numerički modeli korišteni u ovom radu koriste principe mehanike kontinuuma, opisujući materijal kao kontinuiranu masu. Ovi principu neophodni su za opis strujanja fluida i prijenosa topline. Priroda fluida u pokretu često je kaotična, te je zbog toga problematično praćenje pojedinačne čestice. Većina inženjerske primjene fluida u pokretu zahtjeva krajnji odgovor o silama na površinu ili temperaturi, te je zbog toga praktično zamjeniti praćenje pojedinačne čestice s kontrolnim volumenom koji opisuje određeni željeni prostor. Reynoldsov transportni teorem u svojoj generalnoj formi opisuje ovu promjenu. Zakoni očuvanja mase, količine gibanja i energije predstavljaju, u svojoj generalnoj formi, zakone za svako tijelo koje se može opisati kao kontinuum. S obzirom da je broj nepoznatih veličina veći od broja jednadžbi, potrebne su konstitutivne jednadžbe koje bi izjednačile ovo neslaganje. U ovom radu, uvedene su pretpostavke o Newtonskom fluidu. Iako je broj nepoznatih veličina i broj jednadžbi sada izjednačen, za numeričke primjene, ovaj sustav je i dalje nestabilan te se mogu donijeti daljnje pretpostavke o strujanju fluida koji bi smanjile ovu nestabilnost, a time vrijeme i resurse računanja. Strujanje je pretpostavljeno kao nekompresibilno i izotermno.

Modeliranje prijenosa topline

Očuvanje energije vođeno je prvim glavnim stavkom termodinamike, tvrdeći da se energija ne može uništiti niti proizvesti. U svojoj generalnoj formi, jednadžba očuvanja energije je kompleksna za inženjersku primjenu, potrebne su pretpostavke kako bi ju pojednostavili. Tri su glavna mehanizma prijenosa topline: konvekcija, kondukcija i radijacija. Generalno, male promjene gustoće mogu uzrokovati velike promjene u gibanju. Ali, lokalna mjesta gdje su sile advekcije velike, kao blizu ventilatora, promjena temperature ne može značajno promijeniti strujanje. Kroz Navier-Stokes jednadžbe, vidljivo je da temperatura uzrokuje gibanje kroz promjenu gustoće fluida. Ovaj zaključak daje na znanje kako je ovo iterativni postupak gdje su jednadžbe spregnute kroz termodinamičko stanje fluida. U većini inženjerskih problema, kao i u ovom radu, pretpostavka o utjecaju temperature na gibanje fluida može se donijeti kroz odnose Rayleighovog i Reynoldsovog broja. Rayleighov broj govori o odnosu između vremena prijenosa topline difuzijom i vremena prijenosa topline konvekcijom, dok Reynoldsov broj govori o odnosu između inercijskih i viskoznih sila. Ako je Reynoldsov broj puno veći od Rayleighovog, može se smatrati da su advekcijske sile puno snažnije, te time promjena temperature ne može značajno utjecati na strujanje. Ova pretpostavka omogućuje neovisno rješavanje Navier-Stokesovih jednadžbi od energetske jednadžbe. Krajnja jednadžba očuvanja energije je u temperaturnom obliku, te ima oblik:

$$\frac{\partial T}{\partial t} + \nabla\boldsymbol{\cdot}\left(\mathbf{U}T\right) = \nabla\boldsymbol{\cdot}\left(\frac{\nu}{\mathrm{Pr}}\nabla T\right) + \frac{Q}{\rho c_p}, \tag{1}$$

gdje Pr označava Prandtlov broj te govori o omjeru između difuzivnosti količine gibanja i termalne difuzivnosti, a definiran je kao:

$$\mathrm{Pr} = \frac{c_p \mu}{\lambda}. \tag{2}$$

Modeliranje ventilatora

Rotacija ventilatora uzrokuje nestacionarno gibanje fluida, što je u nekim slučajevima skupo za rješavanje. Slijedeća najbolja opcija jeste modeliranje rotirajućih dijelova. Ako bi u računalnoj domeni imali samo jednu os rotacije, te ako bi se sva geometrija rotirala, moguće bi bilo zamijeniti koordinatni sustav te problem pristupiti uz primjenu relativne

brzine. S obzirom da je u ovom radu samo vantilator dio koji se rotira, dok su svi ostali dijelovi stacionarni, potrebno je odabrati dio prostora u kojem se nalazi ventilator i samo u tome dijelu primjeniti relativni pristup. Model se još naziva *engl. Multiple Rotating Frame*. Metoda je slična nestacionarnoj simulaciji koja se zaustavlja u jednom trenutku, te dobiveni rezultati odgovaraju modelu koji bi se pokrenuo na istoj lokaciji rotirajućeg dijela tj. lopatica. Model ovisi o broju lopatica i obliku lopatica. Susjedne površine također utječu na rezultate unutar rotirajuće zone kroz spregnute rubne uvjete koji spajaju rotirajući i stacionarni dio prostora.

Navier-Stokesove jednadžbe unutar rotirajuće zone definiraju se putem relativne brzine:

$$\mathbf{U} = \mathbf{U}_R + \boldsymbol{\omega} \times \mathbf{r}, \tag{3}$$

s vremenskom derivacijom:

$$\frac{\partial \mathbf{U}}{\partial t} = \frac{\partial \mathbf{U}_R}{\partial t} + \underbrace{\frac{\partial \boldsymbol{\omega}}{\partial t} \times \mathbf{r}}_{\substack{\text{tangencijalno} \\ \text{ubrzanje}}} + \underbrace{2\boldsymbol{\omega} \times \mathbf{U}_R}_{\substack{\text{Coriolisovo} \\ \text{ubrzanje}}} + \underbrace{\boldsymbol{\omega} \times (\boldsymbol{\omega} \times \mathbf{r})}_{\substack{\text{centrifugalno} \\ \text{ubrzanje}}}, \tag{4}$$

gdje $\boldsymbol{\omega}$ označava kutnu brzinu, a $\mathbf{r}$ relativni vektor položaja od osi rotacije.

Modeliranje poroznog medija

Kompaktni izmjenjivači topline napravljeni su od fino razmaknutih tankih metalnih rebara. Za rješavanje strujanja fluida kroz takvu geometriju uz rješavanja rubnih slojeva u svakom kanalu, potrebni bi bili deseci milijuna elemenata za jedan izmjenjivač topline. Takve računalne mreže nisu primjenjive za inženjerske probleme. Pomoću tankih metalnih rebara, izmjenjivač topline dopušta strujanje u samo jednom smjeru. Zbog ovoga postoji korist o modeliranju izmjenjivača kao porozni medij. Popularan način modeliranje poroznog medija u računalnoj dinamici fluida je pomoću Darcy-Forchheimer izraza:

$$\nabla p = -\mu \mathbf{D} \cdot \mathbf{U} - \frac{1}{2}\rho \mathbf{F} \cdot (|\mathbf{U}|\mathbf{U})\,. \tag{5}$$

Koeficijenti $\mathbf{D}$ and $\mathbf{F}$ su eksperimentalno određeni kroz izraz $p = f(\mathbf{U})$.

Modeliranje izmjenjivača topline

Izmjenjivači topline predstavljaju toplinski izvor ili ponor, tj. oni mogu smanjiti ili povećati energiju fluida unutar kontrolnog volumena. Zbog toga se u radu razmatra modeliranje izmjenjivača topline kroz izvorski član temperaturne jednadžbe. Član se može modelirati na više načina. Zrnić [4] je u svom radu implementirao tri jednostrujna modela u `foam-extend` softverskom paketu. Ford Otosan kamion koristi kompaktne križne izmjenjivače topline s jednim prolazom bez miješanja obaju struja, te je zbog toga u ovom radu implementiran novi, dvostrujni model. Općenito, učin izmjenjivača topline ovisi o brojnim aspektima kao što su veličina izmjenjivača, tip izmjenjivača i ukupni toplinski kapacitet fluida. Zbog ovoga bitno je generalno opisati izmjenjivač topline. Pogodan način za opisivanje učina izmjenjivača topline koji se koristi i pri njegovom dimenzioniranju je $\epsilon - \mathrm{NTU}$ metoda:

$$q = \epsilon q_{\max} = \epsilon C_{\min} \left(T_{h,i} - T_{c,i}\right) = \epsilon C_{\min} \Delta T_{\max}, \tag{6}$$

Gdje ϵ predstavlja efektivnost izmjenjivača, $C_{\min}$ je minimum od ukupnog toplinskog kapaciteta toplog fluida, C_h i ukupnog toplinskog kapaciteta hladnog fluida, C_c. Dok $\Delta T_{\max} = (T_{h,i} - T_{c,i})$ predstavlja temperaturnu razliku ulaza fluida. Efektivnost izmjenjivača topline ϵ je bezdimenzijski broj, i generalno ovisi o broju prijenosnih jedinica, omjeru minimalnog i maksimalnog ukupnog toplinskog kapaciteta i tipu izmjenjivača topline:

$$\epsilon = f\left(\mathrm{NTU}, \frac{C_{\min}}{C_{\max}}, \text{tip izmjenjivaca}\right). \tag{7}$$

Broj prijenosnih jedinica (*engl. Number of Transfer Units*) NTU, predstavlja bezdimenzijski prijenos topline ili termalnu veličinu izmjenjivača topline, a definiran je kao:

$$\mathrm{NTU} = \frac{UA}{C_{\min}} \tag{8}$$

Analitička derivacija funkcije ϵ moguća je samo za jednostavne tipove izmjenjivača, kao npr. protusmjerni. Kako bi opisali ovu relaciju s križnim izmjenjivačem, potrebna su eksperimentalna testiranja. Uobičajen način za iskazivanje efektivnosti izmjenjivača topline je kroz rješenje putem ovisnosti o ulaznim brzinama obaju fluida, tj. $\epsilon = f\left(\boldsymbol{U}_h, \boldsymbol{U}_c\right)$. Na ovaj način, svi podaci su definirani za potrebne jednadžbe i modeliranje izvorskog člana temperaturne jednadžbe. Općenito, jedan izmjenjivač topline može imati neuniformnu

raspodjelu ulazne brzine zbog nesavršene geometrije ulaza. Isto tako, okružujući fluid može biti blokiran od jedne strane izmjenjivača i time izmjenjivač ne će imati potpuni učin.

Primarna strana izmjenjivača topline modelirana je kao porozni medij. Koeficijenti su tako zadani da dopuštaju strujanje fluida u samo jednom smjeru, imitirajući rebra kompaktnog izmjenjivača. Sekundarna strana fluida modelirana je kao jednodimenzionalni prijenos topline gdje jedan red elementa predstavlja jedan mikro kanal (slika 1).

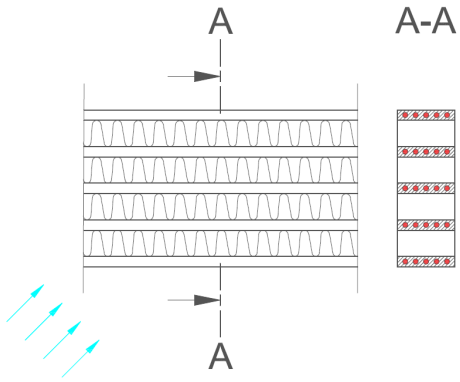

Slika 1: Shematski prikaz *križnog* izmjenjivača topline s oba fluida ne pomiješana: sekundarni (crveno) i primarni (plavo) fluid

Validacija izmjenjivača topline

Validacija za implementirani izmjenjivač topline uključuje provjeru integralnog očuvanja energije. Geometrija korištena za validaciju jednaka je geometriji iz Ford Otosan kamiona. Razmatrana su tri slučaja. Prvi slučaj je simulacija hladnjaka motora (*engl. radiator*) gdje su se provele četiri različite simulacije. U svakoj simulaciji mijenjala se brzina zraka u svrhu promjene učina izmjenjivača. Drugi slučaj je simulacija hladnjaka stlačenog zraka (*engl. intercooler*) gdje su se isto tako provele četiri različite simulacije. Ovoga puta mijenjao se maseni protok stlačenog zraka. Treći slučaj analizirao se njihov zajednički rad gdje su izmjenjivači topline postavljeni na isti način kao u Ford Otosan kamionu.

Sve simulacije su provedene na identičnim postavkama računalne mreže. Bitno je da efektivnost izmjenjivača topline generalno ovisi o ukupnom toplinskom kapacitetu fluida i NTU. U radu se jednostavan model implementirao te se efektivnost smatrala

konstantnom.

Geometrija obuhvaća samo efektivnu površinu izmjene topline svakog izmjenjivača. Simulirana je izolirana cijev u kojoj su postavljeni izmjenjivači te kroz koju struji zrak određene temperature u x smjeru (slika 2). Fizikalna svojstva oba fluida ne ovise o temperaturi te su proglašena konstantim. Energetska jednažba se rješavala odvojeno zbog pretpostavke veliki advekcijskih sila. Izmjenjivači su modelirani kao porozni medij s linearnim padom tlaka u jednom smjeru i strujanjem dominantno u jednom smjeru. Korištene sheme diskretizacije i postavke rješavača iste su kao u poglavlju 5. Validacija je uspješno provedena na svim simulacijama. Rezultati su pokazali dinamičko mijenjanje profila temperatura zraka i sekundara.

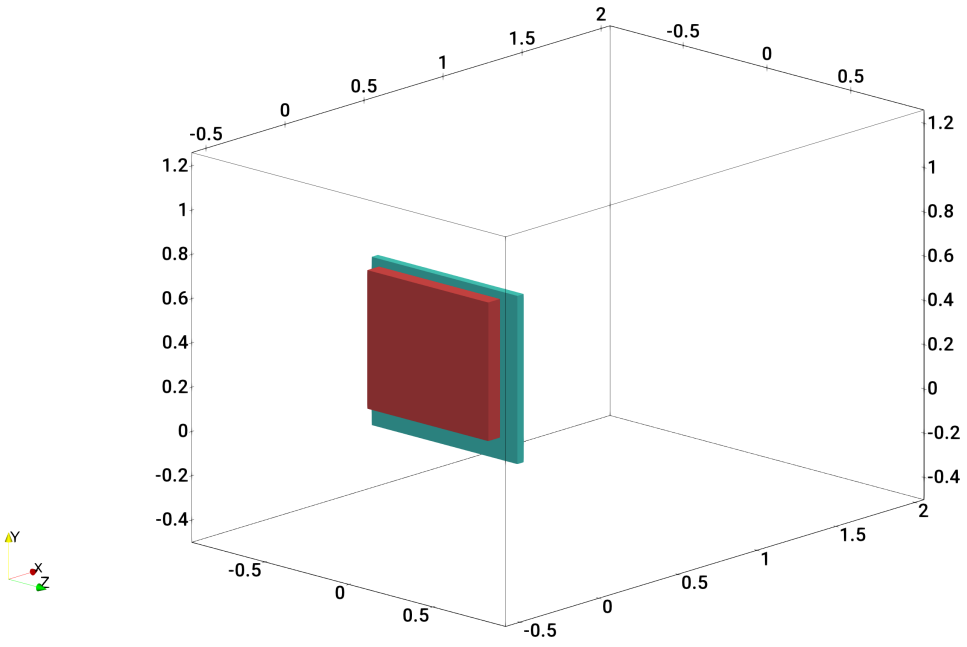

Slika 2: Geometrija za validaciju: hladnjak motora (crveno), hladnjak stlačenog zraka (zeleno).

Rezultati za hladnjak motora

Tablica 1 prikazuje rezultate za 4 simulacije provedene na testiranju hladnjaka motora. Imitiralo se stvarno ponašanje izmjenjivača topline koji pri povišenim brzinama primara smanjuje svoju efektivnost. Model se ponašao stabilno te je greška predaje topline zanemariva što znači da je integralnost modela sačuvana.

U_{air} [m/s]	ϵ [-]	$Q_{\text{air,total}}$ [W]	$Q_{\text{aux,total}}$ [W]	Error [%]
2	0.9096	77493.38	77493.38	1.02e-6
4	0.8361	147025.65	147025.65	0.83e-7
6	0.7454	212994.70	212994.71	1.20e-6
8	0.7606	275257.09	275257.09	1.61e-6

Tablica 1: Hladnjak motora: rezultati simulacija.

Slike 3 i 4 prikazuju postepeno zagrijavanje zraka kako je sve veća predaja topline uslijed povećanja masenog protoka zraka kroz izmjenjivač topline.

Sekundaru hladnjaka motora bitno ne pada temperatura zbog relativno velikog ukupnog toplinskog kapaciteta. Brzina zraka u ovome slučaju može predstavljati brzinu kretanja kamiona uz brzinu strujanja koju nameće ventilator koji se nalazi iza hladnjaka. Upravo je i želja pri hlađenju motora da se temperatura ne mijenja drastično kako ne bi došlo do oštećenja na bloku motora uslijed termalnog opterećenja.

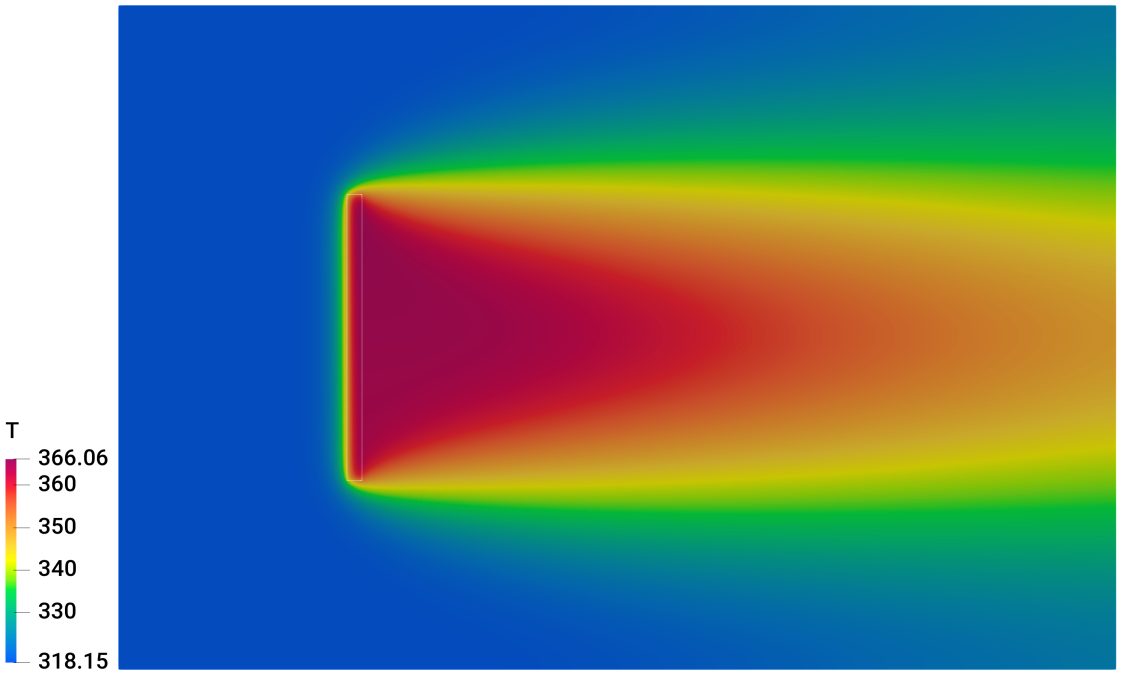

Slika 3: XY presjek hladnjaka motora: temperatura zraka, $U_{\text{air}} = 2$ m/s.

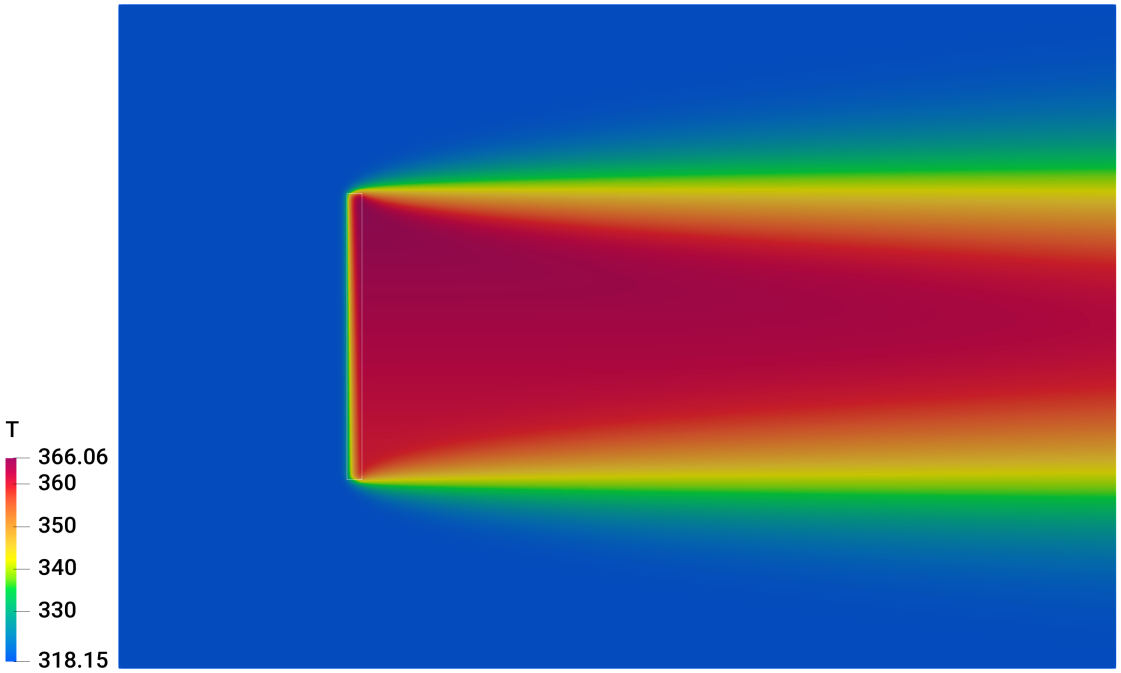

Slika 4: XY presjek hladnjaka motora: temperatura zraka, $U_{\text{air}} = 8$ m/s.

Rezultati za hladnjak stlačenog zraka

Tablica 2 prikazuje rezultate za 4 simulacije provedene na testiranju hladnjaka stlačenog zraka. Imitiralo se stvarno ponašanje izmjenjivača topline koji pri povišenim mesenim protocima sekundara smanjuje svoju efektivnost. Model je zahtjevao podrelaksaciju temperature sekundara te je greška predaje topline zanemariva što znači da je integralnost modela sačuvana.

m_{aux} [m/s]	ϵ [-]	$Q_{\text{air,total}}$ [W]	$Q_{\text{aux,total}}$ [W]	Error [%]
0.1	0.9669	14646.76	14647.06	2.07e-3
0.2	0.9239	29258.04	29258.49	1.56e-3
0.3	0.8603	43528.61	43528.97	8.17e-4
0.4	0.7972	56860.06	56860.28	4.02e-4

Tablica 2: Hladnjak stlačenog zraka: rezultati simulacija.

Slike 5 i 6 prikazuju postepeno zagrijavanje zraka kako je sve veća predaja topline uslijed povećanja masenog protoka sekundara kroz izmjenjivač topline.

Zbog puno većeg ukupnog toplinskog kapaciteta sekundara hladnjaka motora u usporedbi sa sekundarom hladnjaka stlačenog zraka, vidljiva je razlika u ponašanju dvaju izmenjivača toplina pri smanjenju tj. povećanju učina. Stlačeni zrak ima puno manji ukupni toplinski kapacitet nego li sekundar hladnjaka motora. Regulacija temperature zraka vrši se pomoću troputnog ventila koji usmjerava potrebnu količinu stlačenog zraka u izmjenjivač. Da je ukupni toplinski kapacitet stlačenog zraka veći, hladnjak koji se nalazi iza ne bi mogao dovoljno ohladiti motor.

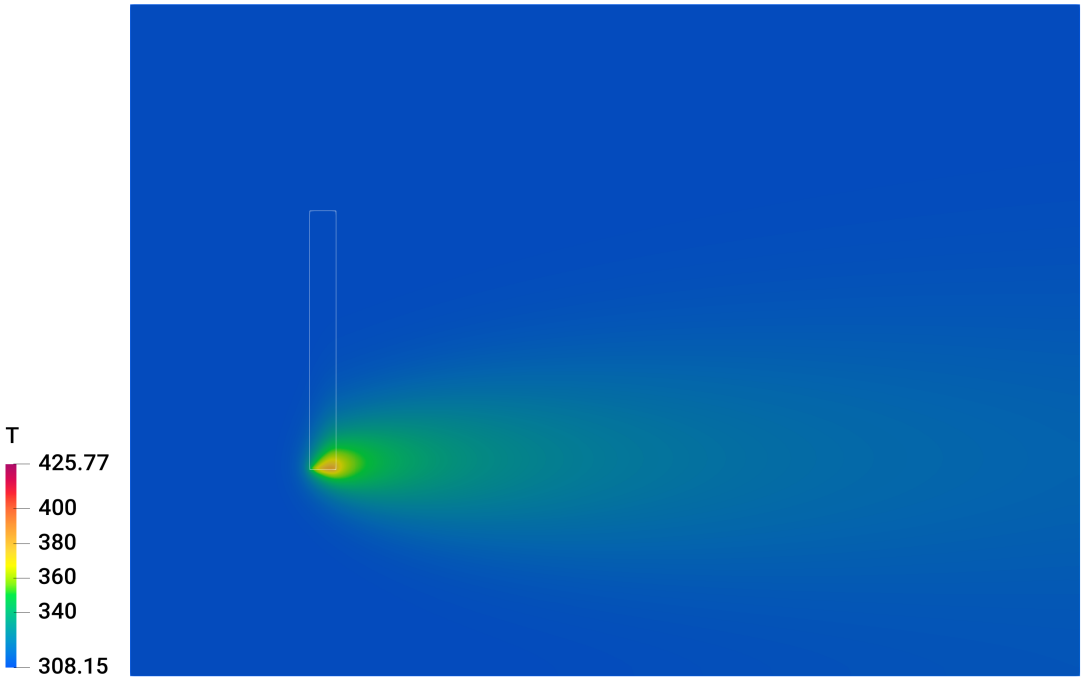

Slika 5: XY presjek hladnjaka stlačenog zraka: temperatura zraka, $m_{\text{aux}} = 0.1$ kg/s.

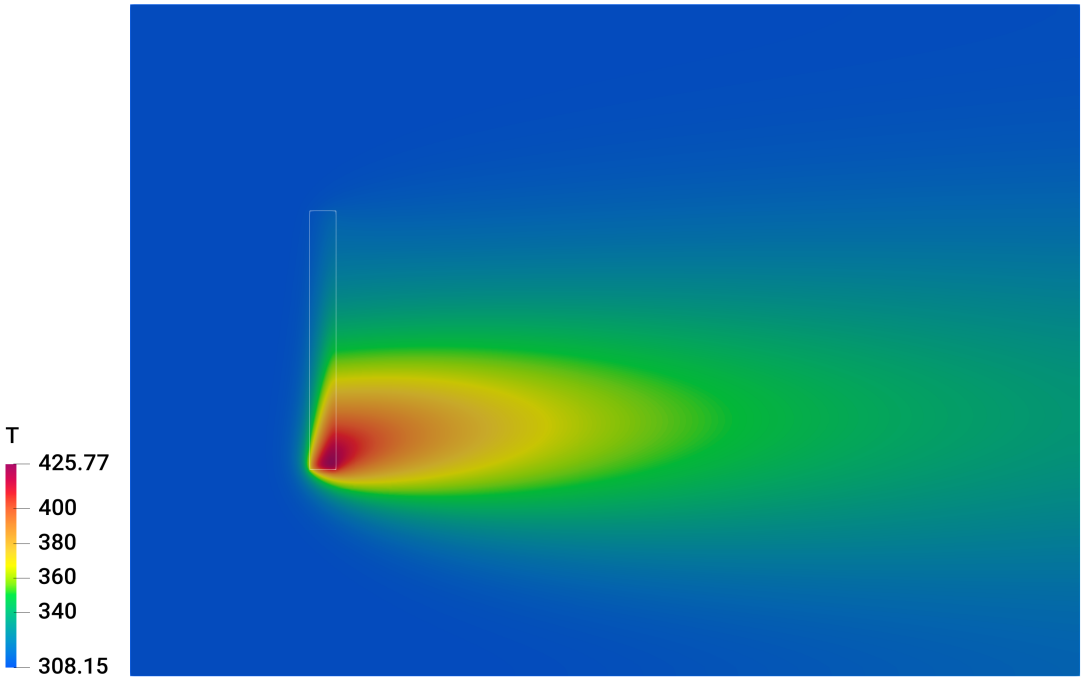

Slika 6: XY presjek hladnjaka stlačenog zraka: temperatura zraka, $m_{\text{aux}} = 0.4$ kg/s.

Rezultati istovremenog rada hladnjaka

Tablice 3, 4 i 5 prikazuju rezultate istovremenog rada hladnjaka. Identične postavke su ponovljene kao pri testiranju pojedinačnog rada.

Simulation no.	U_{air} [m/s]	$Q_{\text{air,sum}}$ [W]	$Q_{\text{aux,sum}}$ [W]	Error [%]
1	2	94999.11	94999.15	3.97e-5
2	4	179475.07	179475.07	6.12e-7
3	6	260163.99	260163.99	9.74e-8
4	8	337145.82	337145.83	7.88e-7

Tablica 3: Rezultati istovremenog rada hladnjaka.

Simulation no.	m_{aux} [m/s]	ϵ [-]	$Q_{\text{aux,total}}$ [W]
1	0.1	0.9669	14282.74
2	0.2	0.9239	29199.78
3	0.3	0.8603	43922.22
4	0.4	0.7972	58591.70

Tablica 4: Rezultati istovremenog rada hladnjaka: hladnjak stlačenog zraka.

Simulation no.	m_{aux} [m/s]	ϵ [-]	$Q_{\text{aux,total}}$ [W]
1	6	0.9096	80716.41
2	6	0.8361	150275.29
3	6	0.7454	216241.77
4	6	0.7606	278554.13

Tablica 5: Rezultati istovremenog rada: hladnjak motora.

Slike 7 i 8 prikazuju temperaturu zraka. Utjecaj hladnjaka stlačenog zraka primarno je lokalan, zbog toga se može očekivati na istom mjestu veliko toplinsko opterećenje simulacije kamiona.

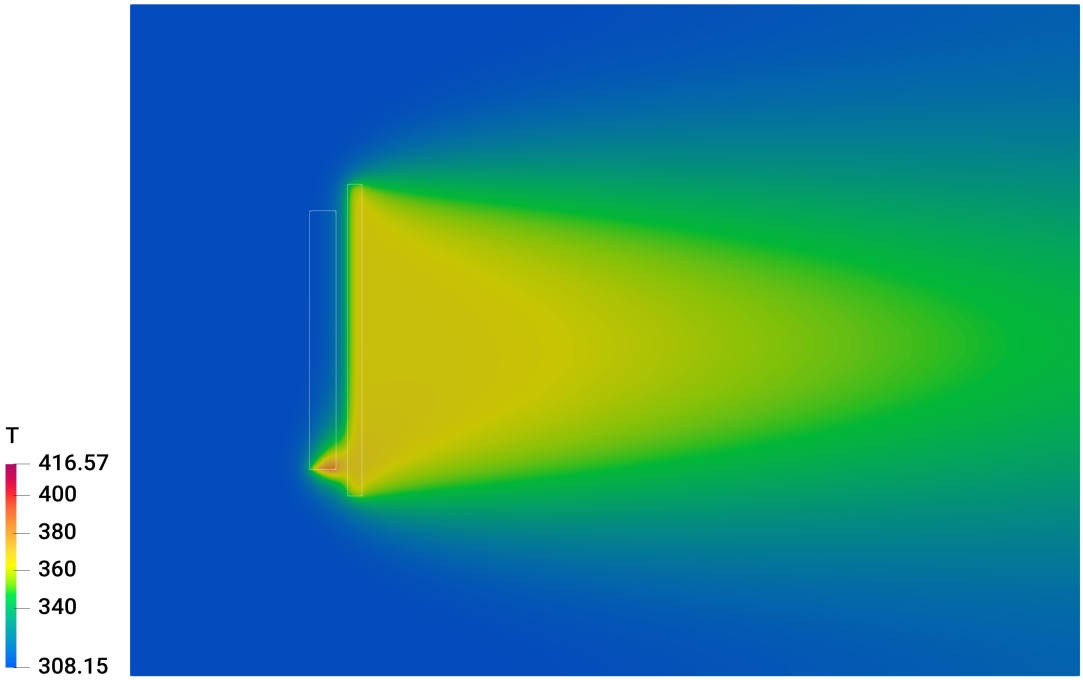

Slika 7: Rezultati istovremenog rada, XZ presjek: temperatura zraka, sim. no. 1.

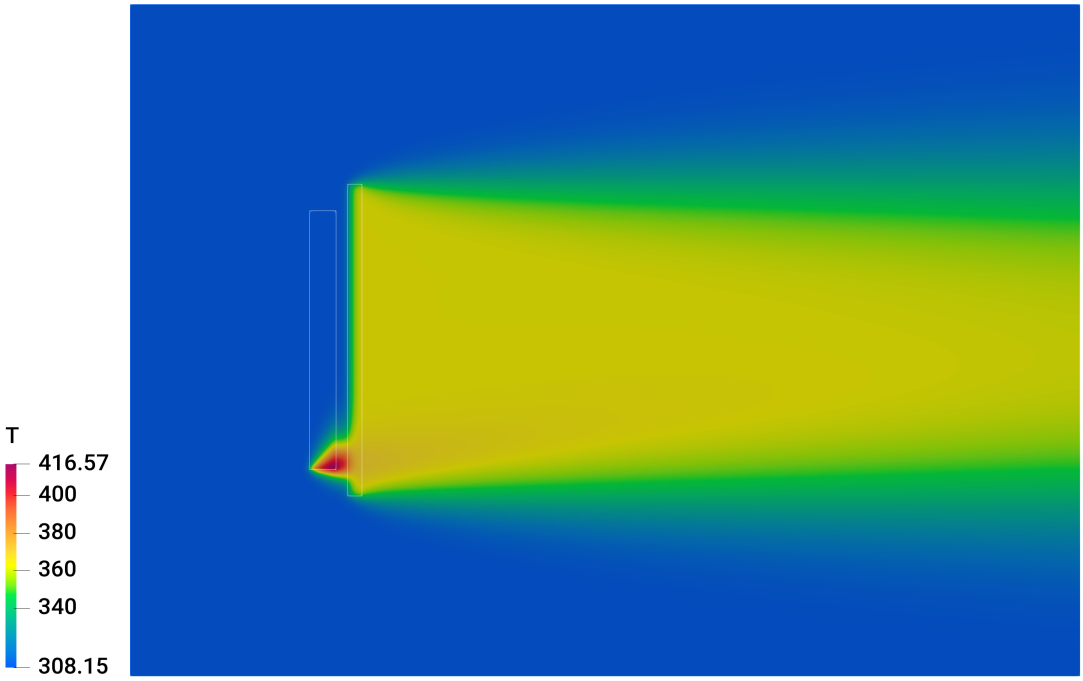

Slika 8: Rezultati istovremenog rada, XZ presjek: temperatura zraka, sim. no. 4.

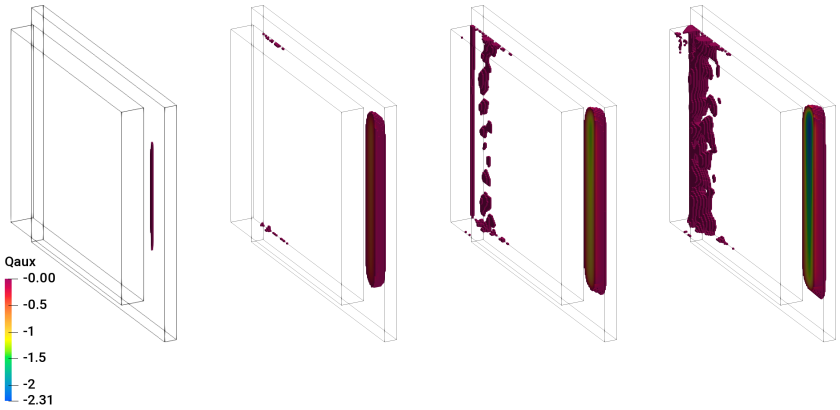

a) sim. no. 1, b) sim. no. 2, c) sim. no. 3, d) sim. no. 4.

Slika 9: Rezultati istovremenog rada hladnjaka, XZ presjek oba hladnjaka: zagrijavanje sekundara.

Iznosi predane topline slični su kao pri pojedinačnom testiranju hladnjaka. Potrebno je naglasiti kako je tempratura zraka pri testiranju hladnjaka motora zadana 318.15 K, dok je pri testiranju hladnjaka stlačenog zraka zadana na 308.15 K. Uzrok ovome je što hladnjak stlačenog zraka povećava temperaturu zraka otprilike 10 K. Hladnjak stlačenog zraka nije značajno promijenio izmjenjenu toplinu iako se brzina zraka povećala četiri puta.

Slika 8 prikazuje kako se visoko temperaturni zrak uzrokovan hladnjakom stlačenog zraka hladi nakon prolaska kroz hladnjak motora. Stoga se taj dio hladnjaka motora zagrijava, što se vidi na slici 9. Ovaj efekt postaje izraženiji pri povišenoj brzini okolnog zraka. Isto tako, hladnjak motora počinje zagrijavati dijelove na izlazu hladnjaka stlačenog zraka.

Računalna mreža Ford Otosan kamiona

Proces pripreme geometrije i izrade računalne mreže odrađen je u softverskom paketu ANSA. Pojednostavljenje geometrije izvedeno je u smislu izostavljanja dijelova kamiona koji ne utječu na strujanje fluida ili nisu potrebni za simulaciju.

Visokokvalitetna površinska mreža je potrebna zbog toga što se najbitnije značajke strujanja fluida odvijaju u blizini površina gdje je potrebna kvalitetna volumenska mreža rubnog sloja. Ovaj dio simulacije je ujedno i vremenski najintenzivniji. Kako bi skratili

vrijeme kreiranja mreže, korišten je *engl. wrapping* algoritam, koji se zasniva na rekurzivnom dijeljenju prostora do najmanjeg detalja. Mana algoritma jeste iznimno velika mreža te se zbog toga dobivena mreža dodatno smanjuje. Ovaj dio procesa odrađen je pomoću konvertiranja trokutastih elemenata u četverokute. Time se smanjila površinska mreža sa 22 milijuna na 4.6 milijuna elemanata (slike 10 do 12).

Implementirani model izmjenjivača topline ovisi o strukturiranoj mreži unutar geometrije izmjenjivača. Zbog toga se prvo kreirala strukturirana mreža za sva tri izmjenjivača (slika 13). Treći izmjenjivač koji se nije spomenuo je kondenzator.

Nakon kreiranja volumenske mreže izmjenjivača, kreirala se volumenska mreža rubnog sloja putem izvlačenja (*engl. extrude*) elemenata površinske mreže. Pet elemenata s konstantim iznosom rasta od 1,2 izvlačen je za potrebe volumenske mreže rubnog sloja. Prvi sloj ima visinu 1 mm.

Posljednji korak u procesu pripreme računalne mreže je kreiranje glavne volumenske mreže. Tetraedar je odabrani element za popunjavanje preostalog prostora zbog visoke kvalitete i svojstva lakog opisivanja kompleksne geometrije. Posljedica ove odluke je veća mreža od volumenske mreže napravljena pomoću heksaedara (slika 14).

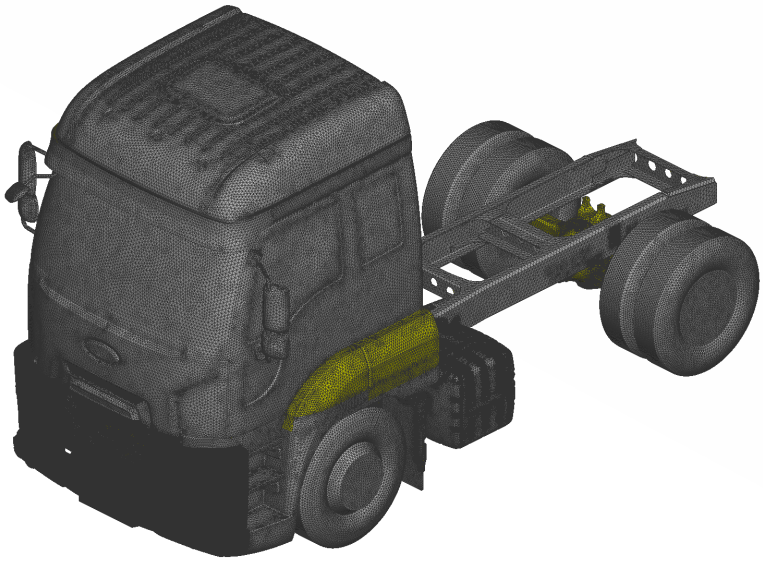

Slika 10: Ford Otosan kamion: izvorna površinska mreža.

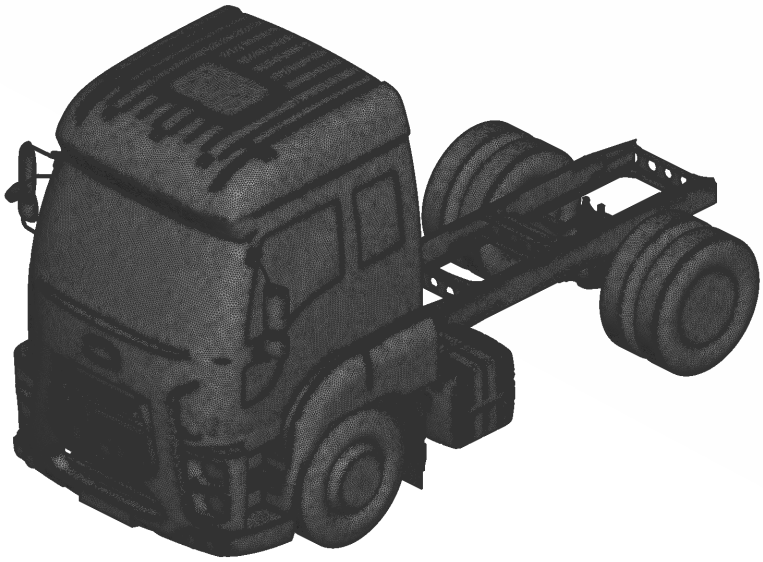

Slika 11: Ford Otosan kamion: *wrapping* algoritam.

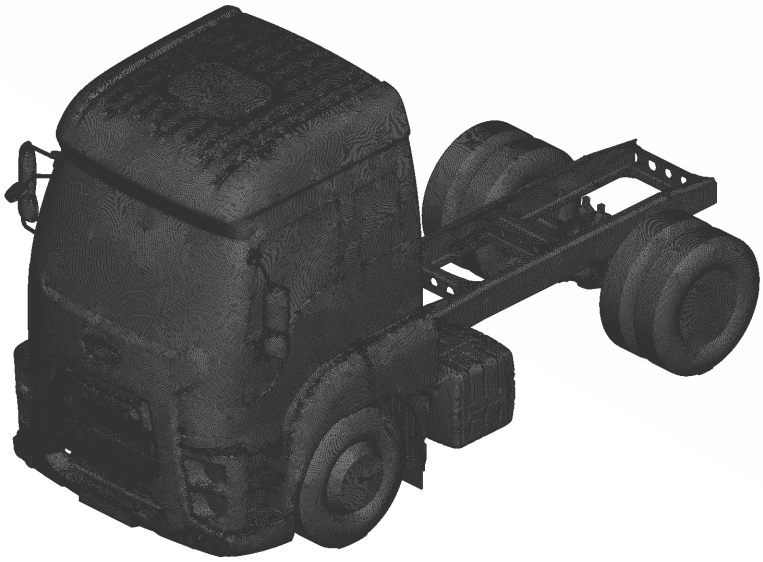

Slika 12: Ford Otosan kamion: finalna površinska mreža.

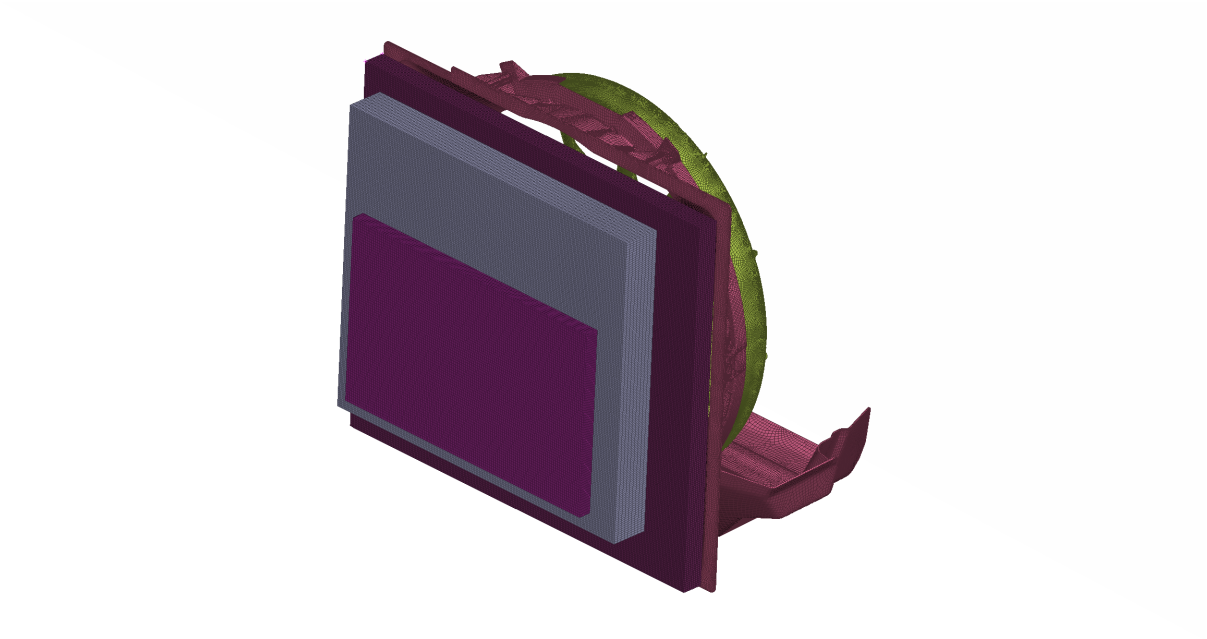

Slika 13: Ford Otosan kamion, izmjenjivači topline: strukturirana volumenska mreža

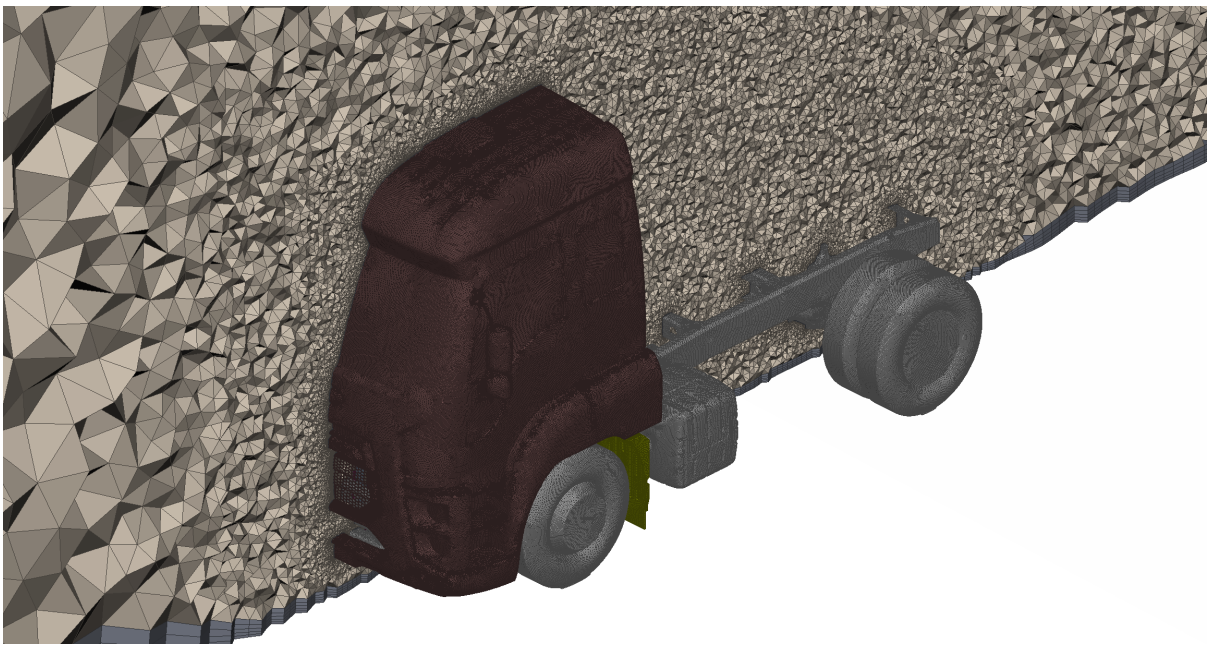

Slika 14: Ford Otosan kamion: volumenska mreža.

Rezultati simulacija Ford Otosan kamiona

Pri simuliranju Ford Otosan kamiona, uzele su se iste pretpostavke u obzir kao pri testiranju izmjenjivača topline. Provedene su dvije simulacije. Prvo je simulirano izotermno strujanje fluida uz korištenje kOmegaSST modela turbulencije. Izmjenjivači su modelirani kao porozni medij, dok se ventilator modelirao pomoću MRF modela. Rezultati ove simulacije prikazani su na slikama 15 i 16.

Nakon dobivenog polja strujanja, simuliralo se toplinsko opterećenje kamiona uslijed izmjenjivača topline. Prijenos topline putem radijacije nije razmatran u radu. Izmjenjen toplinski tok pojedinog izmjenjivača iznosi:

- Hladnjak motora, $Q_{\text{aux,total}} = 60559.40$ W,
- Hladnjak stlačenog zraka, $Q_{\text{aux,total}} = 29041.42$ W,
- Kondenzator, $Q_{\text{aux,total}} = 1885.12$ W.

Slika 16 otkriva povećani protok na donjem području hladnjaka motora te vrtlog na gornjoj strani. Utjecaj ovog vrtloga može prepoznati na slici 18.

Slike 17 i 19 prikazuju utjecaj hladnjaka stlačeng zraka na lokalnu temperaturu zraka i temperaturu površine kamiona.

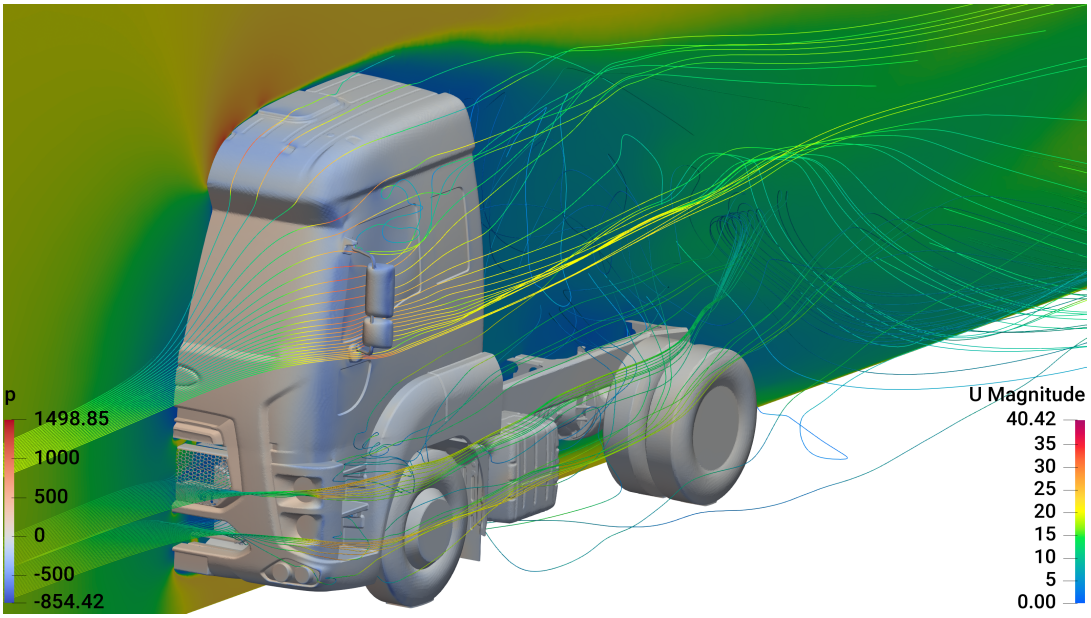

Slika 15: Ford Otosan kamion, izotermno strujanje: aerodinamika.

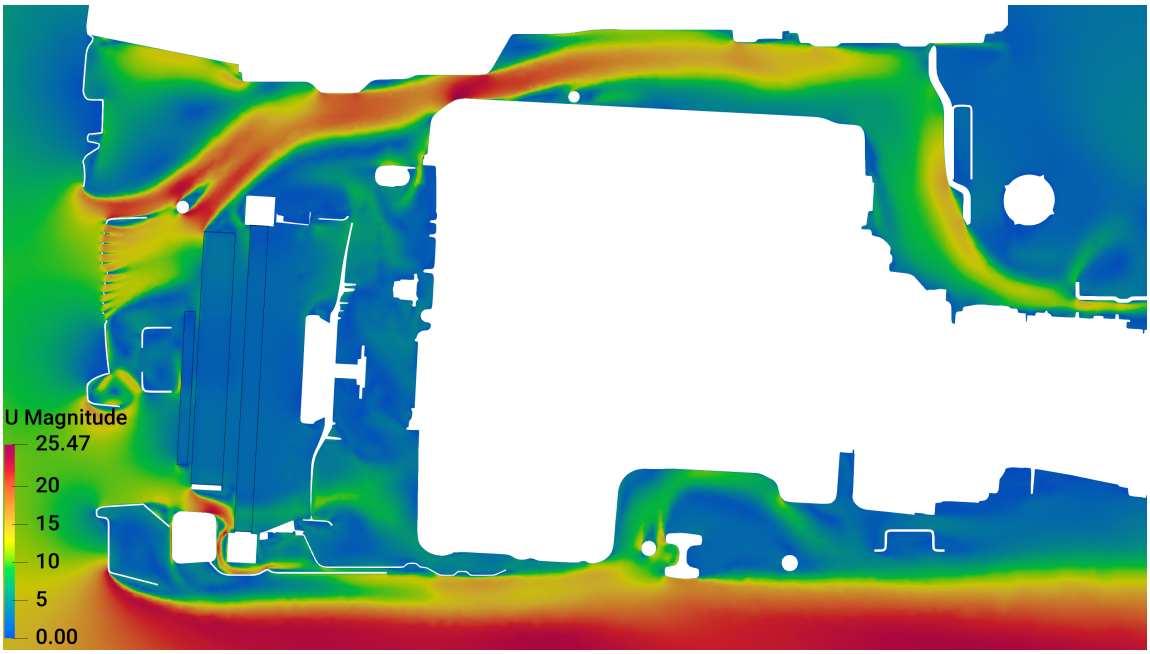

Slika 16: Ford Otosan kamion, izotermno strujanje, presjek: apsolutna brzina.

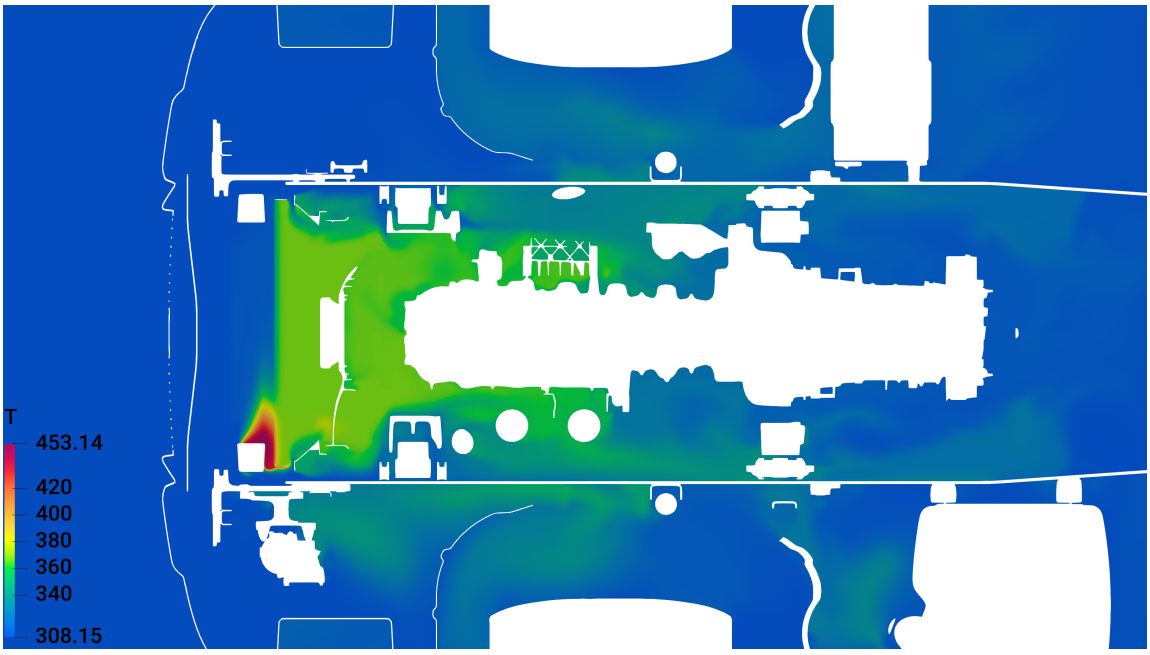

Slika 17: Ford Otosan kamion, rezultati topline, horizontalni presjek: temp. zraka.

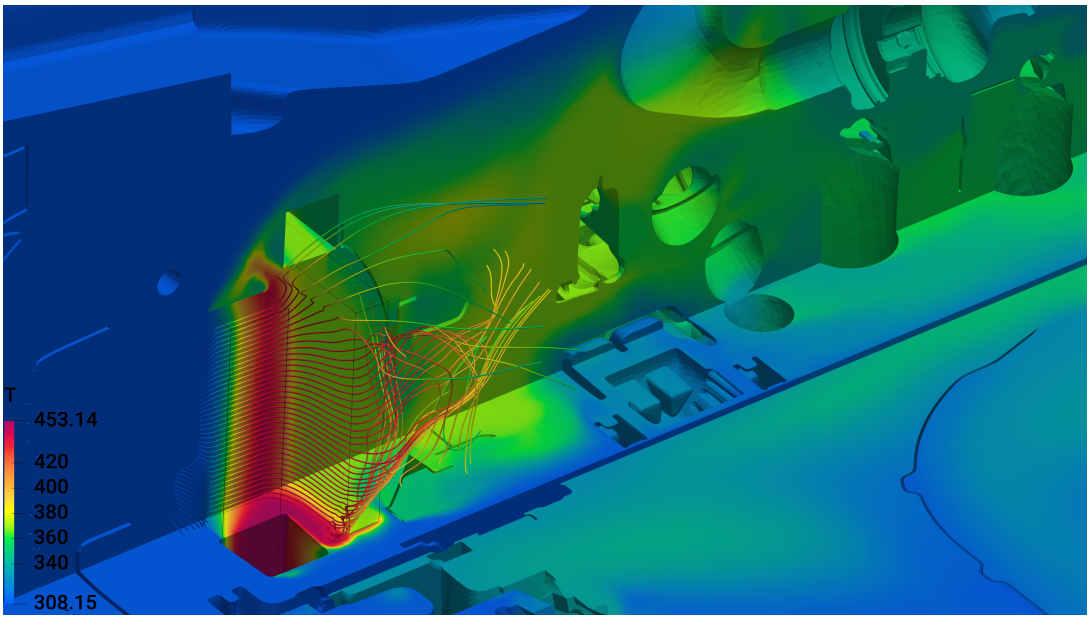

Slika 18: Ford Otosan kamion, rezultati topline, strujnice: temp. zraka.

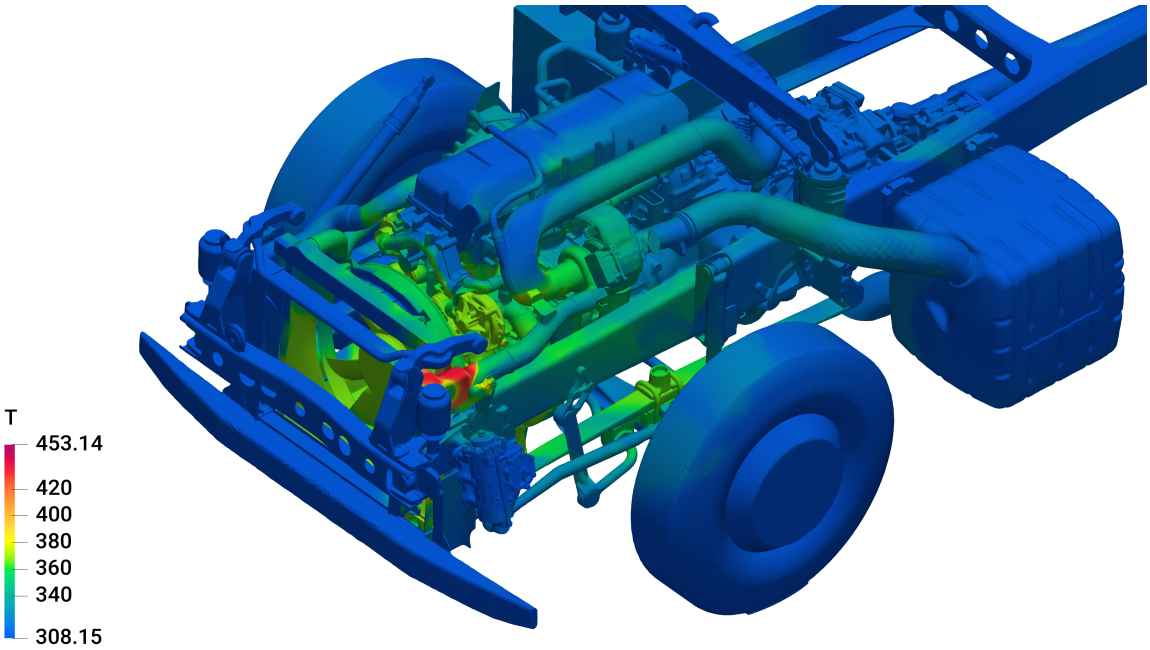

Slika 19: Ford Otosan kamion, rezultati topline, površine: temp. zraka.

Chapter 1

Introduction

1.1 Background

Thermal management of vehicle underhood compartment is one of the first-stage design problems, especially in heavy-duty vehicles where high thermal loading can be exerted for a fair amount of time, *eg.* while climbing a mountain or during extreme weather conditions. It is important to identify hot spots that can cause damage to vital parts of the vehicle during peak thermal loads. Computational Fluid Dynamics (CFD) is a viable tool for performing this type of thermal analysis. Previous methods included a very simple one-dimensional analysis and relied solely on experimental results. While CFD cannot completely replace experimental analysis, it can allow for a valid critical discussion during the design stage of the vehicle.

In this study `foam-extend` [1] framework is used for the development of a novel Dual Stream heat exchanger model. `Foam-extend` is a community-driven fork of OpenFOAM [5], free open source C++ library for solving continuum mechanics problems.

Pre-processing software ANSA [2] from BETA CAE Systems is used for geometry preparation and meshing of the Ford Otosan truck and other test case.

1.2 Previous and Related Studies

Zrnić [4] implemented and validated three heat exchanger models within the `foam-extend` framework. This study included analysis of the cooling system in a light aircraft influ-

enced by a propeller. All three heat exchanger models were of a single stream nature, and the heat exchanger's core was described as a porous media with constant auxiliary fluid temperature. These models are Total Volumetric Heat model, Single Stream model and the Nusselt model.

Ljunskog and Nillson [6] investigated the possibility of developing automated method for obtaining a CFD model of the complete underhood compartment of a car. It included ANSA for geometry cleanup and STAR-CCM+ as CFD solver, while the volume meshing differed. One method used a polyhedral mesh, while the other used a hexahedral mesh. Both methods were compared to wind tunnel measurements. However, there was a large uncertainty in the experimental results.

Nordin [7] investigated alternative underhood cooling flow solutions with the target of reducing cooling drag from battery electric vehicles. Two different approaches of positioning the vehicle's heat exchangers (in series and in parallel) with a number of different air inlet and outlet configurations have been evaluated using CFD simulations.

1.3 Thesis Outline

This study consists of a first chapter that introduces all necesary governing equations and assumptions made for simplification of described transport phenomena. It also includes the heat exchanger model that was used to describe the compact design of Ford Otosan heat exchangers. This model is then validated through simplified geometry consisting of a truck's radiator and intercooler. Simulation is performed on each individual heat exchanger, as well as on their simultaneous work. Chapter 3 consists of the mesh preparation of the Ford Otosan truck. This includes complete geometry clean up, structured volume meshing of heat exchangers, and appropriate boundary cell extrusion with main volume tetrahedral meshing. The final chapter concludes with a simulation setup and run. Results are presented and later discussed.

Chapter 2

Mathematical Model

In the current chapter, mathematical models used in this study are described. Presented numerical models use the principles of continuum mechanics, describing material as a continuous mass rather than discrete particles, enabling the usage of macroscopic physical properties of matter. These principles are essential for describing fluid flow and heat transfer. The chapter consists of basic governing principles of mass, momentum and energy conservation. Heat transfer model is introduced, as well as Multi Rotating Frame (MRF) and the porous media model. Lastly, a Dual Stream heat exchanger model is presented.

2.1 Governing Equations

2.1.1 Conservation Principles

The nature of fluids in motion is often very chaotic, and thus it is very difficult to follow individual particles. In engineering, most applications of fluid motion require a final answer regarding surface forces or temperatures so it is convenient to switch from particle tracking or control mass (CM) to control volume (CV) that deals only with spatial region under consideration. This method of analysis is called the *control volume approach* [8]. In order to switch from control mass to control volume, there is a need for an equivalent conservative form for moving material volume. In general form, the *Reynolds Transport Theorem* describes this change [9]. The conservative forms of mass, linear momentum,

and energy conservation are written as [10]:

- Conservation of mass
$$\frac{\partial \rho}{\partial t} + \nabla\bullet(\rho \mathbf{U}) = 0, \tag{2.1.1}$$
- Conservation of linear momentum
$$\frac{\partial \rho \mathbf{U}}{\partial t} + \nabla\bullet(\rho \mathbf{U}\mathbf{U}) = \rho \mathbf{g} + \nabla\bullet\sigma, \tag{2.1.2}$$
- Conservation of energy
$$\frac{\partial \rho e}{\partial t} + \nabla\bullet(\rho e \mathbf{U}) = \rho \mathbf{g}\nabla\bullet\mathbf{U} + \nabla\bullet(\sigma \cdot \mathbf{U}) - \nabla\bullet\mathbf{q} + Q, \tag{2.1.3}$$

  where

  – ρ is the density,

  – $\mathbf{U}$ is the velocity vector,

  – $\mathbf{g}$ is the gravitational force,

  – σ is the stress tensor,

  – e is the total specific energy,

  – $\mathbf{q}$ is the heat flux and

  – Q is the volume energy source.

The above conservation laws are valid for any continuum. The number of unknown quantities is, however, larger than the number of equations in the system, making the system indeterminate.

2.1.2 Conservation Relations for Newtonian Fluids

In order to close the system, it is necessary to introduce additional, so-called **constitutive relations** [10]. They depend on the properties of the continuous medium in question. In the case of Newtonian fluids, the following set of constitutive relations is used:

- The internal energy equation, defining the internal energy u as a function of pressure P and temperature T:

$$u = u(P, T). \tag{2.1.4}$$

The total energy is calculated as the sum of the kinetic e_M and internal energy (and all others, like chemical, nuclear etc. which will be neglected in this study):

$$e = e_M + u(P, T) = \frac{1}{2}\mathbf{U} \cdot \mathbf{U} + u(P, T), \tag{2.1.5}$$

- The equation of state:

$$\rho = \rho(P, T), \tag{2.1.6}$$

- The Fourier's law of heat conduction:

$$\mathbf{q} = -\lambda \nabla T, \tag{2.1.7}$$

- Generalised form of the Newton's law of viscosity:

$$\sigma = -\left(p + \frac{2}{3}\mu \nabla\!\bullet \mathbf{U}\right)\mathbf{I} + \mu\left[\nabla\mathbf{U} + (\nabla\mathbf{U})^T\right]. \tag{2.1.8}$$

These constitutive relations, together with the governing equations for a continuum create a closed system of partial differential equations for Newtonian fluids:

- Continuity equation:

$$\frac{\partial \rho}{\partial t} + \nabla\!\bullet(\rho\mathbf{U}) = 0, \tag{2.1.9}$$

- Navier-Stokes equations:

$$\frac{\partial \rho\mathbf{U}}{\partial t} + \nabla\!\bullet(\rho\mathbf{U}\mathbf{U}) = \rho\mathbf{g} - \nabla\left(p + \frac{2}{3}\mu \nabla\!\bullet \mathbf{U}\right) + \nabla\!\bullet\left[\mu\left(\nabla\mathbf{U} + (\nabla\mathbf{U})^T\right)\right], \tag{2.1.10}$$

- Energy equation

$$\begin{aligned}\frac{\partial \rho e}{\partial t} + \nabla\!\bullet(\rho e\mathbf{U}) = \rho\mathbf{g} \cdot \mathbf{U} - \nabla\!\bullet(p\mathbf{U}) - \nabla\!\bullet\left(\frac{2}{3}\mu\left(\nabla\!\bullet\mathbf{U}\right)\mathbf{U}\right) \\ +\nabla\!\bullet\left[\mu\left(\nabla\mathbf{U} + (\nabla\mathbf{U})^T\right) \cdot \mathbf{U}\right] + \nabla\!\bullet(\lambda\nabla T) + Q.\end{aligned} \tag{2.1.11}$$

The transport coefficients λ and μ are also functions of the thermodynamic state variables:

$$\lambda = \lambda\left(P, T\right), \tag{2.1.12}$$

$$\mu = \mu\left(P, T\right). \tag{2.1.13}$$

For incompressible isothermal fluids where $\rho = const.$, the system can be further simplified:

$$\nabla\bullet(\mathbf{U}) = 0, \tag{2.1.14}$$

$$\frac{\partial \mathbf{U}}{\partial t} + \nabla\bullet(\mathbf{U}\mathbf{U}) = \mathbf{g} - \nabla p + \nabla\bullet(\nu\nabla\mathbf{U}), \tag{2.1.15}$$

where ν is the kinematic viscosity and p kinematic pressure. All other equations in the system are decoupled.

2.2 Modelling of Heat Transfer

Conservation of energy obeys the first law of thermodynamics, stating that energy cannot be destroyed or produced [8]. Its general form is too complex for engineering applications; assumptions have to be made to make it usable. There are three mechanisms of heat transfer: *conduction*, *convection* and *radiation*. Generally, small changes in temperature of the surrounding air can greatly influence its flow. Also, in cases where advecting forces are great, like those close to a working fan, local temperature changes cannot influence the flow singnificantly. It can be seen from the Navier-Stokes equations that temperature can influence the flow through a change of fluid density. This sounds like an iterative process where equations are coupled through a thermodynamic state. In a greater number of engineering applications, like the one in this study, an assumption can be made on how the temperature influences fluid flow through the ratio of Rayleigh and Reynolds numbers. The Rayleigh number denotes the ratio between the time scale of thermal transfer with the diffusion and time scale of thermal transfer by convection, while the Reynolds number denotes the ratio between inertial forces and viscous forces. Both dimensionless numbers are defined as:

$$\mathrm{Ra} = \frac{\mathbf{g}\Delta\rho L^3}{\rho_0 \mu \kappa}, \tag{2.2.1}$$

$$\mathrm{Re} = \frac{\rho \mathbf{U} L}{\mu}. \tag{2.2.2}$$

If Ra/Re >> 0, the natural convection, *i.e.* buoyancy effect on the flow due to temperature-driven change of density can be neglected. The temperature equation for incompressible fluids with constant thermophysical properties can be written as:

$$\frac{\partial T}{\partial t} + \nabla\boldsymbol{\cdot}(\mathbf{U}T) = \nabla\boldsymbol{\cdot}\left(\frac{\nu}{\mathrm{Pr}}\nabla T\right) + \frac{Q}{\rho c_p}. \tag{2.2.3}$$

This form of equations will be used later in the study. The Prandtl number is a dimensionless number describing the ratio between momentum diffusivity, and thermal diffusivity and is defined as:

$$\mathrm{Pr} = \frac{c_p \mu}{\lambda}. \tag{2.2.4}$$

2.3 Multiple Rotating Frame Model

Rotation of a fan generally produces a time-dependent flow. This is, in some cases, computationally expensive to solve. The next best option is to model the rotating parts. If only rotating blades are considered, it would be natural to change the coordinate system and approach the problem with a relative velocity, *i.e.* present the fan to be stationary while everything around it rotates. This model is called a Single Rotating Frame of Reference (SRF). The shortcoming of this model is that often there are several other parts that do not rotate on the same axis or they don't rotate at all. For this reason, the Multiple Rotating Frame (MRF) model was developed. This model appoints a segment of space around the rotating part and assigns constant speed of rotation around a defined axis. This method would be similar to running a transient simulation and stopping it at the selected state and then observing results at a particular location, *i.e.* blades of the fan. This model greatly depends on the shape of the rotating part, as well as the number of blades. Surroundings also influence the results in the rotating zones via the coupled boundary conditions, connecting moving and stationary parts [11].

The Navier-Stokes equations for cells in the appointed rotating zone must be defined with the help of the relative velocity formulation:

$$\mathbf{U} = \mathbf{U}_R + \boldsymbol{\omega} \times \mathbf{r}, \tag{2.3.1}$$

with its time derivative defined as:

$$\frac{\partial \mathbf{U}}{\partial t} = \frac{\partial \mathbf{U}_R}{\partial t} + \underbrace{\frac{\partial \boldsymbol{\omega}}{\partial t} \times \mathbf{r}}_{\substack{\text{tangential} \\ \text{acceleration}}} + \underbrace{2\boldsymbol{\omega} \times \mathbf{U}_R}_{\substack{\text{Coriolis} \\ \text{acceleration}}} + \underbrace{\boldsymbol{\omega} \times (\boldsymbol{\omega} \times \mathbf{r})}_{\substack{\text{centrifugal} \\ \text{acceleration}}}, \tag{2.3.2}$$

where $\boldsymbol{\omega}$ denotes the angular velocity, and $\mathbf{r}$ the position vector of a cell relative to the rotating frame axis. Eq. (2.3.2) can be added to the conservation equations Eqs. (2.1.9 to 2.1.11) forming the absolute velocity formulation of each equation and for each cell in the rotating zone.

2.4 Modelling of Porosity

Compact heat exchangers are made with finely distributed fins. To solve the fluid flow in such a geometry with the idea of capturing the flow patterns and boundary layers in every single flow channel, one could end up with tens of millions of cells for one heat exchanger. These meshes are not suitable for engineering applications. Due to the nature of the design of compact heat exchanger that allows flow only in one direction, there is a benefit of modelling it as a porous zone. The most popular method for modelling porosity in OpenFOAM is the Darcy-Forchheimer model, considering pressure drop due to viscous and inertial forces [12]:

$$\nabla p = -\mu \mathbf{D} \cdot \mathbf{U} - \frac{1}{2}\rho \mathbf{F} \cdot (|\mathbf{U}|\mathbf{U})\,. \tag{2.4.1}$$

Coefficients $\mathbf{D}$ and $\mathbf{F}$ can be experimentaly determined as $p = f(\mathbf{U})$.

2.5 Heat Exchanger Modelling

Energy transport is well known through Eq. (2.1.11), and in its simplified form with appropriate assumptions, Eq. (2.2.3).

2.5.1 Overview

Heat exchangers act as a heat source, which can either heat up or cool down the surrounding fluid, *i.e.* reduce or increase energy of the fluid inside a control volume. As such, modelling the heat exchanger through the source terms from the last two equations is considered. Three single stream heat exchangers have been implemented and validated by [4] in `foam-extend`. In this study, a new heat exchanger model is implemented to improve the heat transfer conditions between primary and auxiliary fluid.

2.5.2 Dual Stream Model

The developed Dual Stream Model describes a typical *crossflow* heat exchanger. Thermodynamically, the effectiveness of a crossflow exchanger falls between the counterflow and parallelflow arrangements. In a crossflow arrangement, mixing of either fluid stream may or may not occur, depending on the design [3]. Design of heat exchangers in Ford Otosan truck disallows mixing of both fluids. Outer design is in the form of honeycombs, allowing passage of air in only one direction. Inside, geometry is in the form of micro-channels, also allowing flow in only one direction. This information is important for correctly describing the heat transfer, and in order to gain a valid temperature profile. In general, performance of the heat transfer depends on many aspects, such as: flow arrangement, size, mass flow, and total heat capacities of fluids. Thus it is important to describe a heat exchanger in a more general way. One convenient way to describe the heat exchanger, is the $\epsilon - \text{NTU}$ method. This method is used during the design of a heat exchanger, and expresses heat rejection as:

$$q = \epsilon q_{\max} = \epsilon C_{\min} \left(T_{h,i} - T_{c,i}\right) = \epsilon C_{\min} \Delta T_{\max}, \tag{2.5.1}$$

where ϵ is the heat exchanger effectiveness, $C_{\min}$ is the minimum of C_h and C_c, cold fluid's and hot fluid's total heat capacities, respectively; while $\Delta T_{\max} = (T_{h,i} - T_{c,i})$ is the temperature difference between fluid's inlets. The heat exchanger effectiveness ϵ is non-dimensional, and it can be shown that in general it is dependent on the number of transfer units NTU, the total heat capacity rate ratio $\frac{C_{\min}}{C_{\max}}$, and the flow arrangement for a direct-transfer type heat exchanger:

$$\epsilon = f\left(\text{NTU}, \frac{C_{\min}}{C_{\max}}, \text{flow arrangement}\right). \tag{2.5.2}$$

The Number of Transfer Units NTU designates the non-dimensional heat transfer size or thermal size of the exchanger. It is a design parameter defined as [3]:

$$\text{NTU} = \frac{UA}{C_{\min}} \tag{2.5.3}$$

Analytical derivation of function ϵ is possible only for a few simple flow arrangements, such as counterflow exchanger. To describe this relation for crossflow exchanger, there is a need for experimental testing. A common way to express heat exchanger effectiveness through experimental testing is to create a solution regarding inlet velocities, that is, $\epsilon = f(\boldsymbol{U}_h, \boldsymbol{U}_c)$. This way, the inputs are defined for Eq. (2.5.1), and used in modelling of the heat source term. Generally, one heat exchanger can have nonuniform velocity alongside internal geometry due to an imperfect inlet. Also the surrounding fluid can be blocked from one part of the exchanger and thus the heat exchanger will not perform to its full capacity.

Fig. 2.5.1 presents a schematic view on the crossflow heat exchanger with both fluids unmixed with one pass. The primary side is modelled as a porous media. Coefficients are altered to produce flow only in one direction, ulimately imitating the fins that block air flow to the sides of the exchanger. The auxiliary fluid was modelled as one-dimensional heat transfer by making one stack of elements represent one micro-channel.

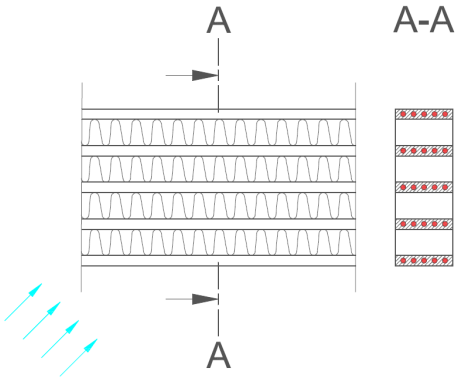

Figure 2.5.1: Schematic view of *crossflow* heat exchanger with both fluids unmixed: auxiliary (red) and primary (blue) fluids

Chapter 3

Validation of the Dual Stream Model

In this chapter, validation is conducted for the implemented dual stream heat exchanger model. Validation is performed in terms of calculating energy imbalance between the coolant and the surrounding air, *i.e.* by verifying the integral form of Dual Stream Model. The geometry of the heat exchanger matches the heat exchanger geometries in the Ford Otosan truck.

In the first two sections simulations are performed on each individual heat exchanger, while the last chapter tests the simultaneous work of the intercooler and the radiator. All simulations were performed using the same case setup with identical high quality mesh properties.

It is important to note that the heat exchanger effectiveness in general depends on the fluid's total heat capacity and NTU. In this study, a simple effectiveness model was developed and the heat exchanger's effectiveness was assumed to be constant.

3.1 Test Case Setup

The heat exchanger's geometry represents only the active surfaces that are involved in the heat transfer, Fig. 3.1.1. The bounding box around the heat exchangers represents an isolated rectangular duct. The direction of the flow matches the x-axis. Thermophysical properties of the surrounding air and of the coolant are assumed to be constant. Due to large advecting forces and a small scale of the bounding box, a change in the air density was neglected and thus the energy equation was solved separately in the form of

temperature equation. The heat exchanger core was modelled as a porous zone with a linear pressure drop and with the flow dominant only in the x-direction. Four different operating conditions were simulated for each heat exchanger. Discretization schemes, as well as the solver settings and zone parameters are identical to those in Chapter 5.

To keep the engine from overheating, the radiator performs a critical part of heat management. Even though over one century has passed since the invention of a Diesel engine, thermodynamic efficiency has not been increased in great amounts. On the contrary, the cooling performance with more complex heat exchanger geometry was increased. Consequently, there is an increasing need for more accurate mathematical models of heat exchangers to better understand the thermal stress of components. In the modern automotive industry, heat exchangers are mostly made as a micro-channel "compact" heat exchanger with one pass, and so are in this study.

In order to increase the thermodynamic efficiency of a Diesel engine, air intake has to be compressed. Downside of this compression is an increase in air temperature. This compressed air is bypassed to the intercooler where the surrounding air cools it down. In terms of design, an intercooler has similar micro channels as a radiator and thus it is modelled in the same manner. In comparison to a radiator, intercooler's coolant is compressed air that has a lower specific heat capacity as well as much lower mass flow rate. Therefore intercooler's total heat capacity can be thirty times lower than radiator's. This is important for suitable placement of heat exchangers. It is only natural that radiator comes behind the intercooler, because intercooler will not heat up the surrounding air as much as a radiator will. The only problem is a very high temperature on the intercooler inlet, so it is of vital importance to correctly model the high temperature drop in the intercooler. This, on the other hand, introduces a numerical problem in terms of high non-linear behaviour that is remedied with explicit relaxation of coolant temperature.

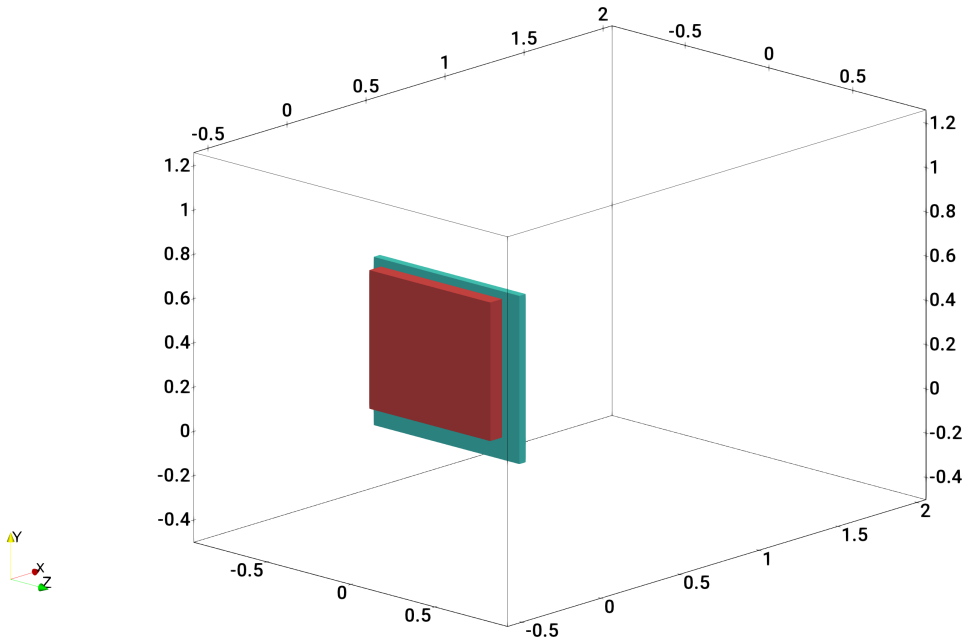

Figure 3.1.1: Test case geometry: radiator (red), intercooler (green) and bounding box.

3.2 Radiator

In order to test radiator's performance there will be four different boundary conditions for the inlet air velocity because it is expected that larger deviations in performance are due to the change in air velocity.

Even though most heat rejection is assumed to come from the radiator, its relatively large auxiliary mass flow provides a small drop in temperature and thus making the non-linear behaviour of the Dual Stream Model less problematic.

Cross section of radiator's volume mesh can be seen in Fig. 3.2.1, while Fig. 3.2.2 shows the placement of the inlet for the auxiliary fluid.

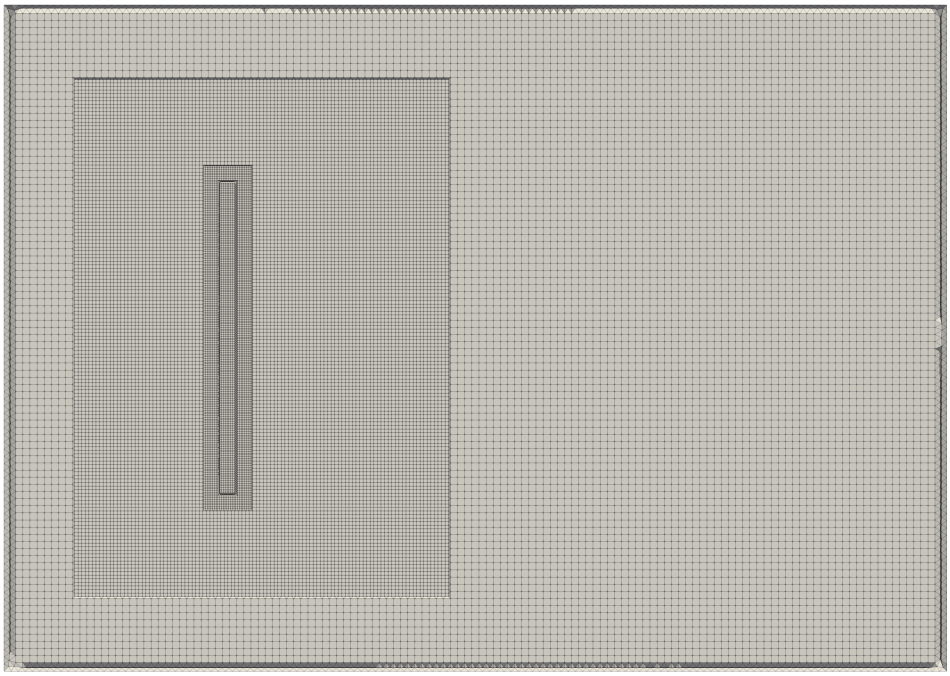

Figure 3.2.1: Radiator: volume mesh.

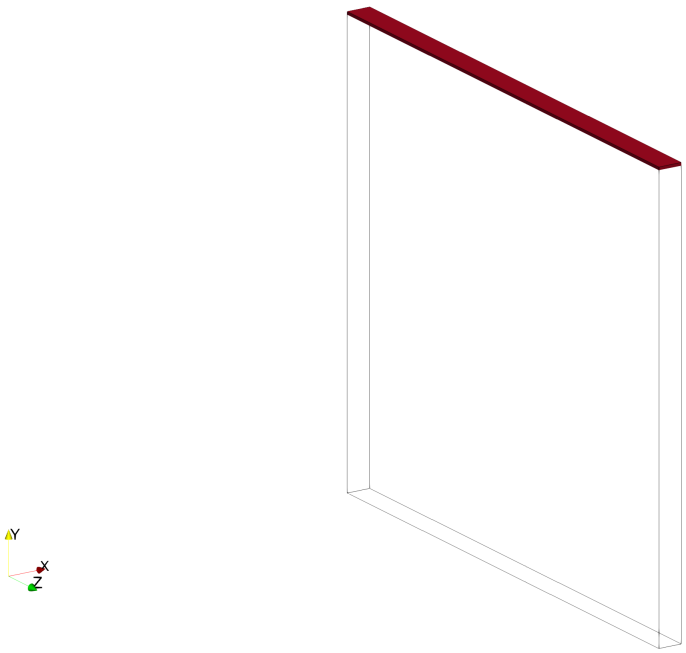

Figure 3.2.2: Radiator: auxiliary fluid inlet.

Parameters and thermophysical properties for radiator simulations are:

- Auxiliary inlet temperature, $T_{\text{aux}} = 368.15$ K,
- Auxiliary mass flow rate, $m_{\text{aux}} = 6$ kg/s,
- Auxiliary specific heat capacity, $c_{\text{aux}} = 3660$ J/(kgK),
- Air inlet temperature, $T_{\text{air}} = 318.15$ K,
- Air velocity magnitude, $U_{\text{air}} = [2, 4, 6, 8]$ m/s,
- Air specific heat capacity, $c_{\text{air}} = 1009$ J/(kgK),
- Air density, $\rho_{\text{air}} = 1.1021$ kg/m^3,
- Heat exchanger effectiveness, $\epsilon = [0.9096, 0.8361, 0.7454, 0.6706]$.

Table 3.2.1 presents the results where air velocity magnitude and heat exchanger's effectiveness were changed during four different simulations. Effectiveness was gradually decreased to imitate real crossflow exchanger where drop in heat effectiveness is expected due to higher velocity of the surrounding air. The model behaved stable and the heat rejection error is neglectible so the integrality of the model is preserved. Figs. 3.2.3 to 3.2.6 show gradually warmer air at the outlet as the air velocity magnitude increases. This is an expected behaviour due to increase in heat rejection, as seen in Table 3.2.1.

U_{air} [m/s]	ϵ [-]	$Q_{\text{air,total}}$ [W]	$Q_{\text{aux,total}}$ [W]	Error [%]
2	0.9096	77493.38	77493.38	1.02e-6
4	0.8361	147025.65	147025.65	0.83e-7
6	0.7454	212994.70	212994.71	1.20e-6
8	0.7606	275257.09	275257.09	1.61e-6

Table 3.2.1: Radiator: simulations results.

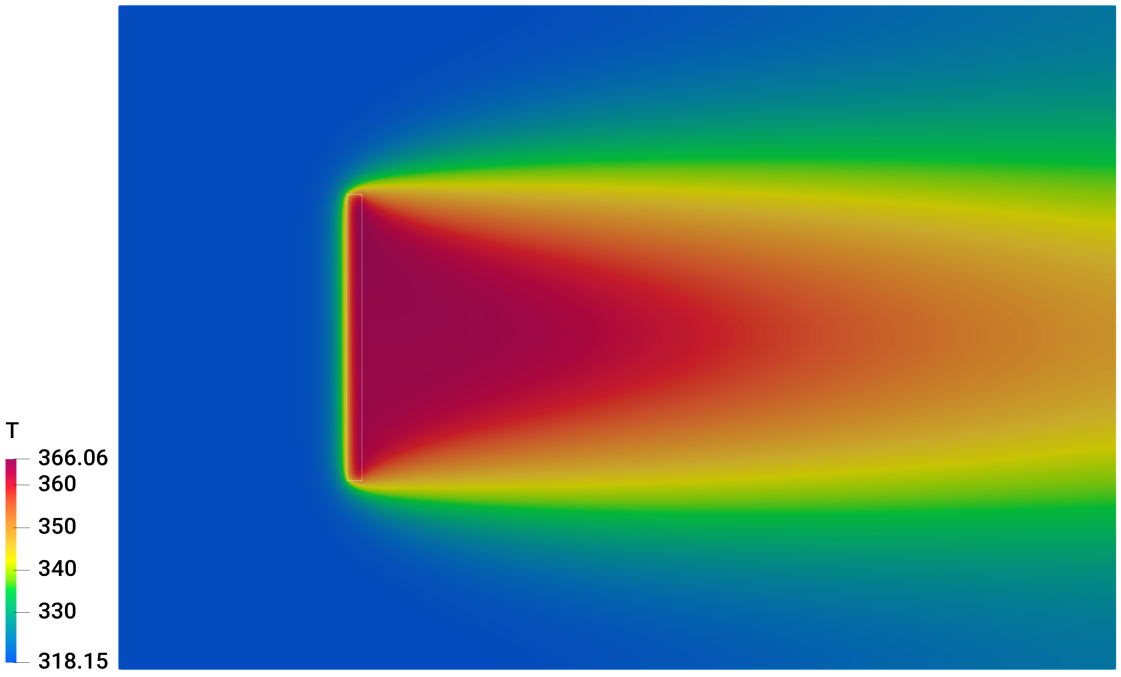

Figure 3.2.3: Radiator XY cross section: air temperature, $U_{\text{air}} = 2$ m/s.

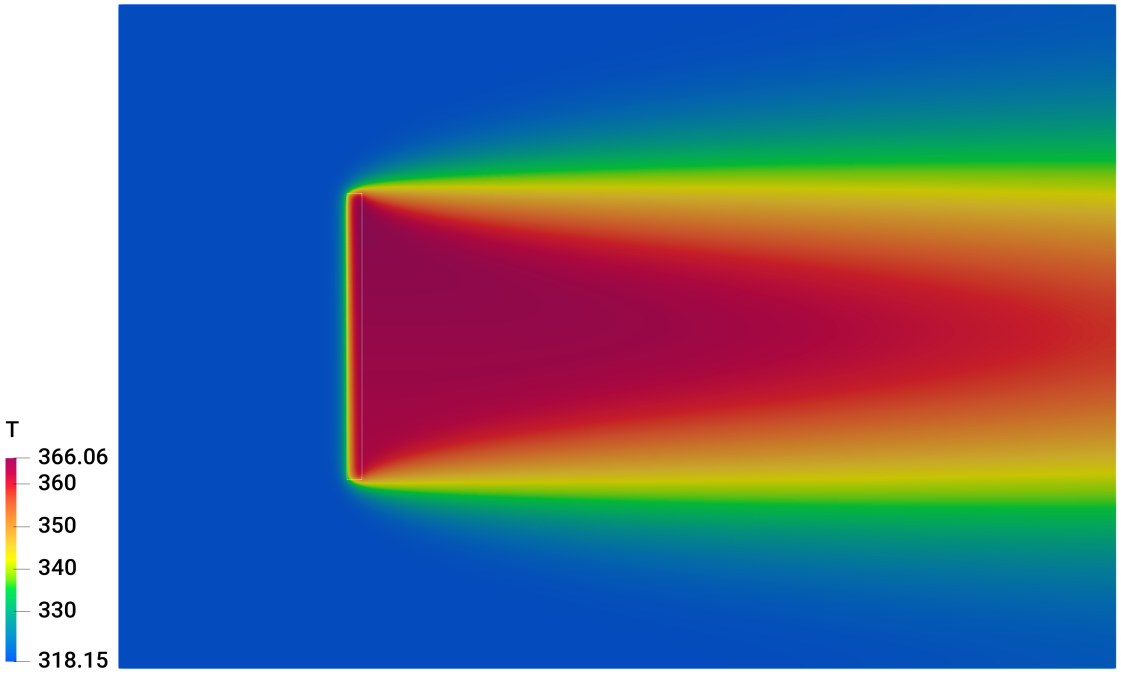

Figure 3.2.4: Radiator XY cross section: air temperature, $U_{\text{air}} = 4$ m/s.

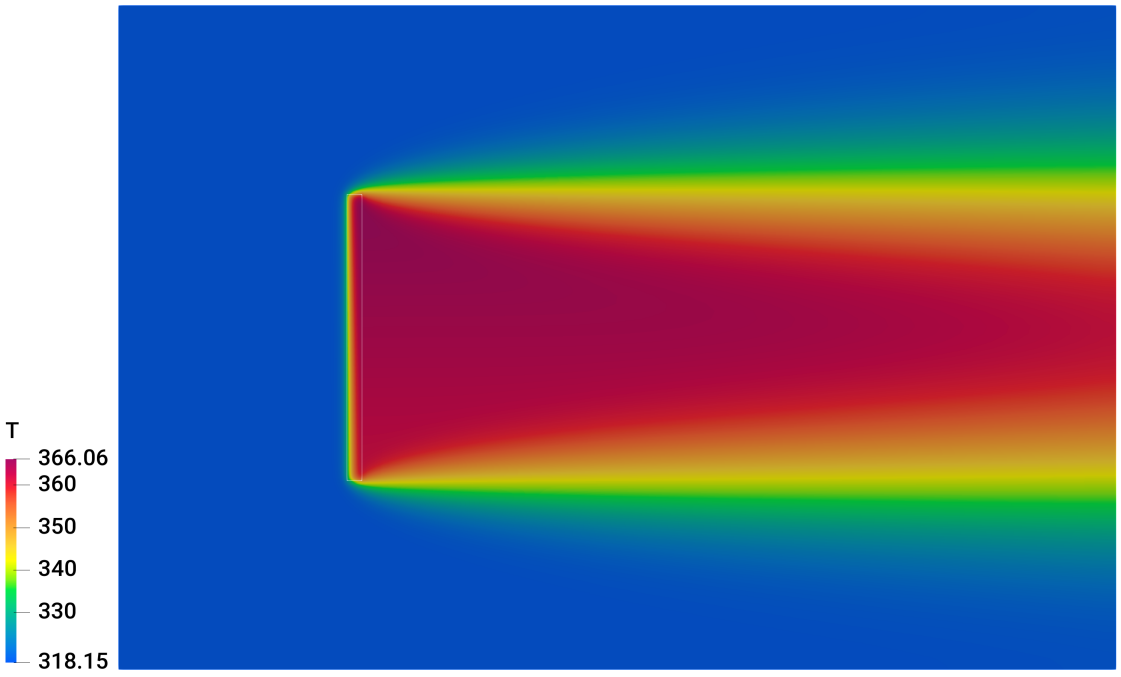

Figure 3.2.5: Radiator XY cross section: air temperature, $U_{\text{air}} = 6$ m/s.

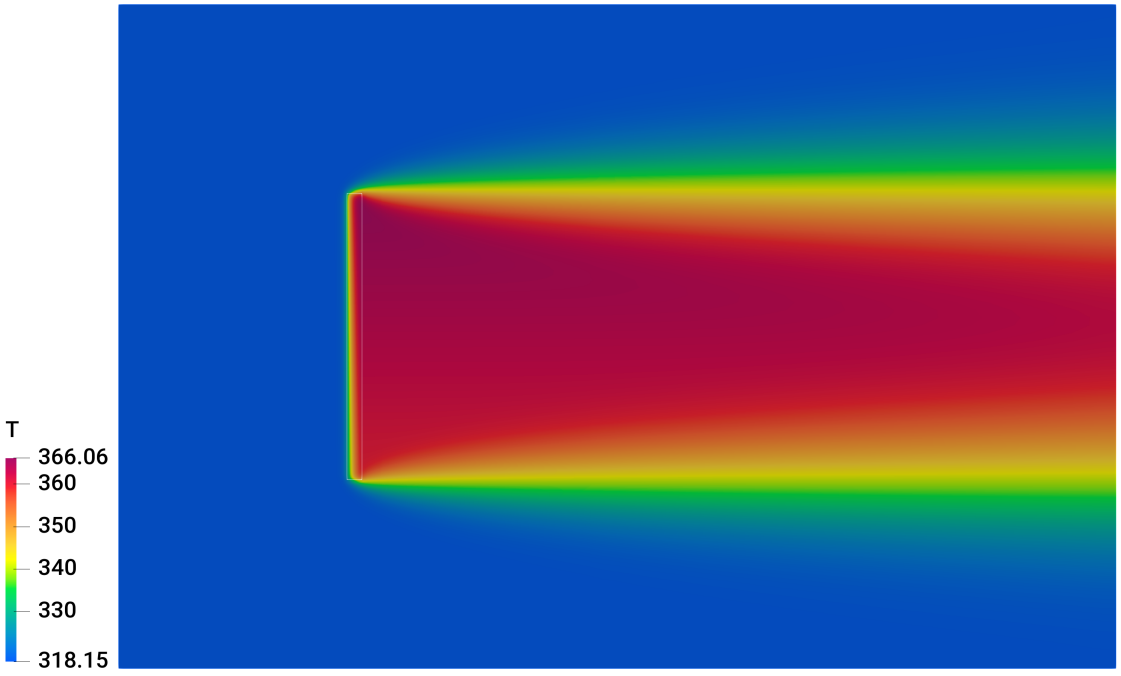

Figure 3.2.6: Radiator XY cross section: air temperature, $U_{\text{air}} = 8$ m/s.

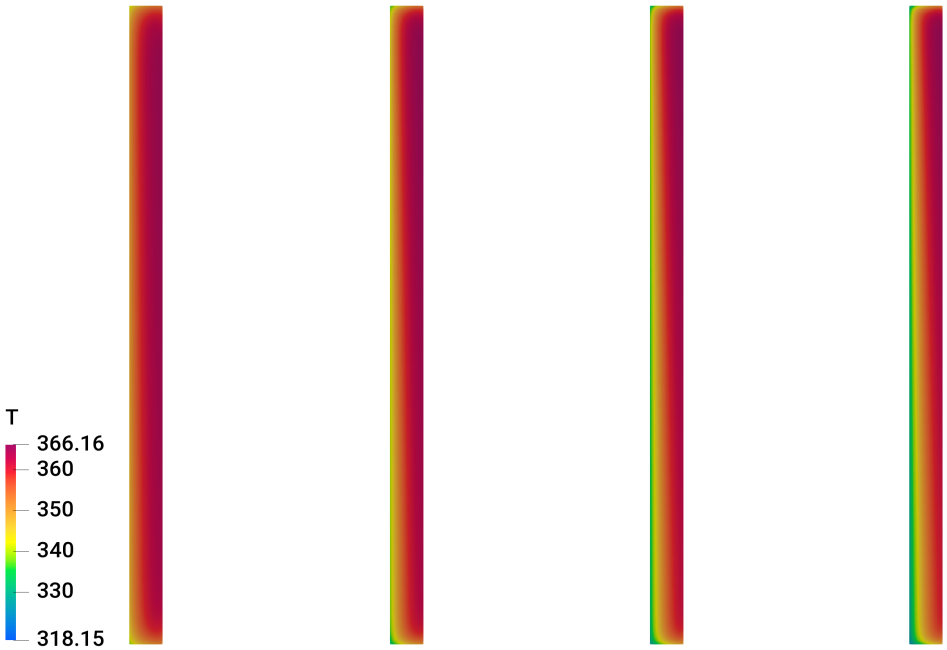

a) $U_{\text{air}} = 2$ m/s, b) $U_{\text{air}} = 4$ m/s, c) $U_{\text{air}} = 6$ m/s, d) $U_{\text{air}} = 8$ m/s.

Figure 3.2.7: Radiator XY cross section: radiator's air temperature.

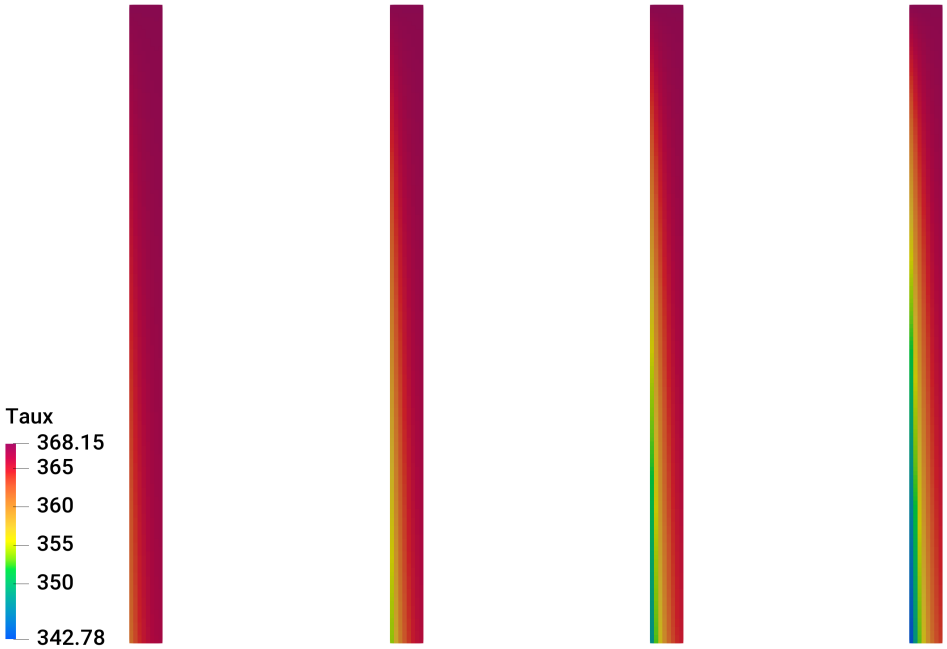

a) $U_{\text{air}} = 2$ m/s, b) $U_{\text{air}} = 4$ m/s, c) $U_{\text{air}} = 6$ m/s, d) $U_{\text{air}} = 8$ m/s.

Figure 3.2.8: Radiator XY cross section of: radiator's coolant temperature.

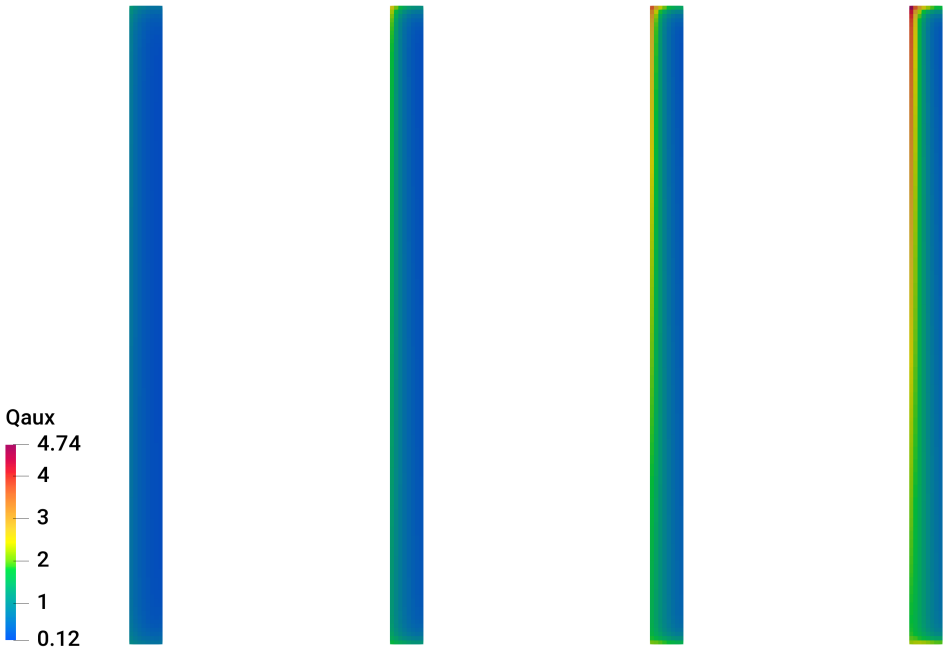

a) $U_{\text{air}} = 2$ m/s, b) $U_{\text{air}} = 4$ m/s, c) $U_{\text{air}} = 6$ m/s, d) $U_{\text{air}} = 8$ m/s.

Figure 3.2.9: Radiator XY cross section: radiator's heat rejection.

Analysing Figs. 3.2.7 to 3.2.9 it can be seen that the gradual increase in air velocity magnitude also affects the auxiliary temperature profile. Temperature drop as well as temperature gradients become more severe and heat rejection becomes more obvious.

3.3 Intercooler

In order to test intercooler's performance there will be four different boundary conditions for the auxiliary mass flow rate because it is expected that larger deviations in performance are due to the change in mass flow rate. Temperature drop is expected to be much larger than in previous section when radiator was tested.

Simulating intercooler introduced a numerical stability problem because of this large temperature drop. This issue was remedied with explicit relaxation of auxiliary temperature.

Cross section of intercooler's volume mesh can be seen in Fig. 3.3.1, while Fig. 3.3.2 shows the placement of the inlet for the auxiliary fluid.

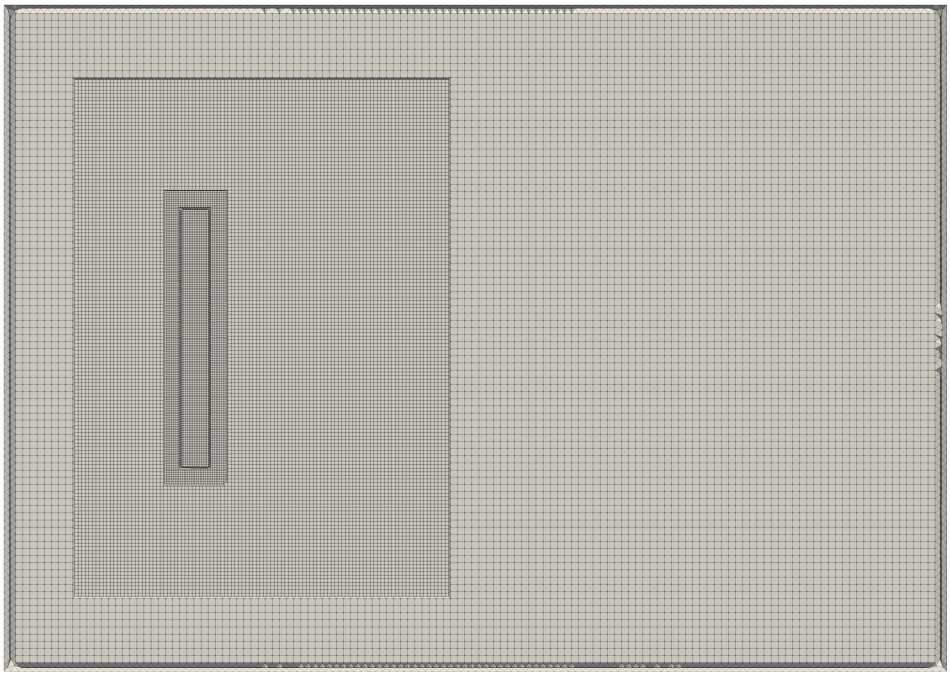

Figure 3.3.1: Intercooler: volume mesh.

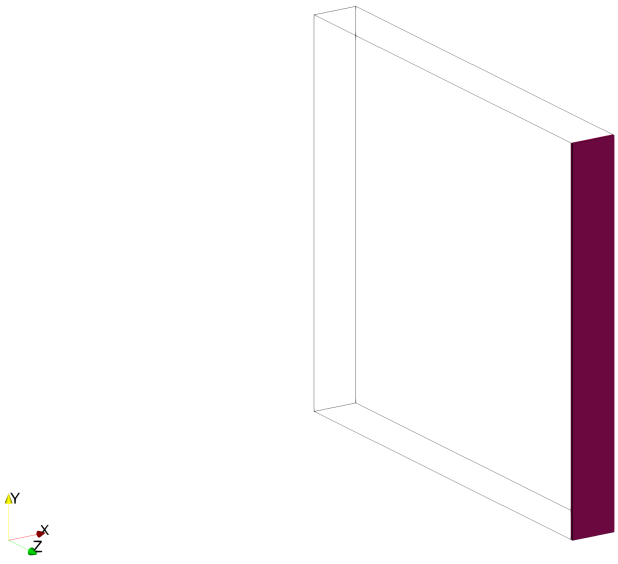

Figure 3.3.2: Intercooler: auxiliary fluid inlet.

Parameters and thermophysical properties for intercooler simulations are:

- Auxiliary inlet temperature, $T_{\text{aux}} = 453.15$ K,
- Auxiliary mass flow rate, $m_{\text{aux}} = [0.1, 0.2, 0.3, 0.4]$ kg/s,
- Auxiliary specific heat capacity, $c_{\text{aux}} = 1009$ J/(kgK),
- Air inlet temperature, $T_{\text{air}} = 308.15$ K,
- Air velocity magnitude, $U_{\text{air}} = 2$ m/s,
- Air specific heat capacity, $c_{\text{air}} = 1009$ J/(kgK),
- Air density, $\rho_{\text{air}} = 1.1021$ kg/m^3,
- Heat exchanger effectiveness, $\epsilon = [0.9769, 0.9239, 0.8603, 0.7972]$.

Table 3.3.1 presents the results where auxiliary mass flow rate and heat exchanger's effectiveness were changed during four different simulations. Effectiveness was gradually decreased to imitate real crossflow exchanger where drop in heat effectiveness is expected due to higher mass flow rate of auxiliary fluid. Heat rejection error is neglectible so the integrality of the model is preserved. Figs. 3.3.3 to 3.3.6 show gradually warmer air at the outlet as the air velocity magnitude increases. This is an expected behaviour due to increase in heat rejection, as seen in Table 3.3.1. But more importantly, the figures show large temperature gradients because of low total heat capacity of auxiliary fluid and higher auxiliary inlet temperature.

m_{aux} [m/s]	ϵ [-]	$Q_{\text{air,total}}$ [W]	$Q_{\text{aux,total}}$ [W]	Error [%]
0.1	0.9669	14646.76	14647.06	2.07e-3
0.2	0.9239	29258.04	29258.49	1.56e-3
0.3	0.8603	43528.61	43528.97	8.17e-4
0.4	0.7972	56860.06	56860.28	4.02e-4

Table 3.3.1: Intercooler: simulations results.

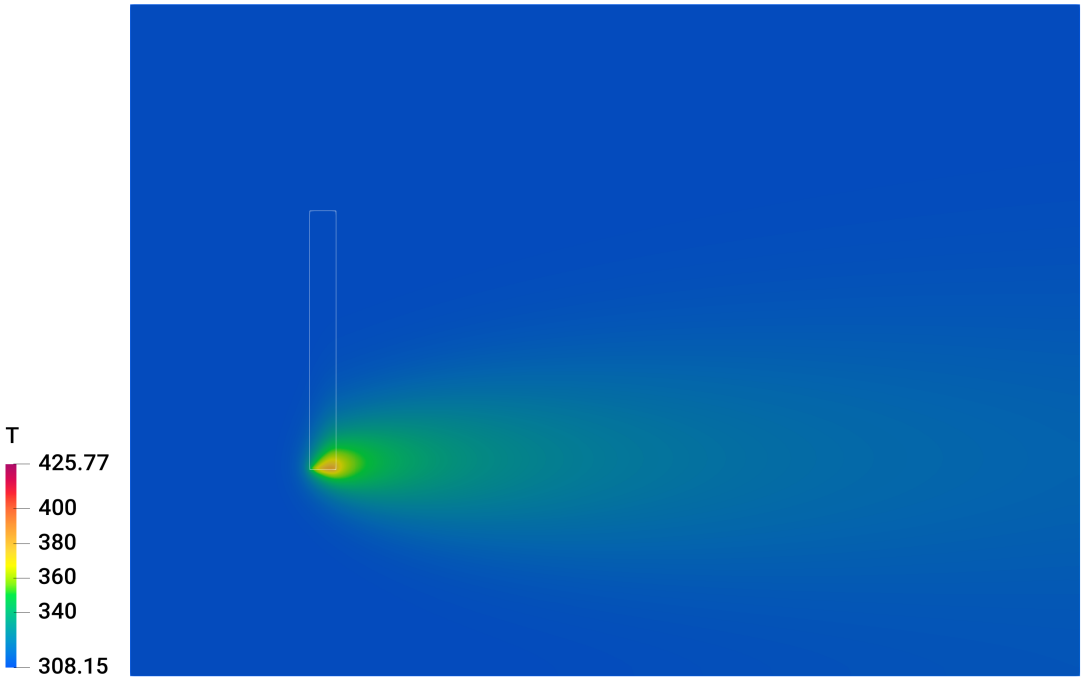

Figure 3.3.3: Intercooler XZ cross section: air temperature, $m_{\text{aux}} = 0.1$ kg/s.

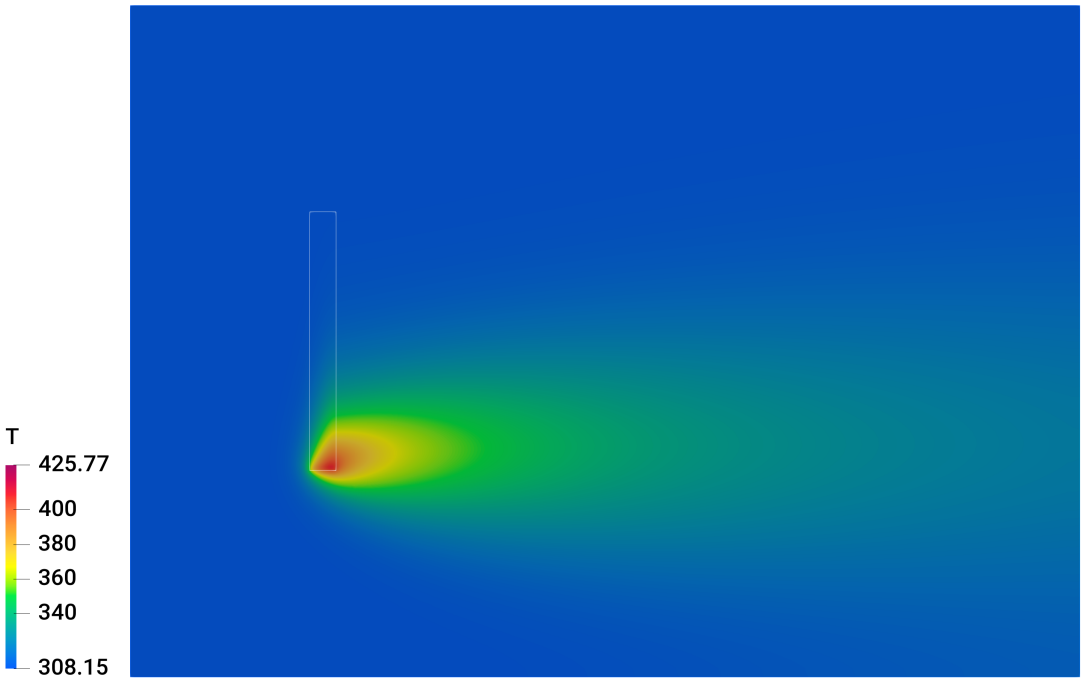

Figure 3.3.4: Intercooler XZ cross section: air temperature, $m_{\text{aux}} = 0.2$ kg/s.

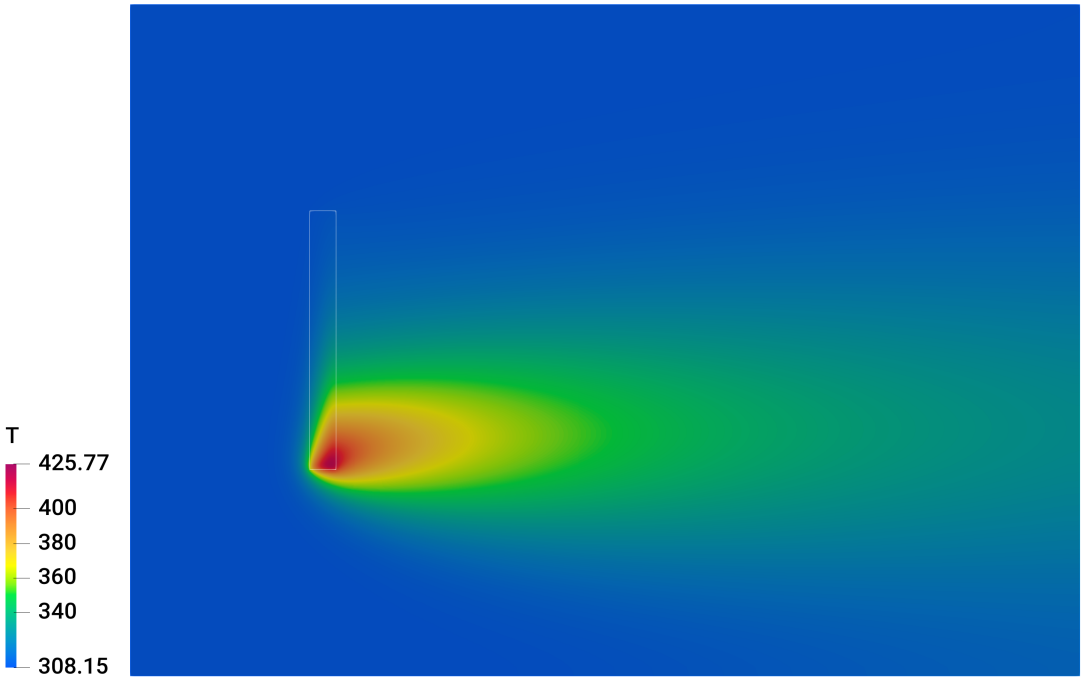

Figure 3.3.5: Intercooler XZ cross section: air temperature, $m_{\text{aux}} = 0.3$ kg/s.

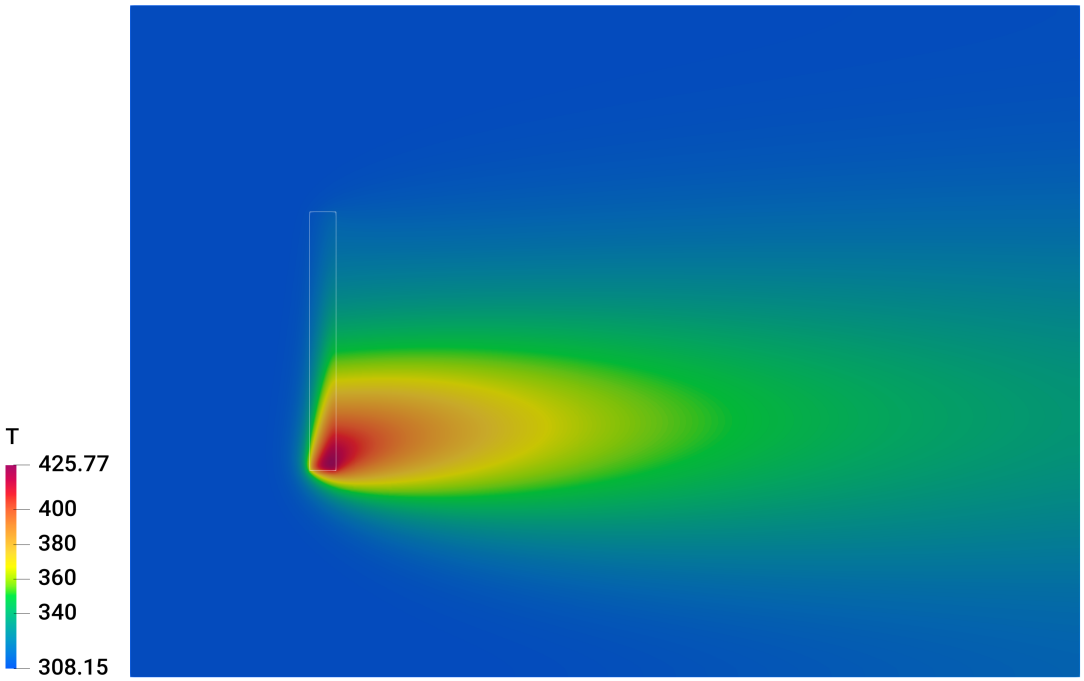

Figure 3.3.6: Intercooler XZ cross section: air temperature, $m_{\text{aux}} = 0.4$ kg/s.

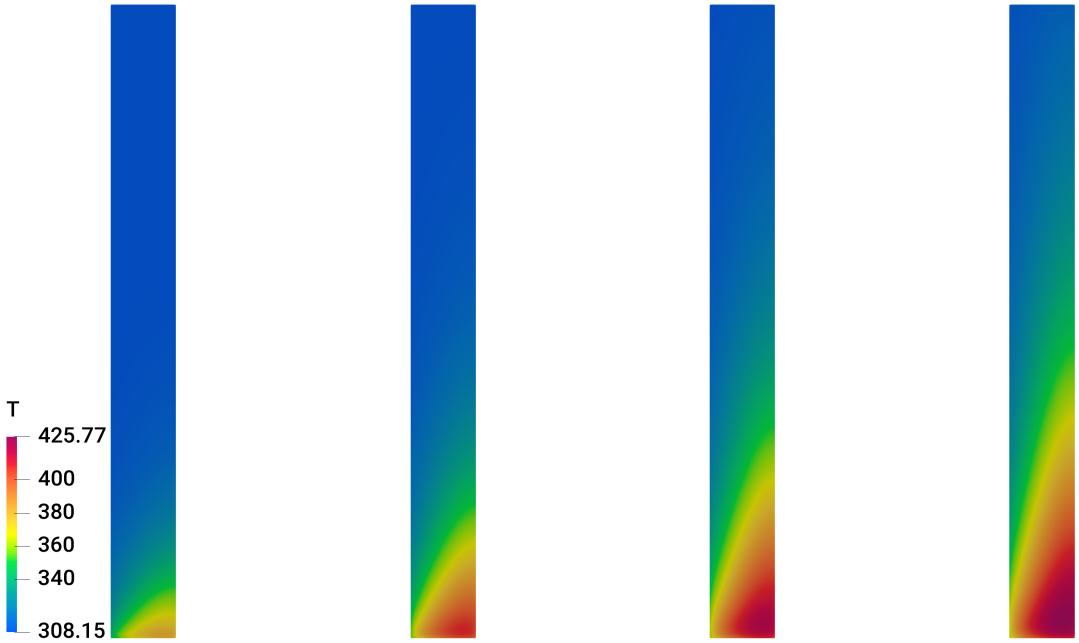

a) $m_{\text{aux}} = 0.1$ kg/s, b) $m_{\text{aux}} = 0.2$ kg/s, c) $m_{\text{aux}} = 0.3$ kg/s, d) $m_{\text{aux}} = 0.4$ kg/s.

Figure 3.3.7: Intercooler XZ cross section: intercooler's air temperature.

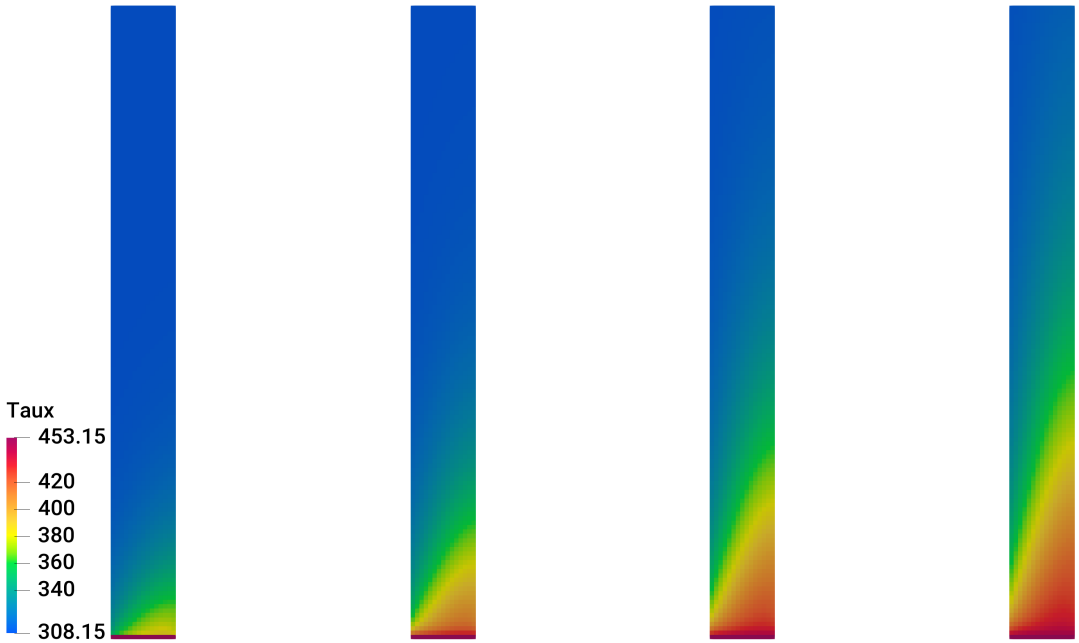

a) $m_{\text{aux}} = 0.1$ kg/s, b) $m_{\text{aux}} = 0.2$ kg/s, c) $m_{\text{aux}} = 0.3$ kg/s, d) $m_{\text{aux}} = 0.4$ kg/s.

Figure 3.3.8: Intercooler XZ cross section: intercooler's coolant temperature.

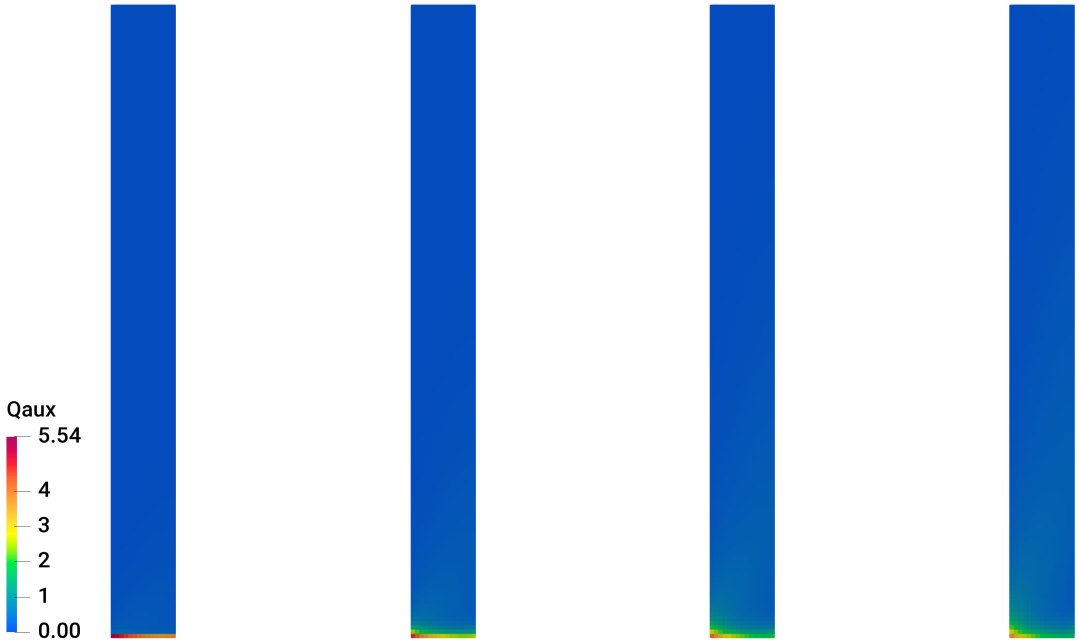

a) $m_{\text{aux}} = 0.1$ kg/s, b) $m_{\text{aux}} = 0.2$ kg/s, c) $m_{\text{aux}} = 0.3$ kg/s, d) $m_{\text{aux}} = 0.4$ kg/s.

Figure 3.3.9: Intercooler XZ cross section: intercooler's heat rejection.

Through Figs. 3.3.7 to 3.3.9 it can be seen that the gradual increase in mass flow rate also affects the auxiliary temperature profile. Temperature drop is almost constant through the simulations, but the temperature and heat rejection gradients smooth down as the auxiliary mass flow rate increases. Running of simulations for intercooler was not as stable as they were for radiator. This is because of high auxiliary temperature gradients that were not present in the radiator's case. This problem was solved with explicit relaxation of auxiliary temperature.

3.4 Simultaneous Operation of the Intercooler and the Radiator

In the previous two sections, both heat exchangers were successfully validated for the implemented Dual Stream Model. To introduce additional complexity to the implemented model, in this section both heat exchangers will be active at the same time. Identical four simulations with corresponding heat exchanger parameters are performed. To analyse

working conditions, the placement and size of heat exchangers correspond to real Ford Otosan geometry that will be introduced in Chapter 4. Before the results are presented, it must be noted that the radiator analysis was performed using a temperature of the surrounding air at 318.15 K, while analysis of the intercooler at 308.15 K. This is due to an assumption that the intercooler in general will increase local temperature by 10 K and thus the radiator was analysed using the corresponding air temperature. Parameters and thermophysical properties for simulations are equal to previous two sections. Cross section of the volume mesh can be seen in Fig. 3.4.1, while Fig. 3.4.2 shows the placement of the inlet for the auxiliary fluids.

Tables 3.4.1 to 3.4.3 presents the results of four simulations. Similar results are observed as in previous two sections. It is interesting that intercooler's heat rejection was not changed significantly even though air velocity magnitude increased from 2 m/s to 8m/s. The reason behind this is its low total heat capacity. Similar results for radiator's heat rejection are observed because the air temperature in this section was set to 308.15 K, while in the first section the air temperature was set to 318.15 K. Figs. 3.4.3 to 3.4.6 show gradually warmer air at the outlet as the air velocity magnitude increases, as it did in the previous two sections. Only in Fig. 3.4.6 the influence of intercooler's heat can be seen on downstream air temperature, but the local temperature around intercooler's inlet increases and this is an expected hot spot in Ford Otosan simulation.

Simulation no.	U_{air} [m/s]	$Q_{\text{air,sum}}$ [W]	$Q_{\text{aux,sum}}$ [W]	Error [%]
1	2	94999.11	94999.15	3.97e-5
2	4	179475.07	179475.07	6.12e-7
3	6	260163.99	260163.99	9.74e-8
4	8	337145.82	337145.83	7.88e-7

Table 3.4.1: Simultaneous operation results.

Simulation no.	m_{aux} [m/s]	ϵ [-]	$Q_{\text{aux,total}}$ [W]
1	0.1	0.9669	14282.74
2	0.2	0.9239	29199.78
3	0.3	0.8603	43922.22
4	0.4	0.7972	58591.70

Table 3.4.2: Simultaneous operation results: intercooler.

Simulation no.	m_{aux} [m/s]	ϵ [-]	$Q_{\text{aux,total}}$ [W]
1	6	0.9096	80716.41
2	6	0.8361	150275.29
3	6	0.7454	216241.77
4	6	0.7606	278554.13

Table 3.4.3: Simultaneous operation results: radiator.

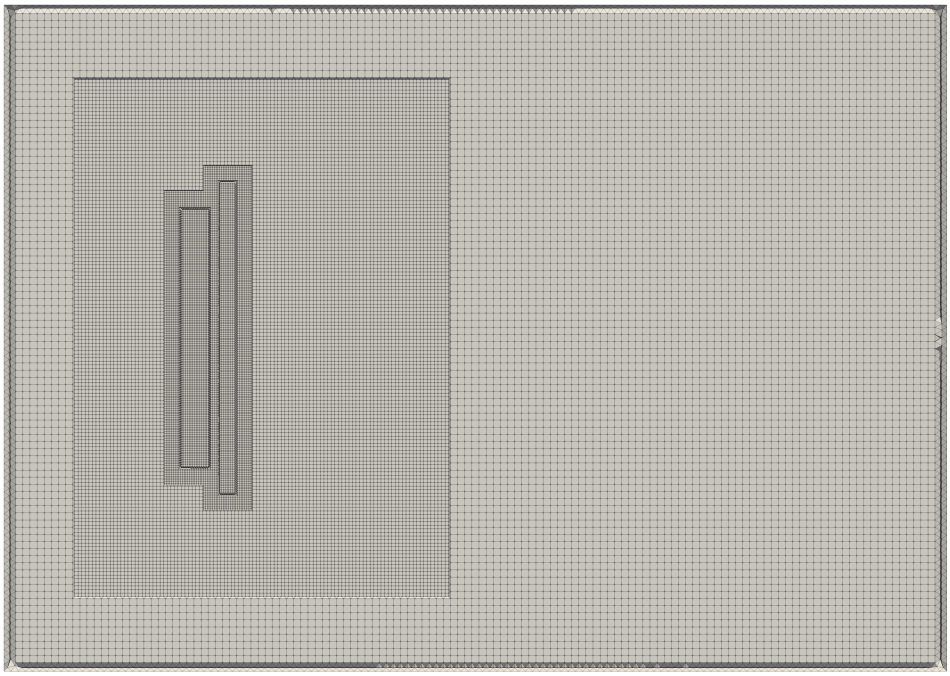

Figure 3.4.1: Simultaneous operation: volume mesh.

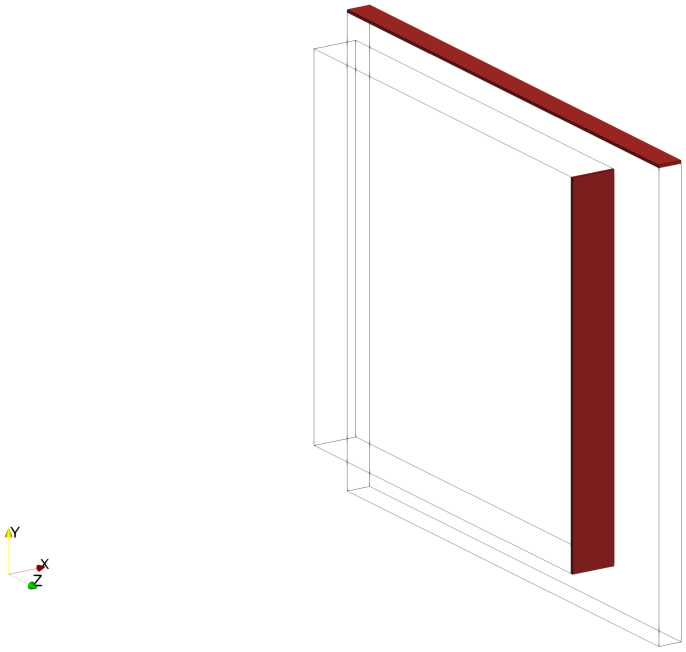

Figure 3.4.2: Simultaneous operation: auxiliary fluid inlet.

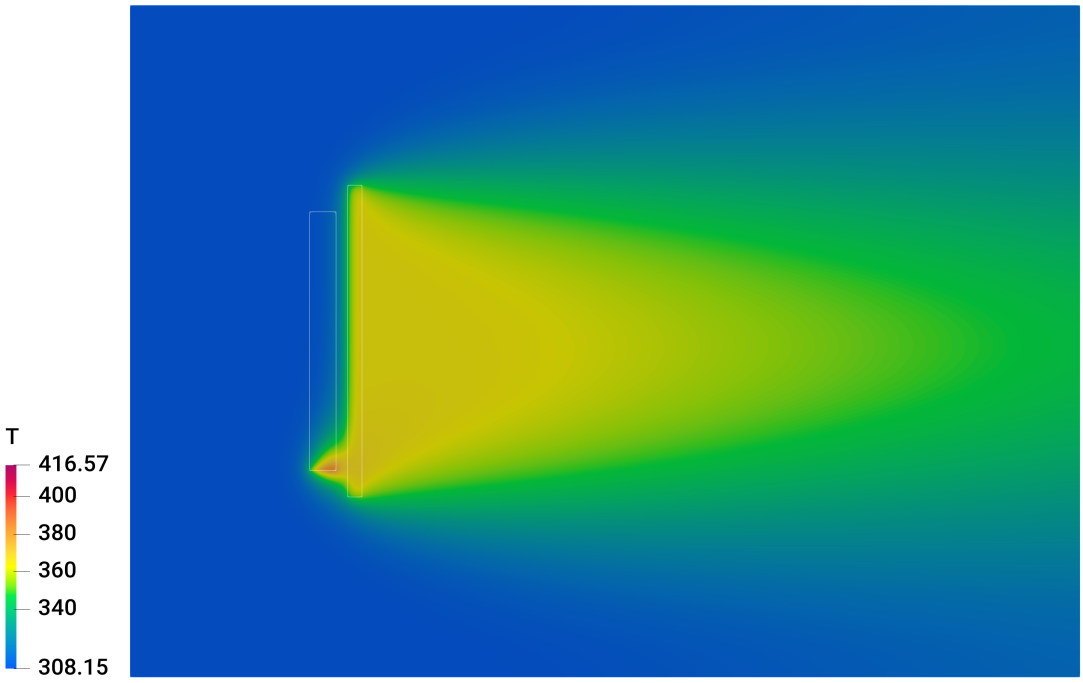

Figure 3.4.3: Simultaneous operation, XZ cross section: air temperature, sim. no. 1.

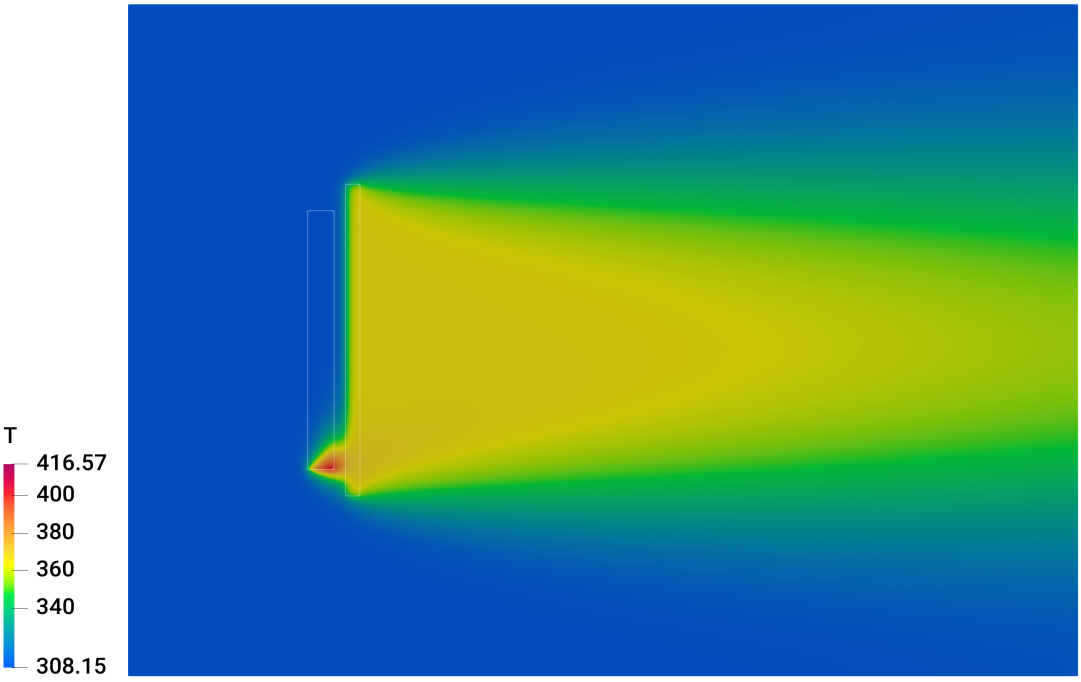

Figure 3.4.4: Simultaneous operation, XZ cross section: air temperature, sim. no. 2.

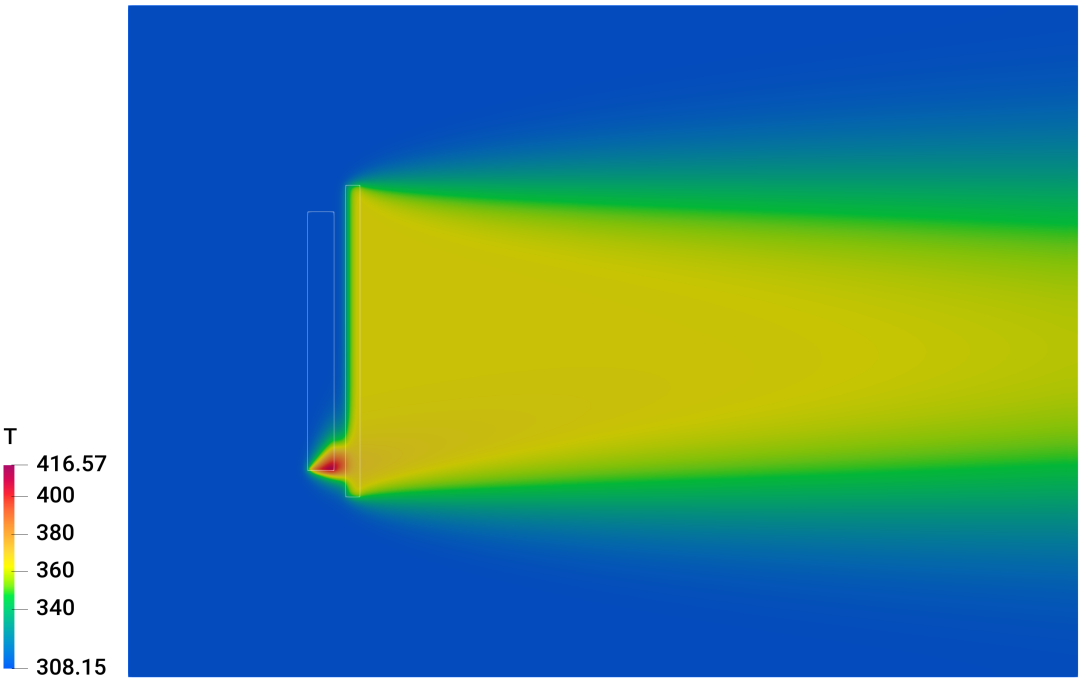

Figure 3.4.5: Simultaneous operation, XZ cross section: air temperature, sim. no. 3.

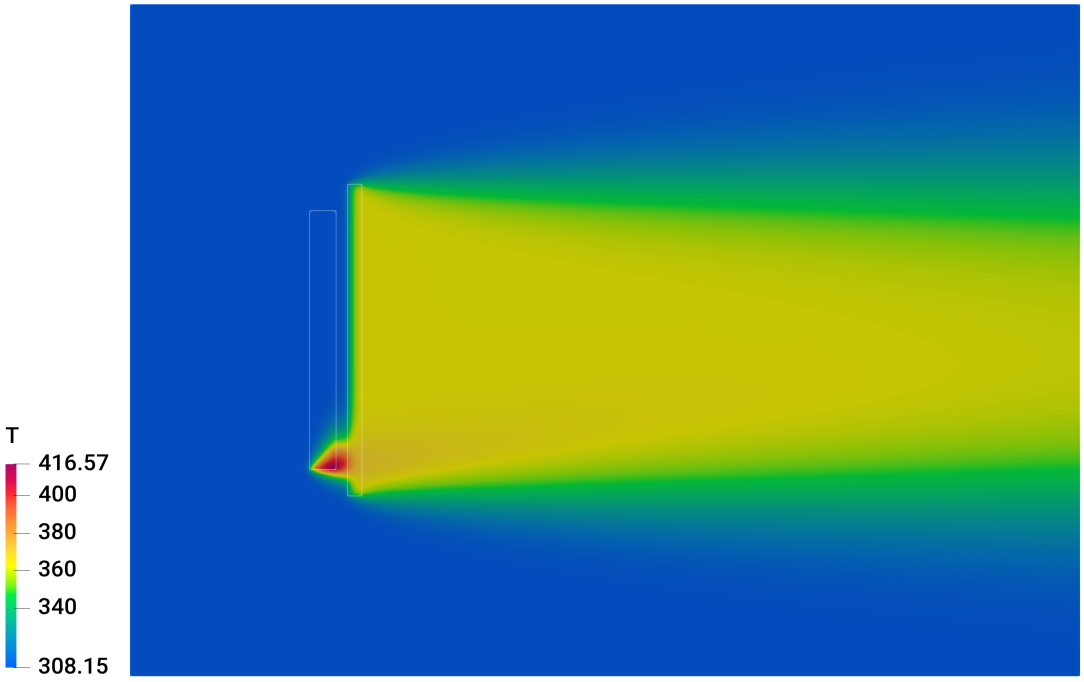

Figure 3.4.6: Simultaneous operation, XZ cross section: air temperature, sim. no. 4.

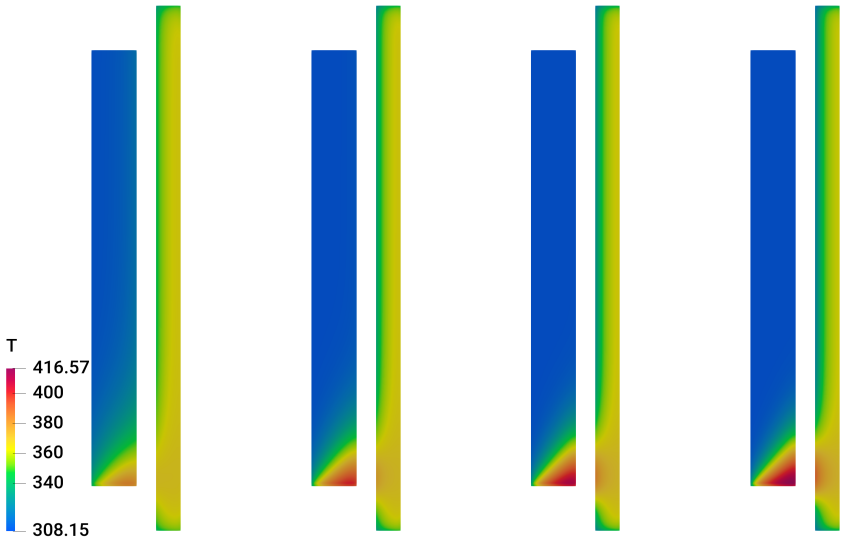

a) sim. no. 1, b) sim. no. 2, c) sim. no. 3, d) sim. no. 4.

Figure 3.4.7: Simultaneous operation, XZ cross section of intercooler and radiator: air temperature.

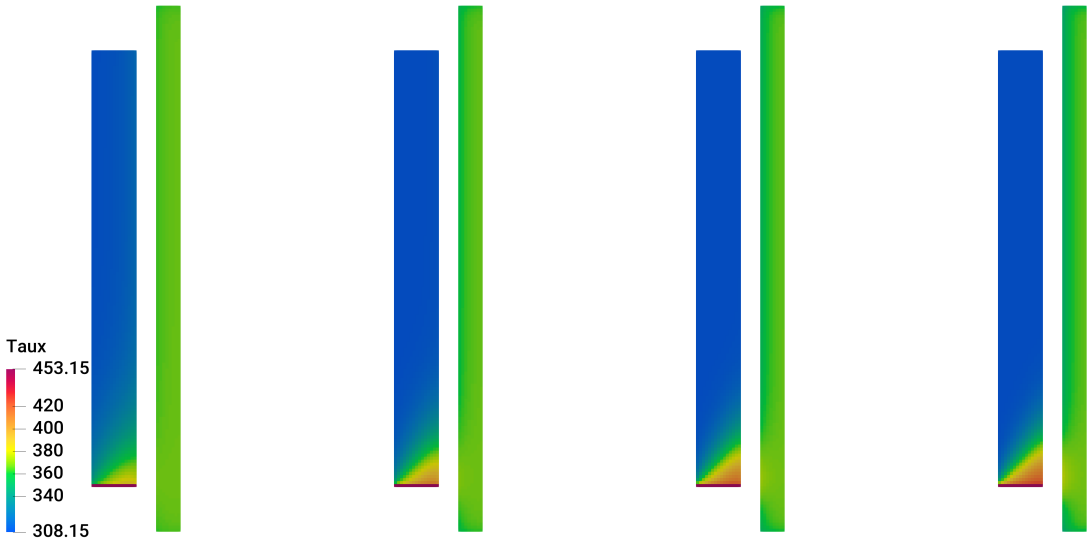

a) simulation no. 1, b) simulation no. 2, c) simulation no. 3, d) simulation no. 4.

Figure 3.4.8: Simultaneous operation, XZ cross section of intercooler and radiator: coolant temperature.

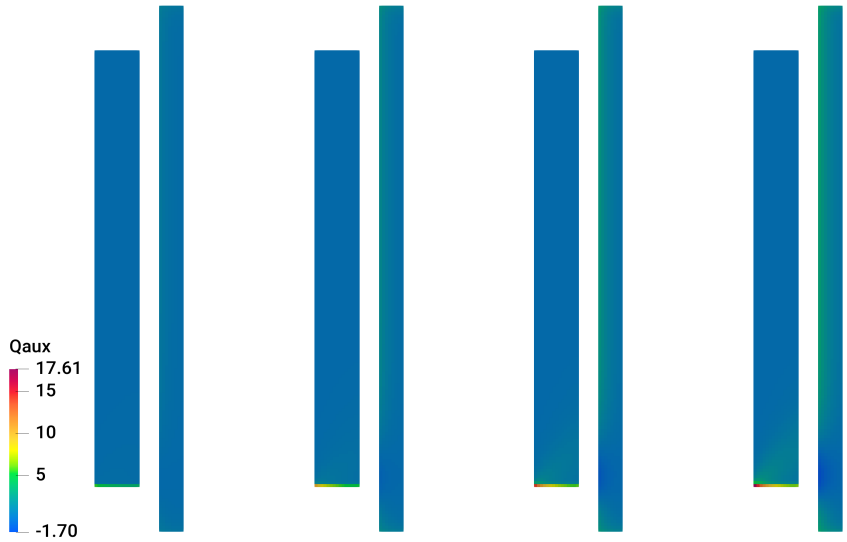

a) sim. no. 1, b) sim. no. 2, c) sim. no. 3, d) sim. no. 4.

Figure 3.4.9: Simultaneous operation, XZ cross section of intercooler and radiator: heat rejection.

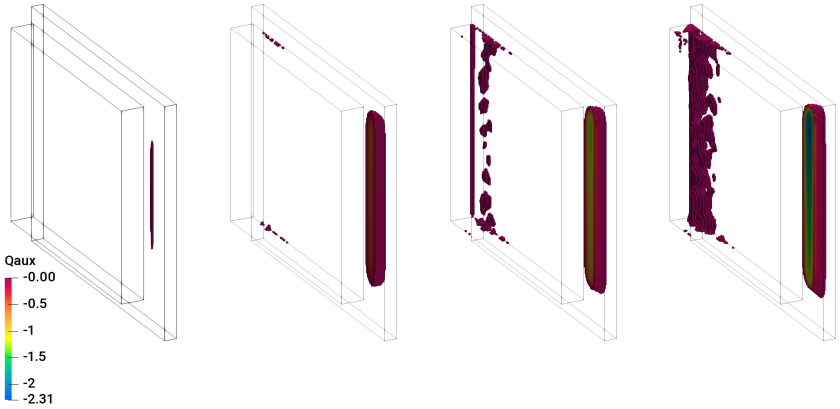

a) sim. no. 1, b) sim. no. 2, c) sim. no. 3, d) sim. no. 4.

Figure 3.4.10: Simultaneous operation, heat rejection: heating of coolants.

In Fig. 3.4.7 it can be seen that high air temperature, influenced by intercooler's inlet cools down when passing through the radiator. Due to high total heat capacity of radiator's auxiliary fluid, in Fig. 3.4.8 it cannot be seen at first glance, but Fig. 3.4.9 reveals that the part of the radiator actually heats up. This effect is seen as negative heat rejection, and Fig. 3.4.10 isolates this effect. Another effect is seen on Fig. 3.4.10, as the heat rejection from the radiator increases it heats up parts of intercooler's outlet as well.

3.5 Closure

Chapter 3 presented successful validation of the implemented Dual Stream Model. Section 1 and 2 analysed individual work of each heat exchanger. Individual analysis offered reliable results. Intercooler analysis needed explicit relaxation of the auxiliary fluid temperature due to low total heat capacity. Simultaneous work analysis performed in Section 3 provided insight in Dual Stream Model's interconnectivity between fluids, *i.e.* parts of the intercooler heated up parts of the radiator and vice versa, as seen in Fig. 3.4.10.

Chapter 4

Meshing of the Ford Otosan Truck

4.1 Overview

In this Chapter the complete geometry preparation and meshing process of the Ford Otosan truck's underhood compartment is presented. The pre-processing was performed in ANSA, a software for preparation of CAD models for CFD simulations. Preparation begins with importing the triangulated surface of the truck. Figs. 4.1.1 to 4.1.3 show a model of the Ford Otosan truck with yellow surfaces representing a wrongly oriented unit vector of triangles on that surface. Other common problems with under-defined surfaces are in the form of non-closed volume, holes in surfaces, or intersected triangles. The major drawback of a triangulated surface is the lack of complex functions for performing changes to the model in common engineering CAD software. For this reason, ANSA was chosen for the pre-processing task because it enables the user to make changes to the existing model, but limited in comparison to NURBS. One of the most automated tools for altering the surface mesh is surface wrapping. The specialty of this automated tool is good and robust solving of a complex geometry. The algorithm, called octree encoding, is based on recursive dividing of space to the smallest detail.

Simplification of the model is conducted in the form of removing unnecessary details which do not influence flow significantly, or are not in the scope of interest for thermal management (Fig. 4.1.4). For example, electrical installations and everything placed inside the cabin will be removed because the cabin will be closed for the penetration of outside air.

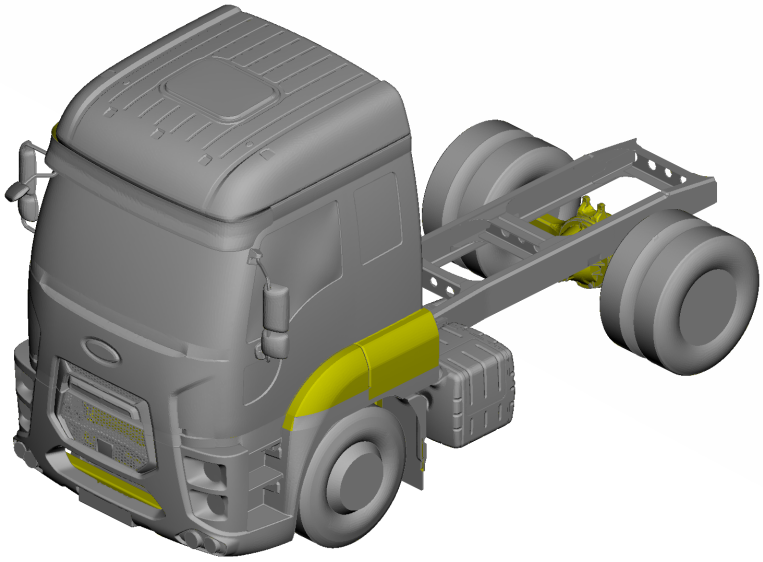

Figure 4.1.1: Ford Otosan truck model.

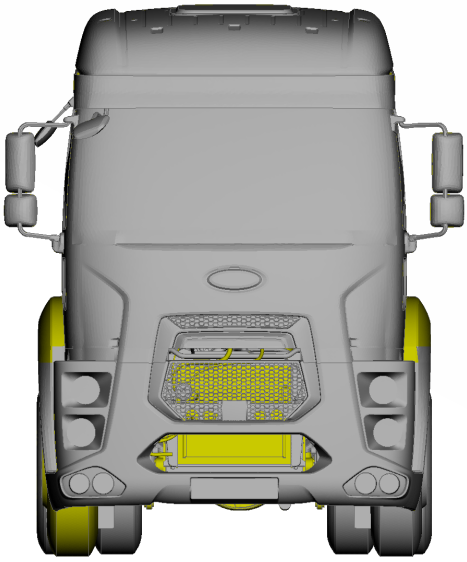

Figure 4.1.2: Ford Otosan truck model: front view.

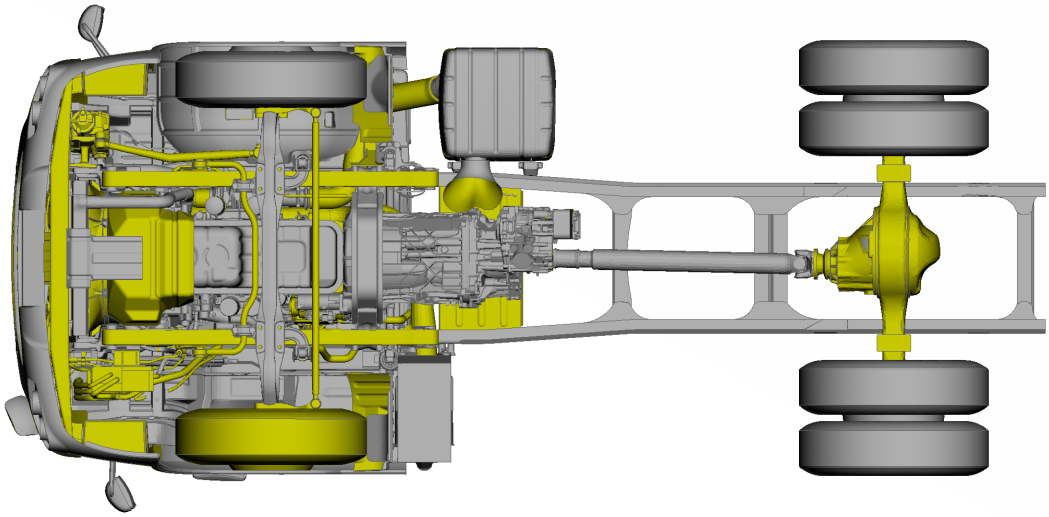

Figure 4.1.3: Ford Otosan truck model: bottom view.

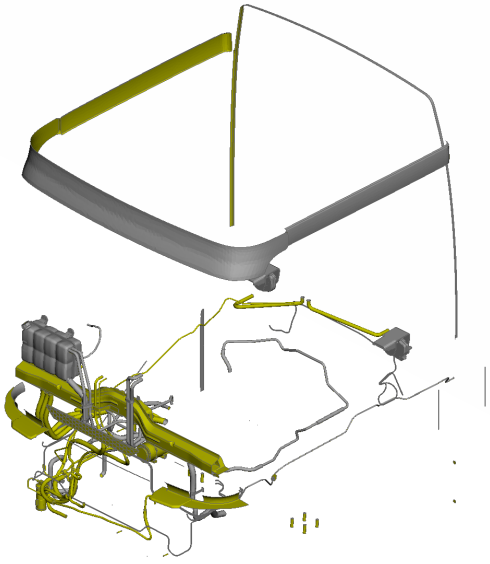

Figure 4.1.4: Ford Otosan truck model: removed parts.

4.2 Surface Mesh

A very high quality of the surface mesh is required. The most important aspects of fluid flow evolve around surfaces, where the quality of the volume mesh in the boundary region is of vital importance. This part of the geometry preparation is often the most time-consuming. The wrapping algorithm greatly reduces the engineer's need for intervention, but it still requires manual corrections. The most common problems are sharp edges, intersections, and generally low quality cells. The results of the wrapping algorithm are very high quality cells with a total size of 22 million. The downside of this algorithm is a large mesh size which cannot be afforded. In this study, reduction in mesh size was done in a manner of turning the resulting mesh into a mixed type which mostly contains quadrilaterals and just a small number of triangles. This change in the cell type of surface mesh is possible in ANSA with additional interventions after the treatment. The final surface mesh consists mostly of quadrilaterals, with a total size of 4.6 million elements.

Figs. 4.2.1 to 4.2.3 represent described process of importing original surface, wrapping and converting to quadrilaterals for obtaining the final surface mesh.

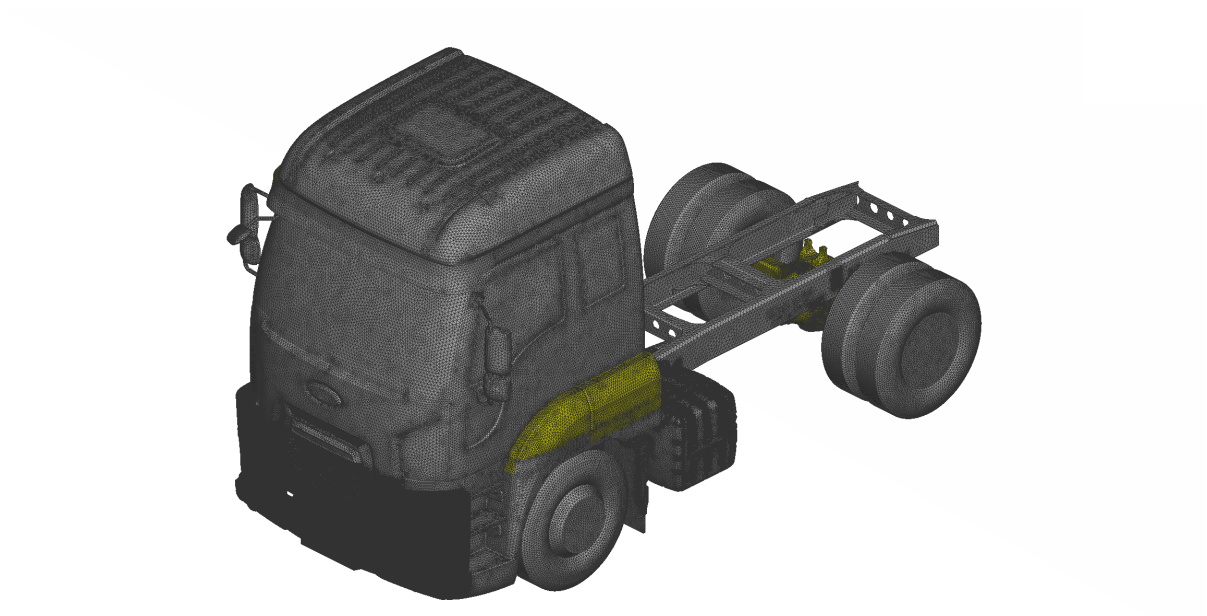

Figure 4.2.1: Ford Otosan truck: original surface mesh.

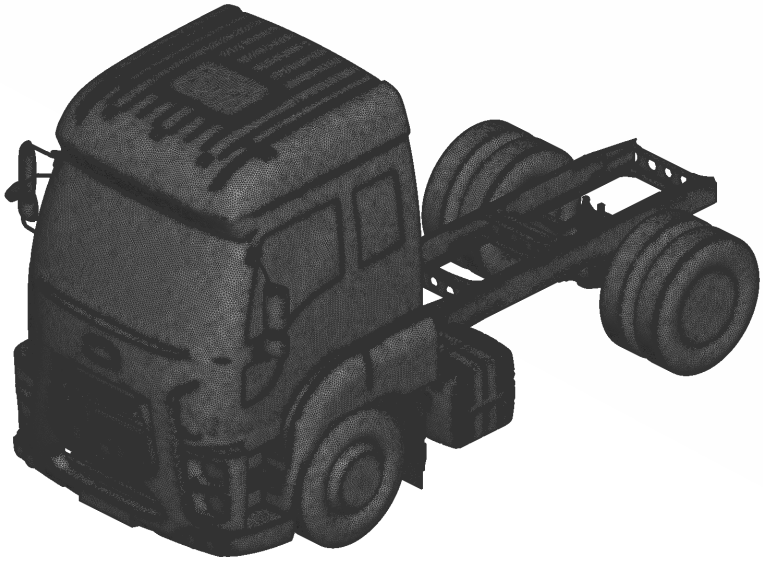

Figure 4.2.2: Ford Otosan truck: wrapping algorithm.

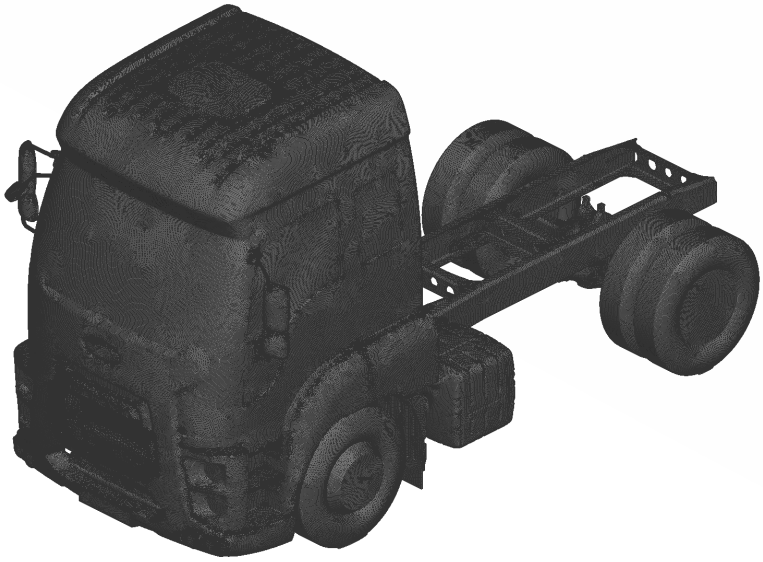

Figure 4.2.3: Ford Otosan truck: final surface mesh.

Figs. 4.2.4 to 4.2.9 are views on two details that more precisely show the process of surface converting. The wrapping results are visually the best, but the size of the mesh is too large.

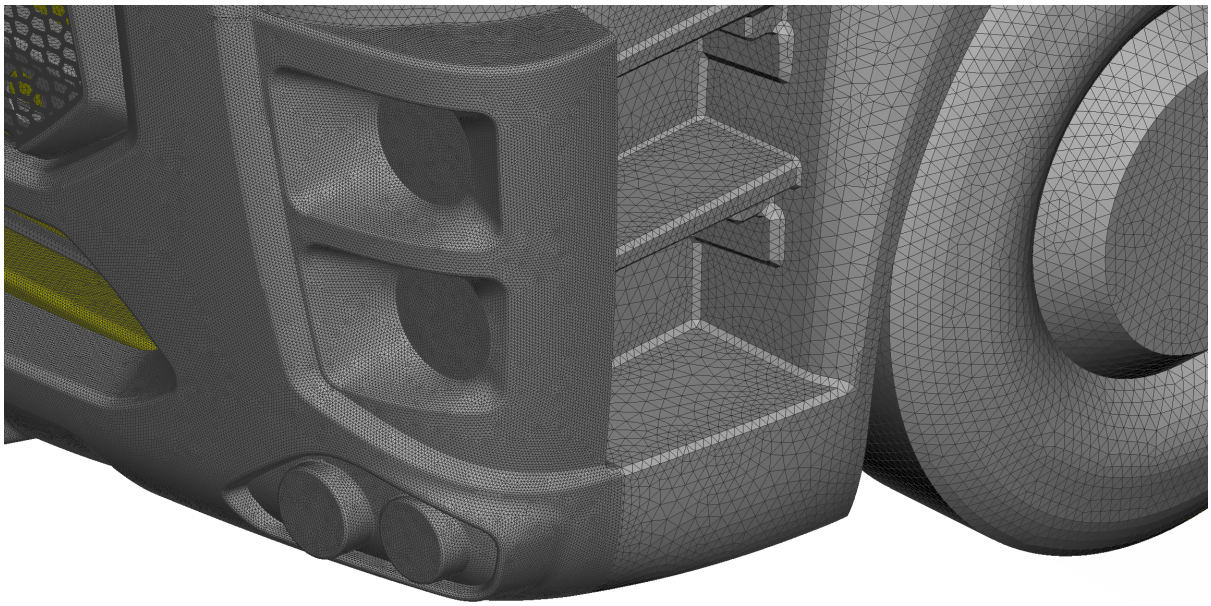

Figure 4.2.4: Ford Otosan truck, detail 1: original surface mesh

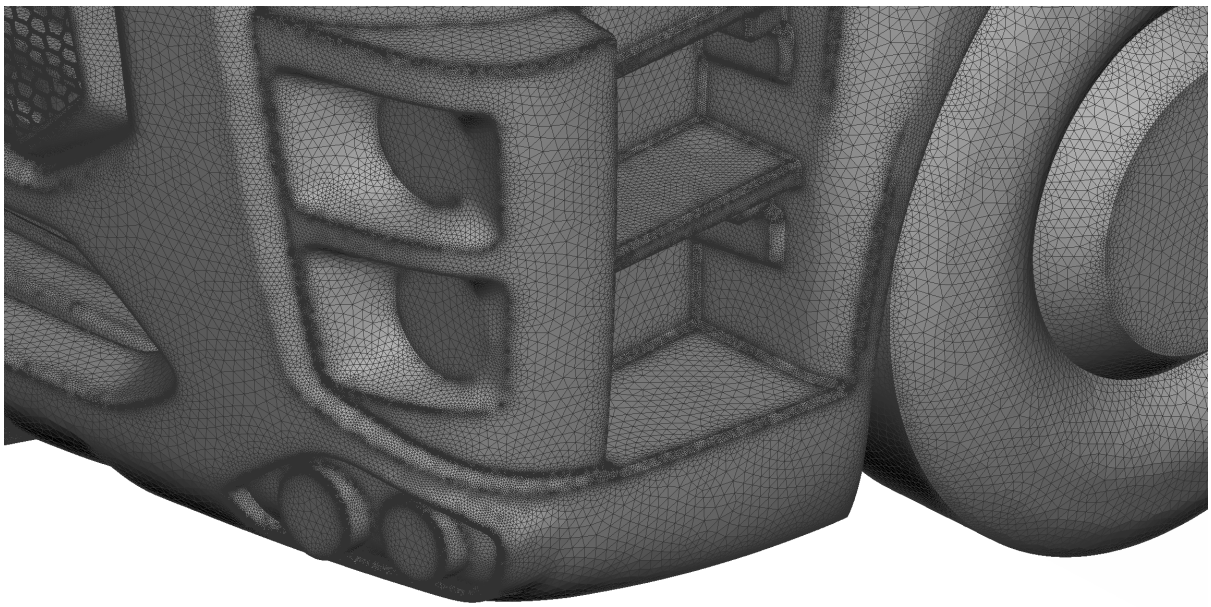

Figure 4.2.5: Ford Otosan truck, detail 1: wrapping algorithm.

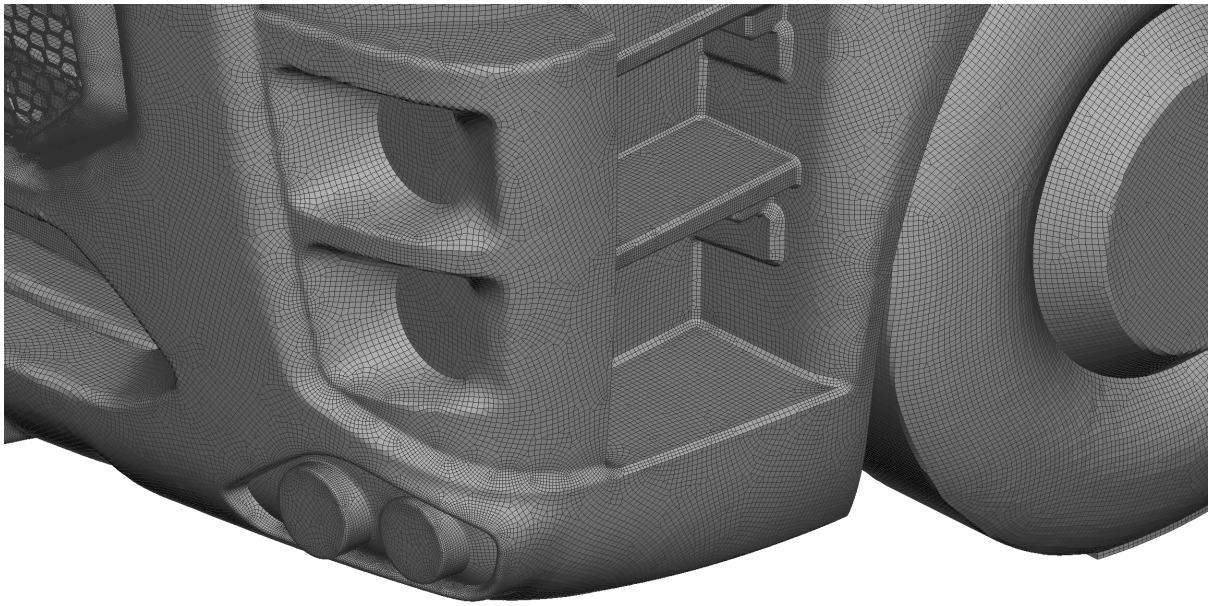

Figure 4.2.6: Ford Otosan truck, detail 1: final surface mesh.

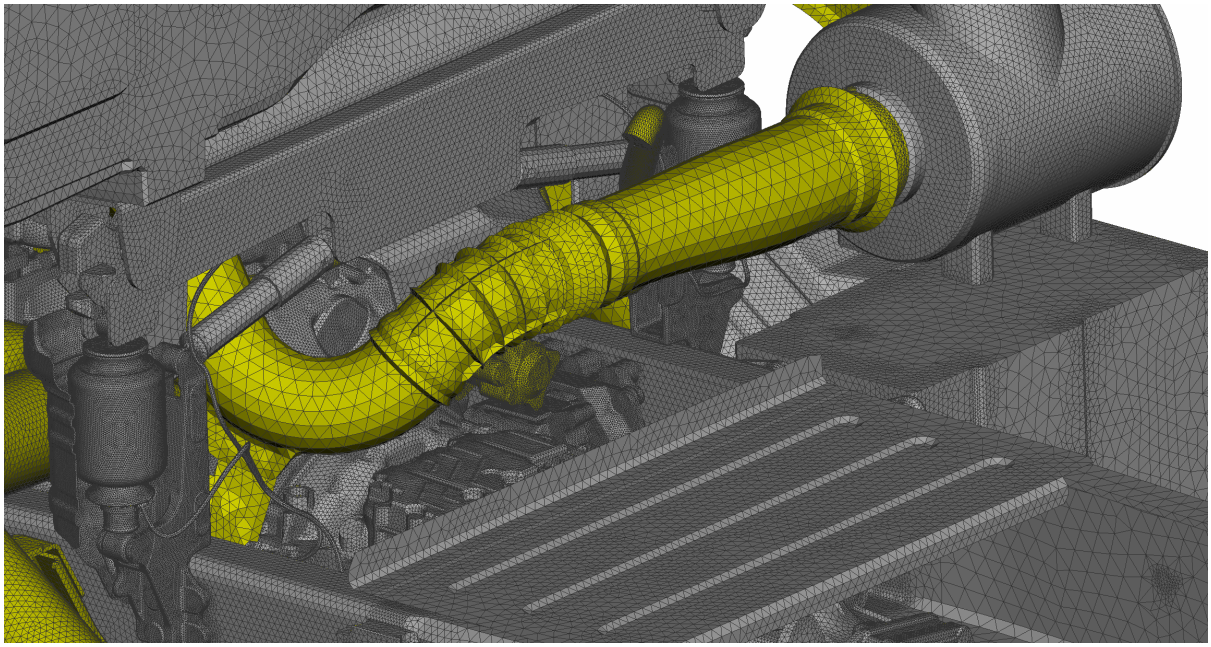

Figure 4.2.7: Ford Otosan truck, detail 2: original model.

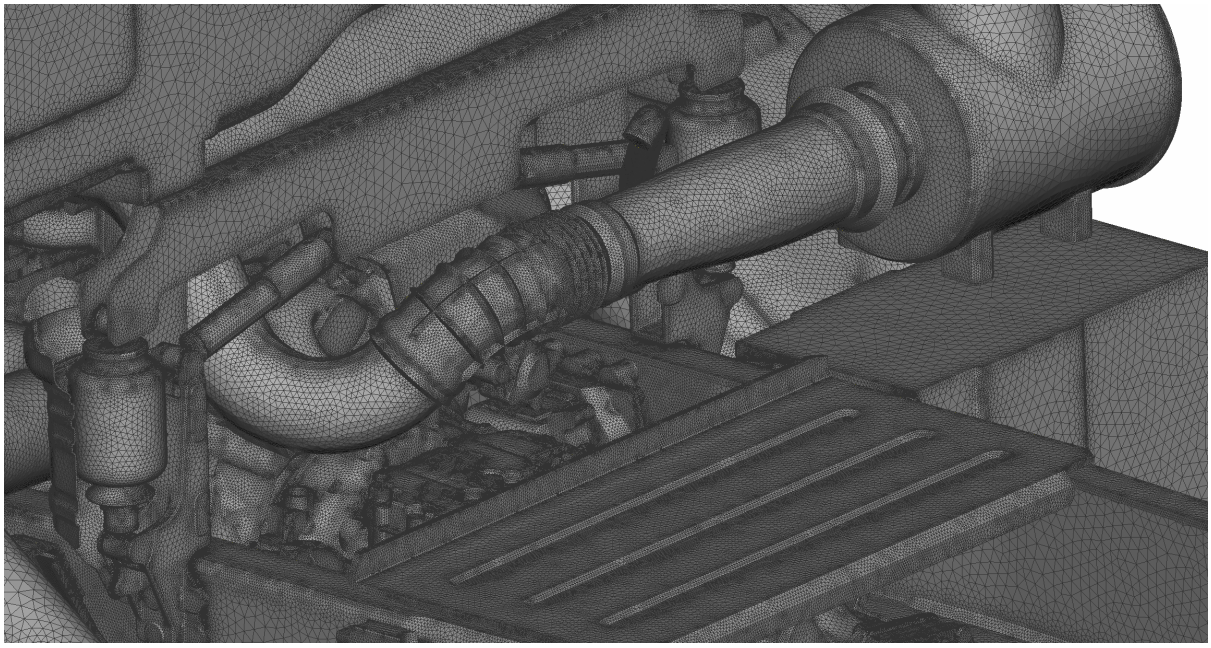

Figure 4.2.8: Ford Otosan truck, detail 2: wrapping algorithm.

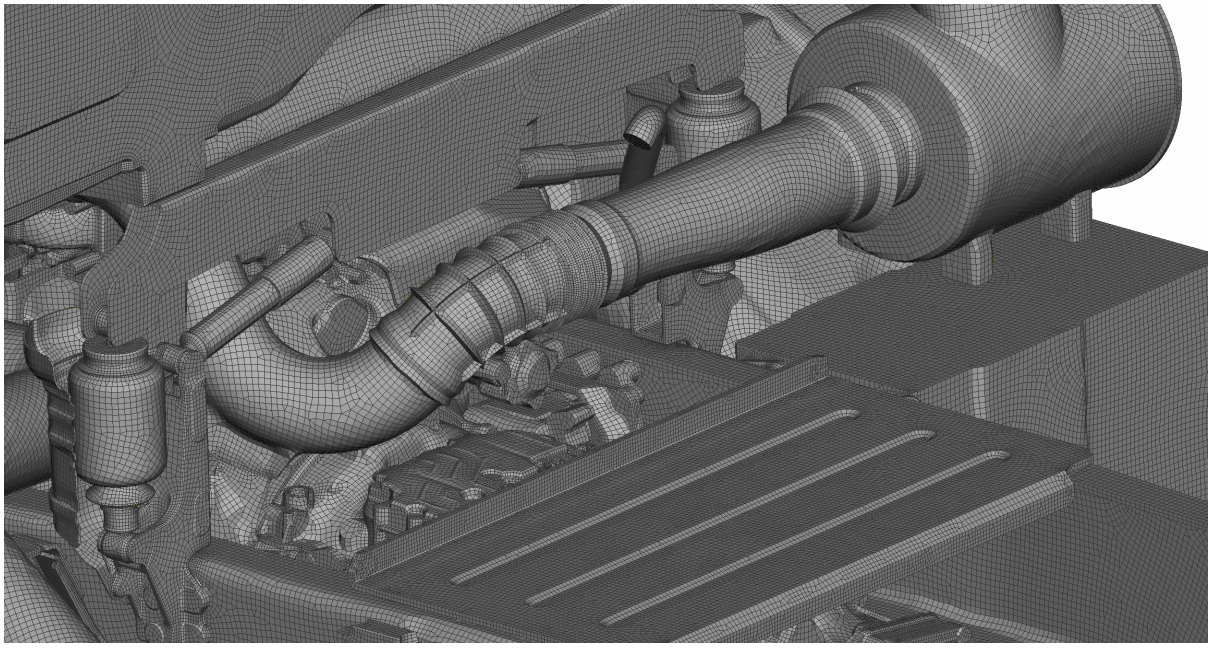

Figure 4.2.9: Ford Otosan truck, detail 2: final surface mesh.

Fig. 4.2.10 represent the final surface mesh of the underhood compartment along with the chassis and other supporting parts. The fan with its case that is mounted behind the radiator is presented in Fig. 4.2.11.

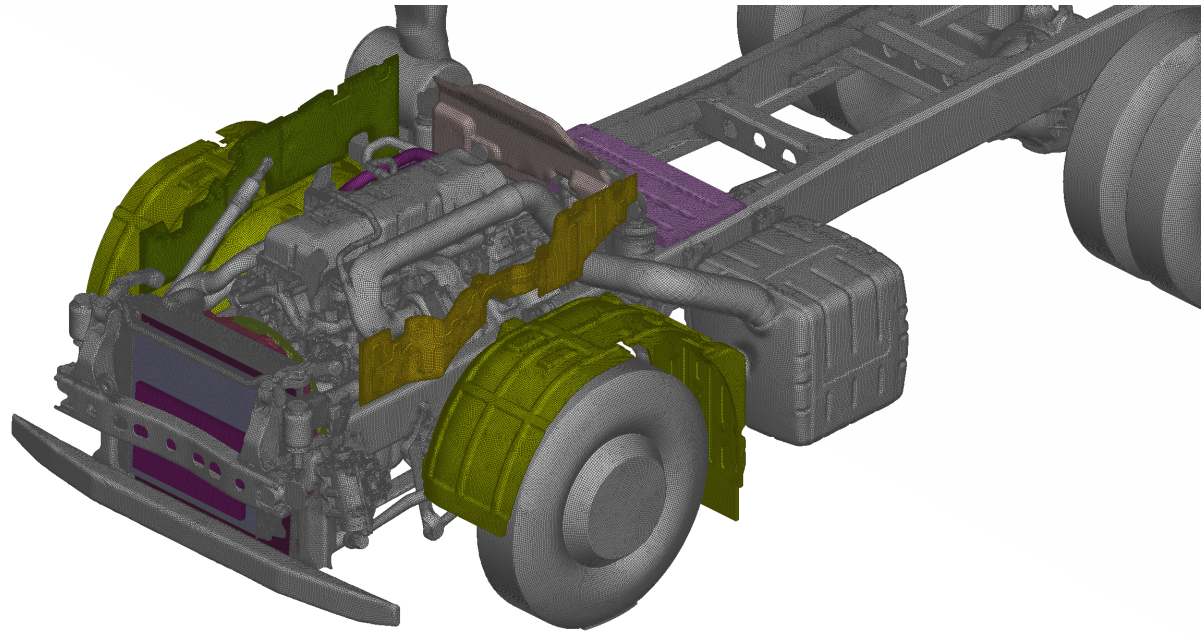

Figure 4.2.10: Ford Otosan truck, underhood: final surface mesh

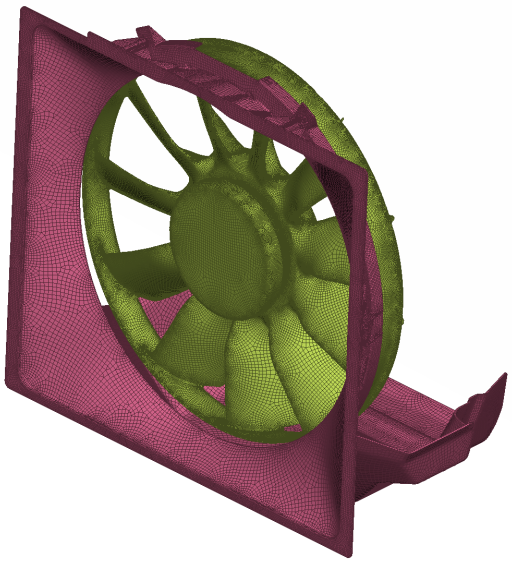

Figure 4.2.11: Ford Otosan truck, fan and its case: final surface mesh

4.3 Volume Mesh

The implemented Dual Stream model depends on a structured mesh within the exchanger region. Therefore, the best starting point in creating the volume mesh is the meshing of heat exchangers. Fig. 4.3.1 presents three structured volume meshes of the heat exchangers and the surface mesh of the fan and its case. A structured volume mesh for heat exchangers was created with the `map` function. These zones represent effective thermal zones of heat exchangers, and they are modelled as porous media. After the creation of a structured volume mesh, a boundary layer zone volume mesh was created with the extrusion of five cells with a constant growth factor of 1.2. Fig. 4.3.7 shows the problematic area where the exclusion of boundary layer cells happened due to a lower quality surface mesh at that spot. The final step was to create the main volume mesh. Because of a very complex geometry of the engine, chassis and other relevant underhood parts, the chosen cell type was tetrahedron. Downside of this decision is a larger mesh in comparison to hexahedron dominant volume meshes, but their ability to define any type of surface with high quality was considered more important. Finally, Tables 4.3.1 and 4.3.2 show two main quality criteria for the generated mesh.

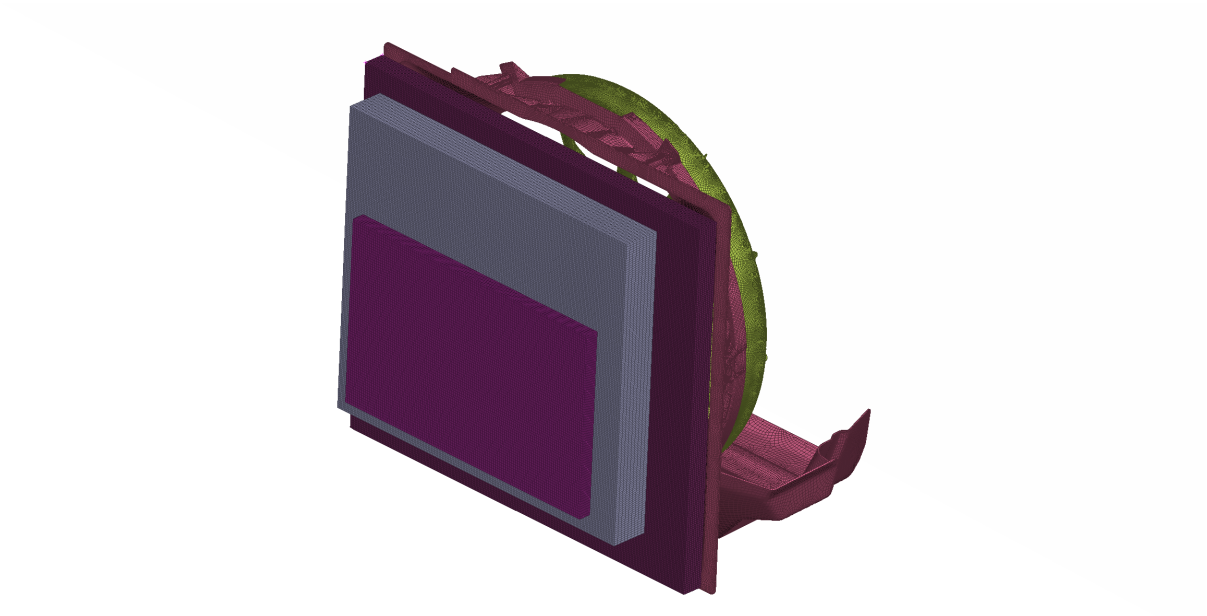

Figure 4.3.1: Ford Otosan truck, heat exchangers: structured volume mesh

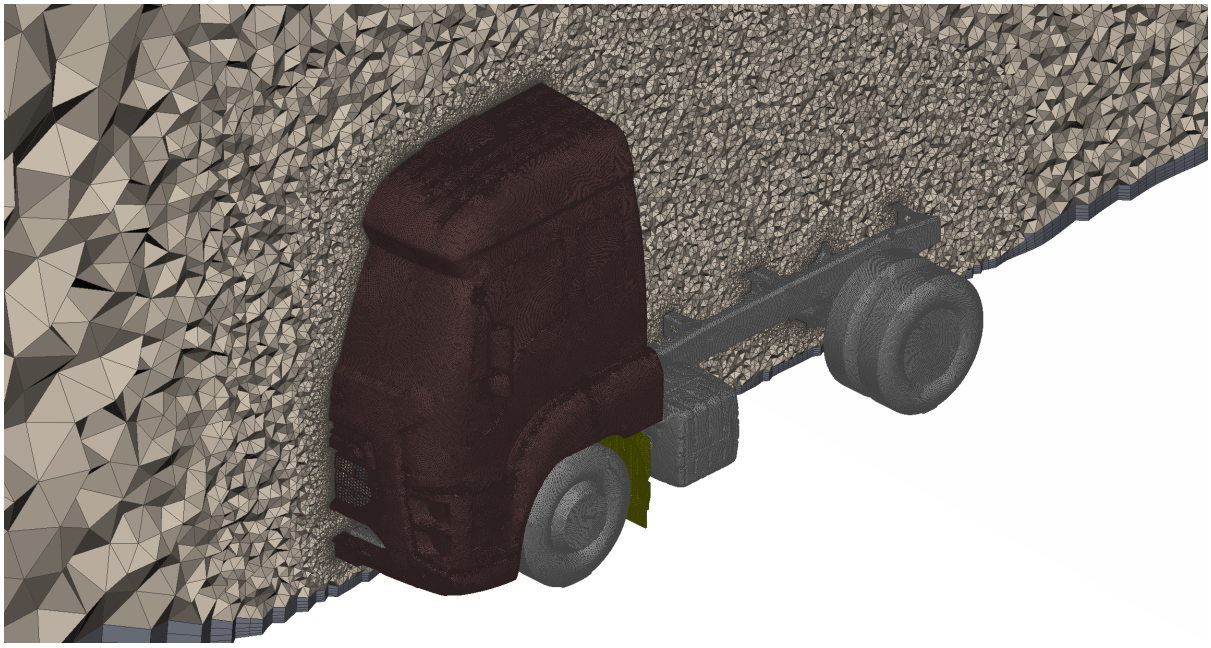

Figure 4.3.2: Ford Otosan truck: volume mesh.

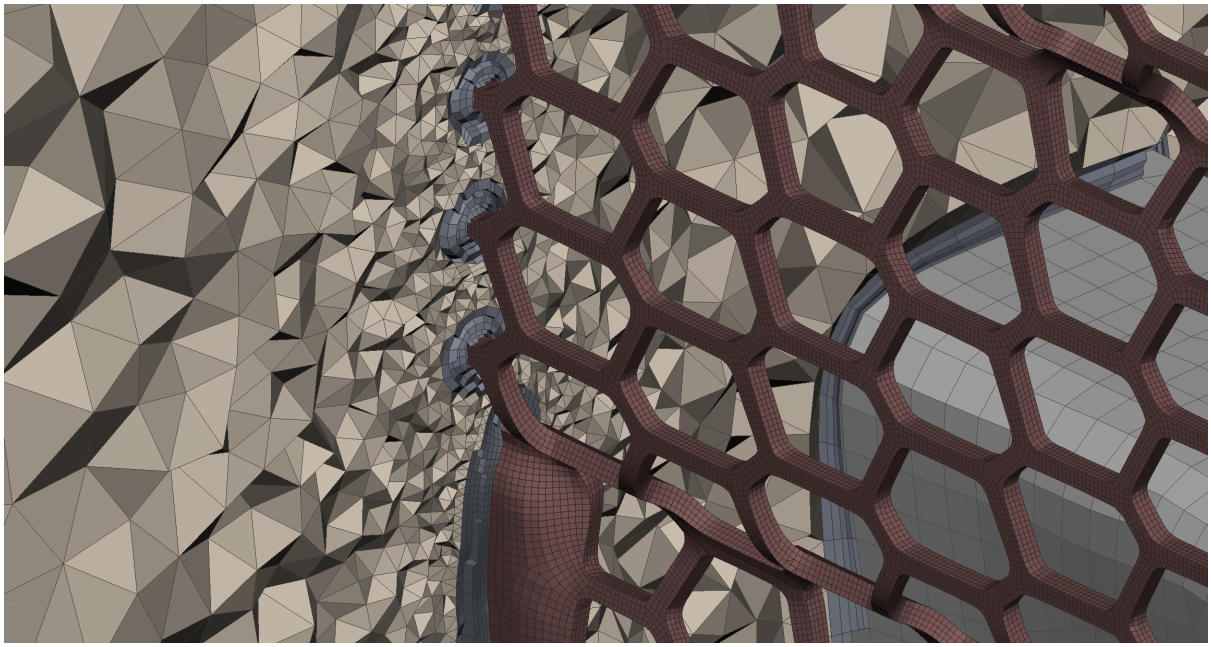

Figure 4.3.3: Ford Otosan truck, mask detail: volume mesh

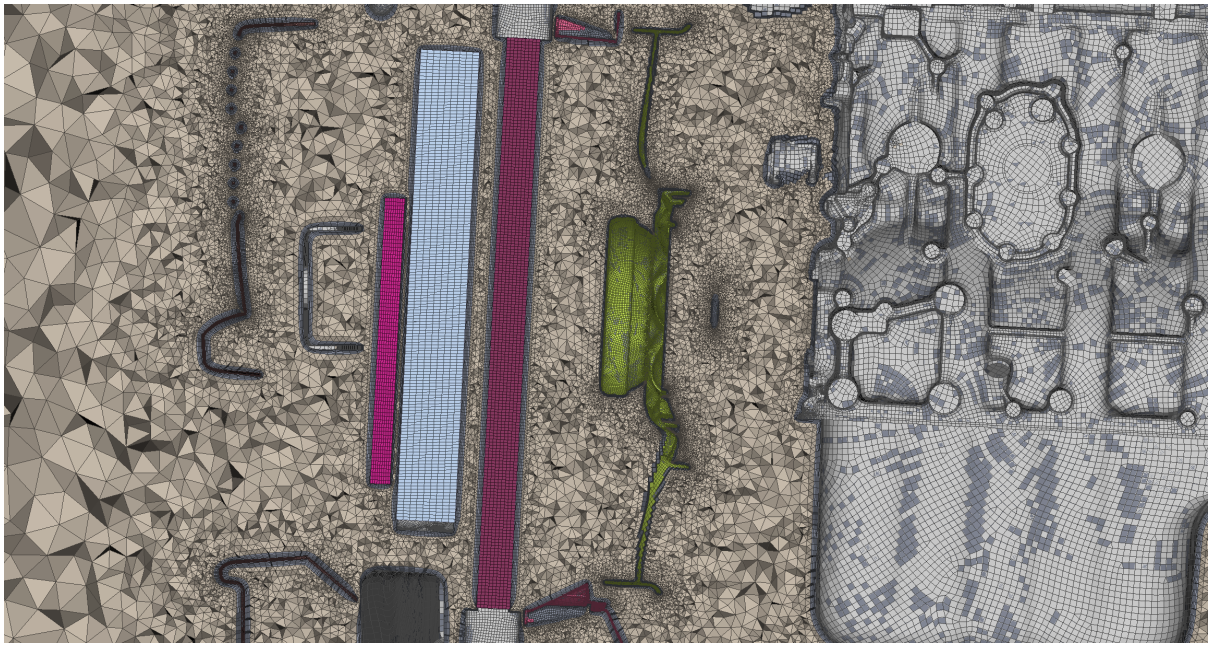

Figure 4.3.4: Ford Otosan truck, cross section detail: volume mesh

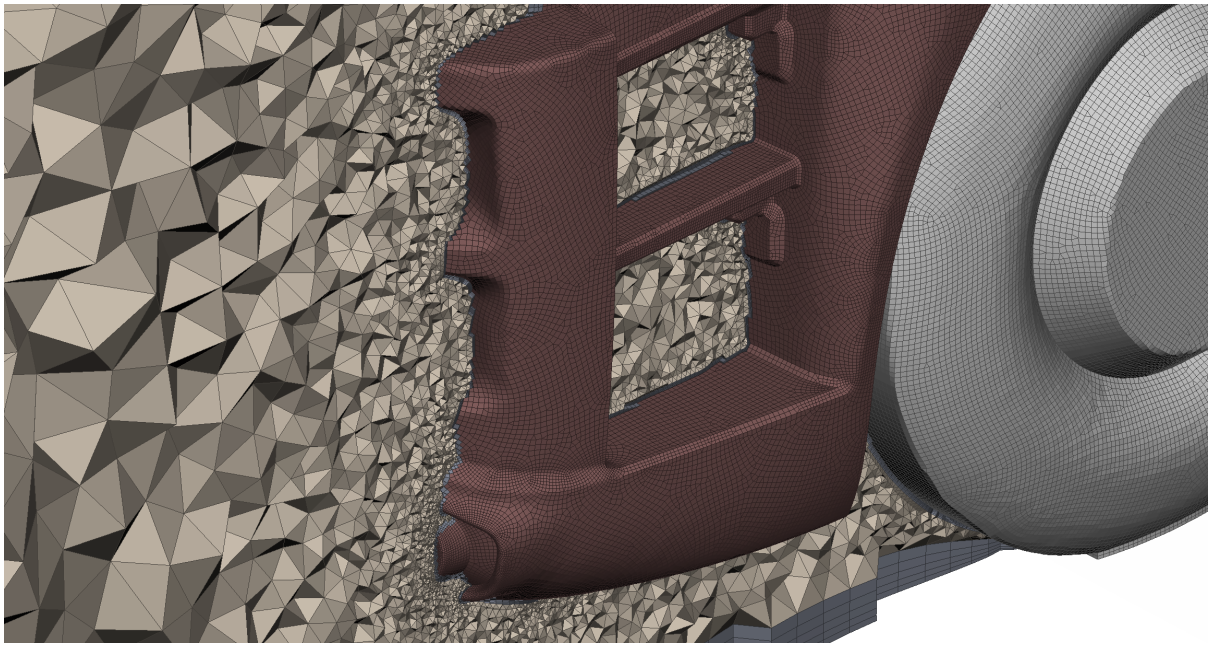

Figure 4.3.5: Ford Otosan truck, detail 1: volume mesh

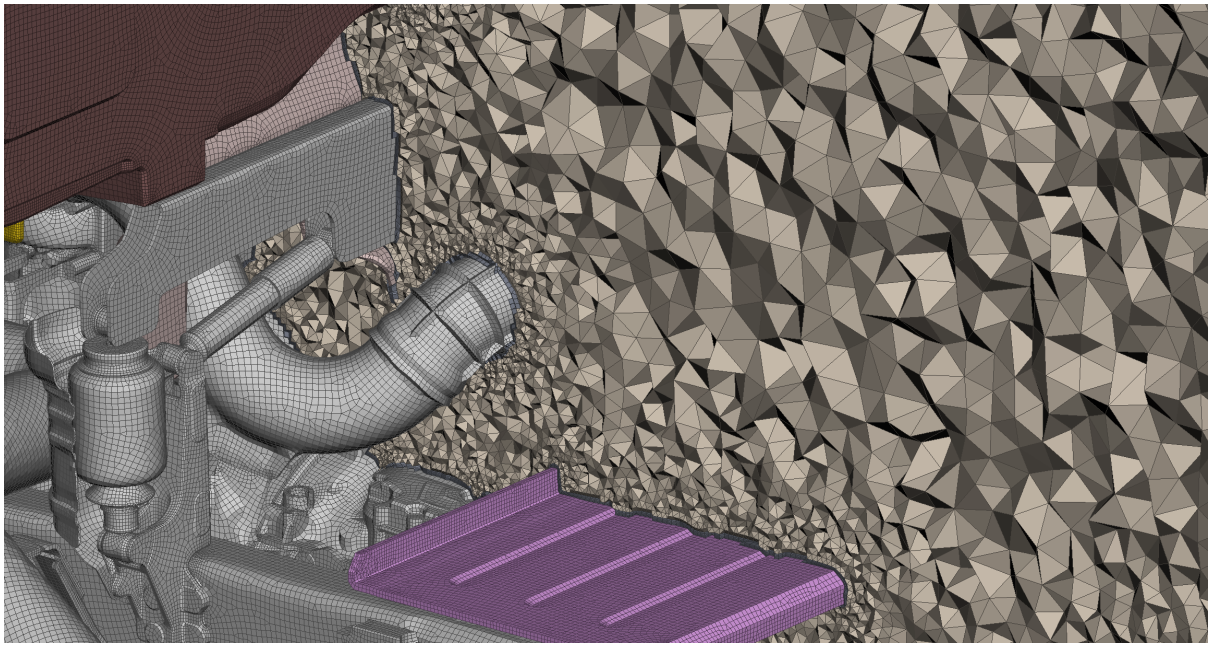

Figure 4.3.6: Ford Otosan truck, detail 2: volume mesh

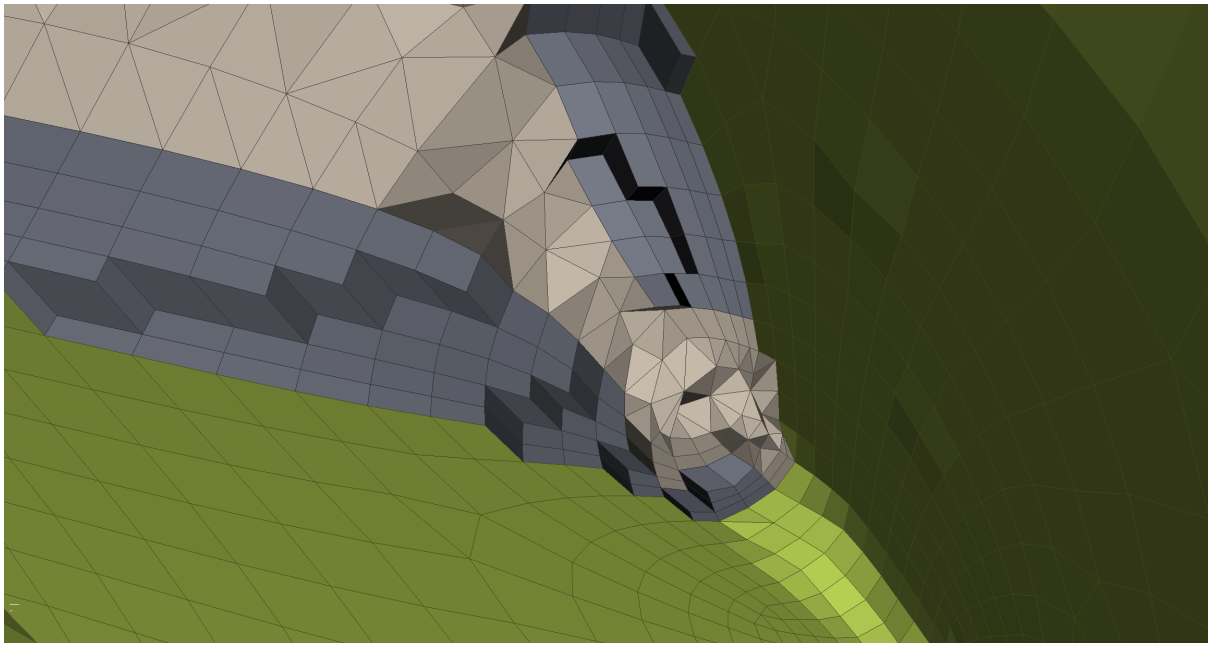

Figure 4.3.7: Ford Otosan truck, problematic are: volume mesh

Used element size boxes can be seen in Fig. 4.3.2. Main goal of this study was to investigate underhood thermal management so a coarse mesh was produced on trailing edges of the truck.

Figs. 4.3.3 to 4.3.6 are views of various parts of the truck geometry and its volume mesh.

Solid Skewness Quality SKEW FACTOR [OPENFOAM]

Solid Skewness Table						
ID of Element with min value					**MIN Value**	
4772776					3.81282e-06	
ID of Element with max value					**MAX Value**	
17760250					4.74598	
Class					**No of Elements**	**Perc(%)**
1	**From:**	-∞	**To:**	**0**	0	0
2	**From:**	**0**	**To:**	**1**	104919195	98.2173
3	**From:**	**1**	**To:**	**2**	1404874	1.31514
4	**From:**	**2**	**To:**	**3**	464335	0.434675
5	**From:**	**3**	**To:**	**4**	35028	0.0327905
6	**From:**	**4**	**To:**	**5**	86	8.05066e-05
7	**From:**	**5**	**To:**	**6**	0	0
8	**From:**	**6**	**To:**	**7**	0	0
9	**From:**	**7**	**To:**	**8**	0	0
10	**From:**	**8**	**To:**	**9**	0	0
11	**From:**	**9**	**To:**	**10**	0	0
12	**From:**	**10**	**To:**	**12**	0	0
13	**From:**	**12**	**To:**	**14**	0	0
14	**From:**	**14**	**To:**	**16**	0	0
15	**From:**	**16**	**To:**	**18**	0	0
16	**From:**	**18**	**To:**	**50**	0	0
17	**From:**	**50**	**To:**	+∞	0	0
Out of any class range					0	0
TOTAL					106823518	

Table 4.3.1: Ford Otosan truck: skewness quality of volume mesh.

Solid Non Orthogonality Quality NON ORTHOGONALITY [OPENFOAM]

Solid Non Orthogonality Table						
ID of Element with min value					MIN Value	
4659964					0.0253097	
ID of Element with max value					MAX Value	
27261791					79.053	
Class					No of Elements	Perc(%)
1	From:	-∞	To:	0	0	0
2	From:	0	To:	5	1278882	1.19719
3	From:	5	To:	10	2458535	2.30149
4	From:	10	To:	15	9806971	9.18054
5	From:	15	To:	20	21574087	20.196
6	From:	20	To:	25	24214933	22.6682
7	From:	25	To:	30	19914780	18.6427
8	From:	30	To:	35	12520676	11.7209
9	From:	35	To:	40	6520974	6.10444
10	From:	40	To:	45	3560375	3.33295
11	From:	45	To:	50	2211243	2.07
12	From:	50	To:	55	1401101	1.3116
13	From:	55	To:	60	897355	0.840035
14	From:	60	To:	65	322106	0.301531
15	From:	65	To:	70	141276	0.132252
16	From:	70	To:	75	175	0.000163822
17	From:	75	To:	80	49	4.587e-05
18	From:	80	To:	85	0	0
19	From:	85	To:	90	0	0
20	From:	90	To:	+∞	0	0
Out of any class range					0	0
TOTAL					106823518	

Table 4.3.2: Ford Otosan truck: non orthogonal quality of volume mesh.

Chapter 5

Result of Thermal Management

In Chapter 3, validation was performed on the newly implemented Dual Stream heat exchanger model. The incompressible flow was considered due to velocities being lower than 0.3 Mach. Another assumption was made to neglect buoyant forces, that is, to neglect changes in air density. The reason behind the last assumption is because of high advecting forces near heat exchanger zones due to a fan. This gives the opportunity to decouple the momentum equation and energy equation. Results were made in a manner of two simulations. In both simulations, the chosen turbulence model was the kOmegaSST by Menter [13]. The first simulation was carried using a coupled incompressible solver `MRFPorousFoam`. The Heat exchanger zones were modelled as porous zones with a linear pressure drop, while the fan is modelled as MRF zone. The second simulation was carried out with incompressible energy equation in a form of temperature equation with modelling of source terms for heat exchangers. The focus in this study is not about resolving aerodynamic properties of the truck, but to investigate heat exchanger influence on the surrounding air and surfaces of underhood parts. With that said, thermal radiation is not solved, and only advective heat transfer is considered. Because of the lack of information regarding surface temperatures, and to achieve only the heat exchanger influence on surface temperatures, zero gradient boundary condition for temperature equation was applied on all walls.

5.1 Simulation Settings and Solving

In the current chapter, the parameters required for conducting simulations are presented in the form of tables resembling OpenFOAM dictionaries. Heat exchanger parameters and thermophysical data were selected from Chapter 3.

ddtSchemes	
default	steadyState
gradSchemes	
default	cellLimited leastSquares 1
divSchemes	
default	none
div(phi,U)	Gauss linearUpwind grad(U)
div(phi,T)	Gauss vanLeerDC
div(phi,k)	Gauss upwind
div(phi,omega)	Gauss upwind
div((nuEff*dev(T(grad(U)))))	Gauss linear
laplacianSchemes	
default	Gauss linear limited 0.5
laplacian(rAU,p)	Gauss midPoint corrected
interpolationSchemes	
default	linear
interpolate(grad(p))	midPoint

Table 5.1.1: Discretization schemes.

Figs. 5.1.1 and 5.1.2 show the convergence history. Both simulations show stable convergence while the energy equation required more iterations to converge, but it was significantly faster than the cold flow simulation.

In Fig. 5.1.3 the heat rejection of each individual exchanger can be observed through iterations. While in Chapter 3 under-relaxation was required only for the intercooler, in this case both exchangers required it. Condenser has a small part of total heat rejection and thus no oscialtions were observed at the start of the simulation.

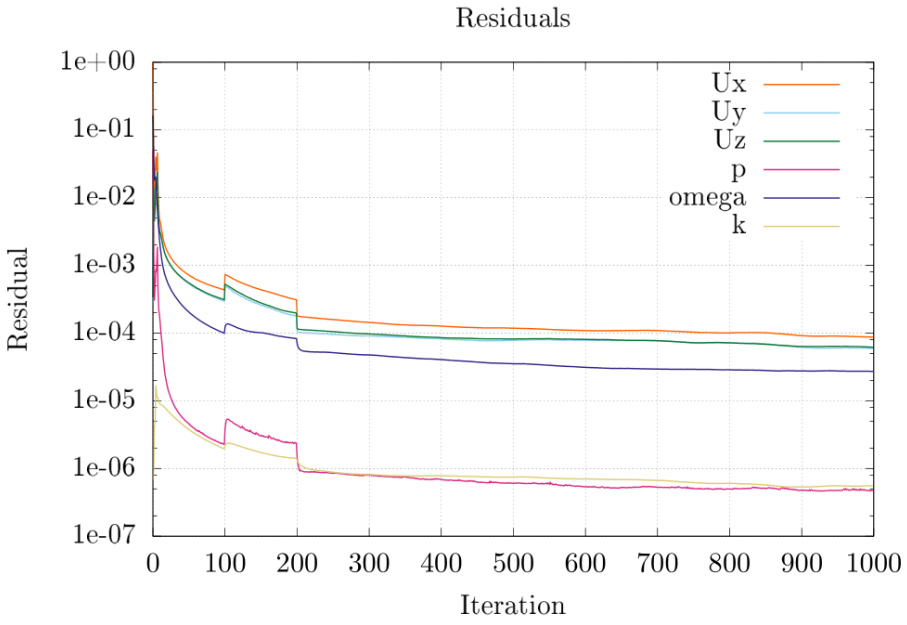

Figure 5.1.1: Cold flow residuals.

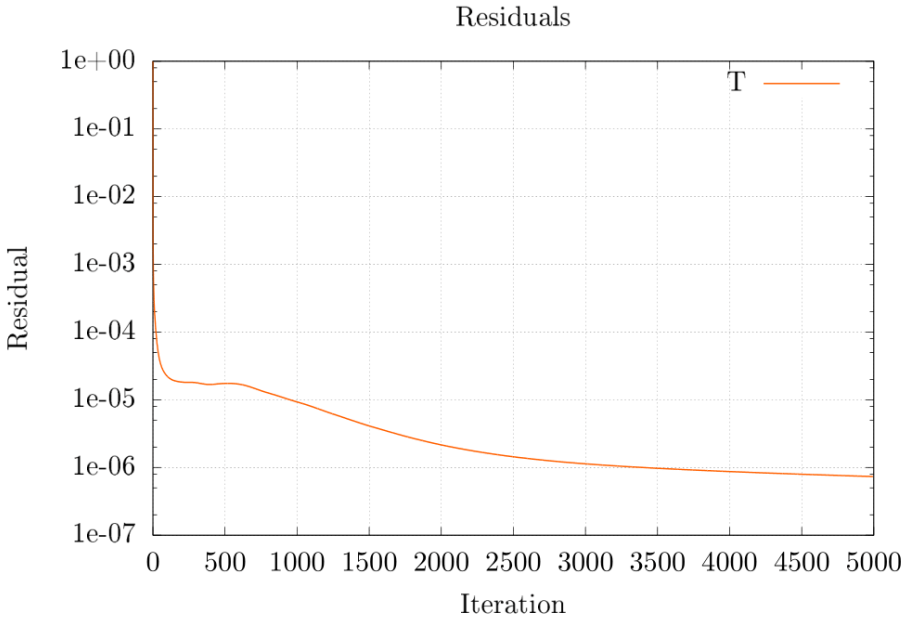

Figure 5.1.2: Temperature residual.

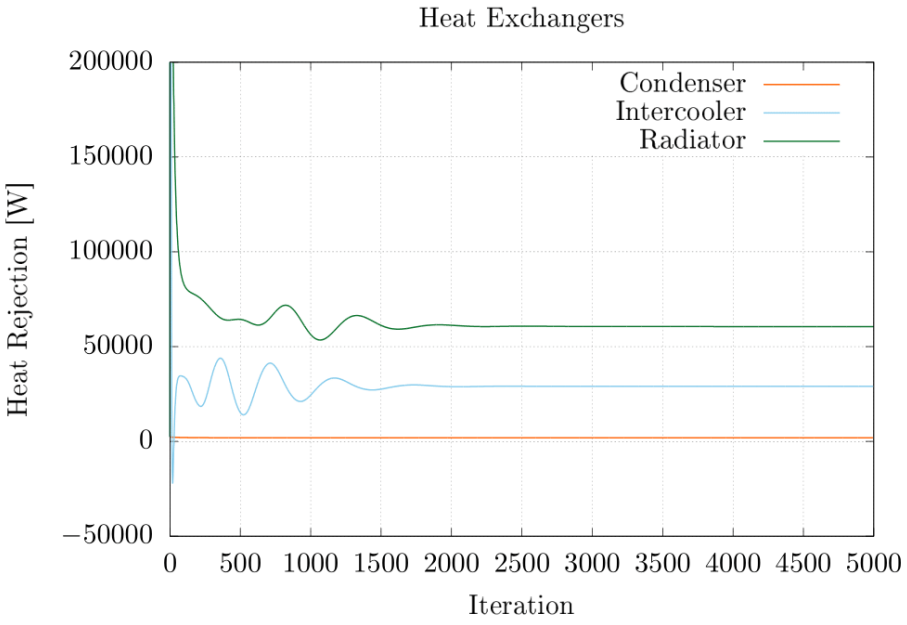

Figure 5.1.3: Heat rejection iterations.

fan		
origin	[0 1 0 0 0 0 0]	(2.34593 0 1.095678)
axis	[0 0 0 0 0 0 0]	(0.998632 0 -0.05229)
omega	[0 0 -1 0 0 0 0]	20.94395102
Radiator | Intercooler | Condenser		
Coordinate System		
e1		(0.998632 0 -0.05229)
e2		(0 -1 0)
Darcy		
d	[0 -2 0 0 0 0 0]	(5e7 -1000 -1000)
f	[0 -1 0 0 0 0 0]	(0 0 0)

Table 5.1.2: MRF zone and porous zones parameters.

Patch	U	p	k	omega	T
inlet	fixedValue value uniform (20 0 0)	zeroGradient	fixedValue value uniform 0.24	fixedValue value uniform 1.78	fixedValue value uniform 318.15
outlet	inletOutlet inletValue uniform (0 0 0) value uniform (20 0 0)	fixedValue value uniform 0	zeroGradient	zeroGradient	zeroGradient
road	fixedValue value uniform (20 0 0)	zeroGradient	kqRWallFunction value uniform 0.24	omegaWallFunction value uniform 1.78	zeroGradient
slips	slip value uniform (20 0 0)	slip value uniform 0	slip value uniform 0.24	slip value uniform 1.78	slip value uniform 318.15
truck	fixedValue value uniform (0 0 0)	zeroGradient	kqRWallFunction value uniform 0.24	omegaWallFunction value uniform 1.78	zeroGradient

Table 5.1.3: Boundary conditions.

Radiator		
Maux	[1 0 -1 0 0 0 0]	6
Taux	[0 0 0 1 0 0 0]	368.15
caux	[0 2 -2 -1 0 0 0]	3660
ϵ	[0 0 0 0 0 0 0]	0.91
Intercooler		
Maux	[1 0 -1 0 0 0 0]	0.2
Taux	[0 0 0 1 0 0 0]	453.15
caux	[0 2 -2 -1 0 0 0]	1009
ϵ	[0 0 0 0 0 0 0]	0.89
Condenser		
Maux	[1 0 -1 0 0 0 0]	0.16
Taux	[0 0 0 1 0 0 0]	333.15
caux	[0 2 -2 -1 0 0 0]	3141
ϵ	[0 0 0 0 0 0 0]	0.02

Table 5.1.4: Heat exchanger parameters.

5.2 Results

Previous section introduced the parameters used in the simulations. Results are given in a form of figures. The heat rejection values per heat exchanger are as follows:

- Radiator's heat rejection, $Q_{\text{aux,total}} = 60559.40$ W,
- Intercooler's heat rejection, $Q_{\text{aux,total}} = 29041.42$ W,
- Condenser's heat rejection, $Q_{\text{aux,total}} = 1885.12$ W.

Figs. 5.2.1 to 5.2.10 present the cold flow simulation results, while Figs. 5.2.11 to 5.2.16 present the energy simulation results.

In Figs. 5.2.1 and 5.2.2 local acceleration of fluid is seen below the intercooler, possibly influencing the radiator's performance.

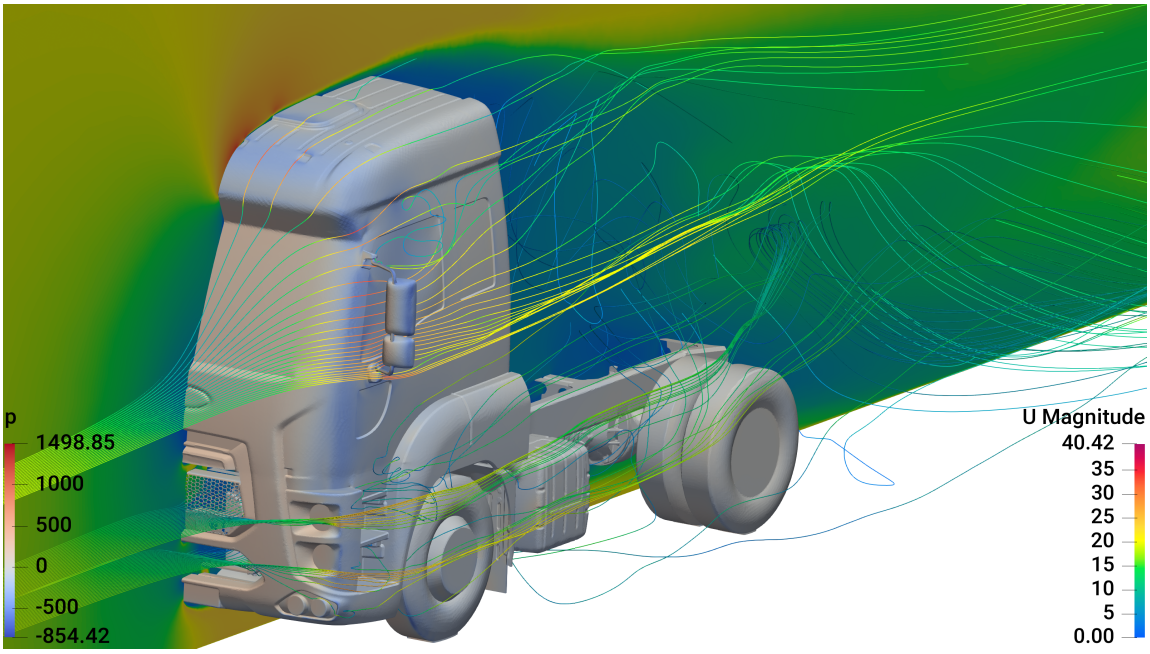

Figure 5.2.1: Ford Otosan truck cold flow: aerodynamics.

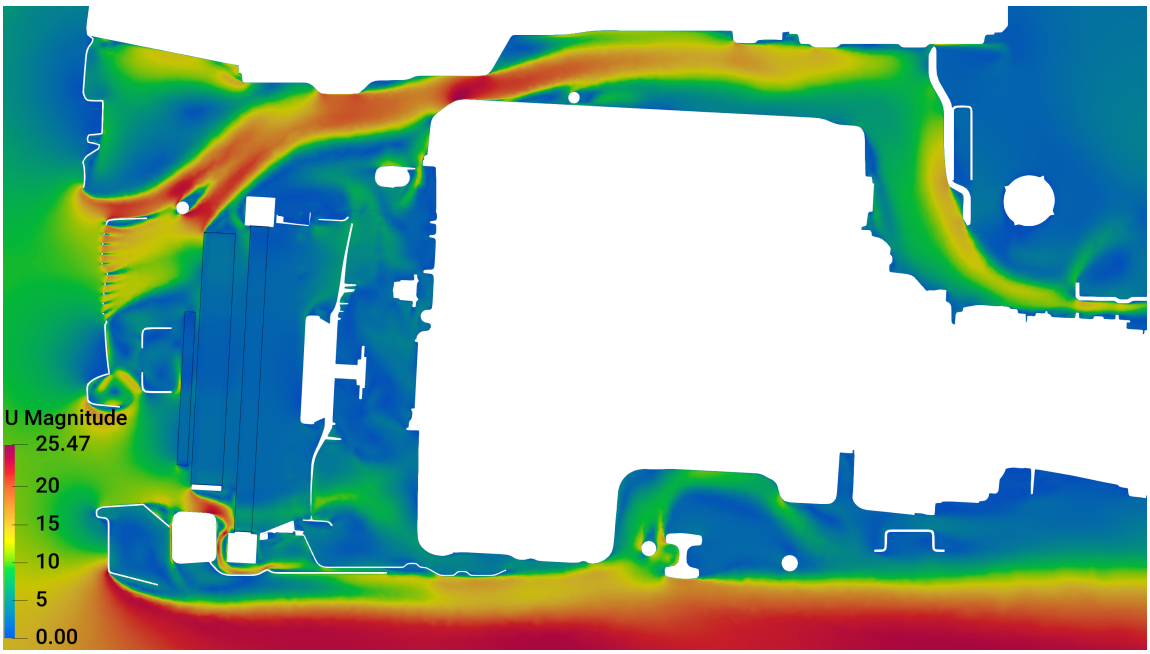

Figure 5.2.2: Ford Otosan truck cold flow, cross section: velocity magnitude.

Largest pressure drop can be seen on intercooler in Fig. 5.2.3. Fig. 5.2.4 reveal local turbulence below the intercooler and in front of the condeser.

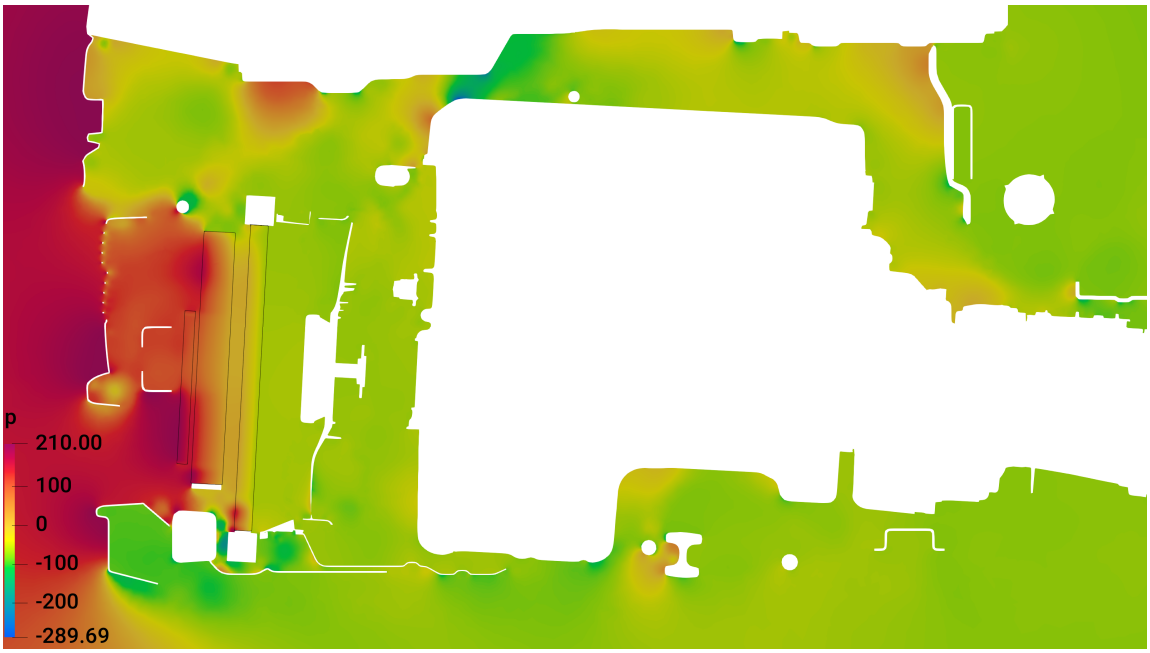

Figure 5.2.3: Ford Otosan truck cold flow, cross section: pressure.

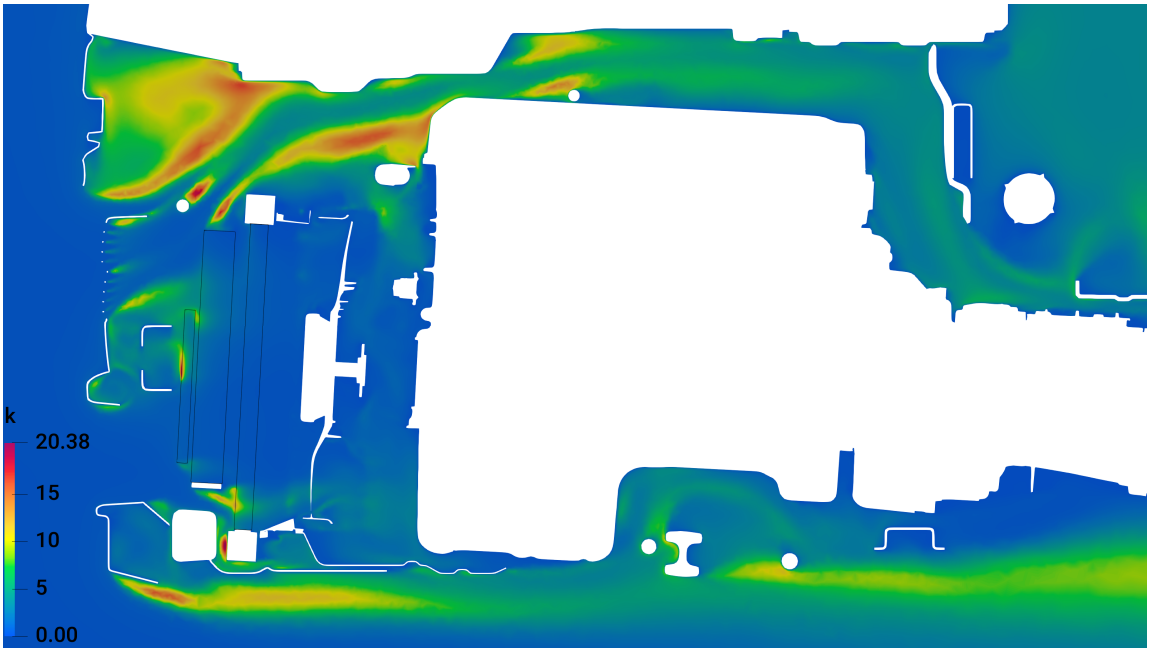

Figure 5.2.4: Ford Otosan truck cold flow, cross section: turbulent kinetic energy.

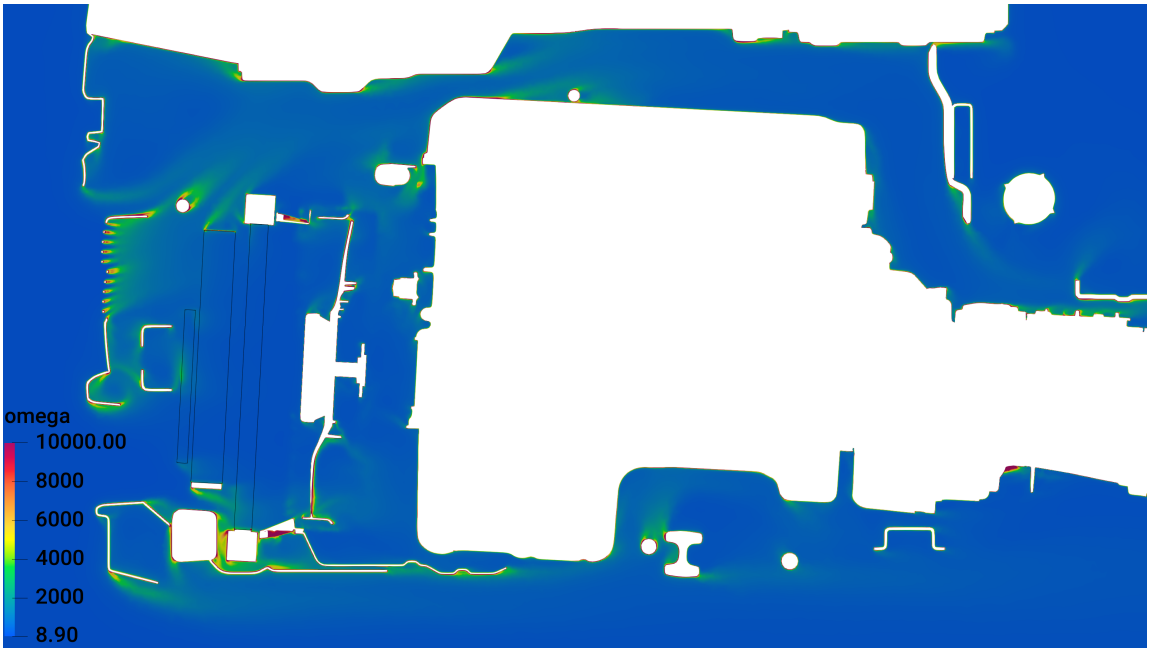

Figure 5.2.5: Ford Otosan truck cold flow, cross section: specific turb. dissipation rate.

From Fig. 5.2.6 the axial component of velocity on streamlines can be seen. Small vortex above the intercooler can possibly increase the heating of compressed air near the outlet, as seen in Fig. 3.4.10

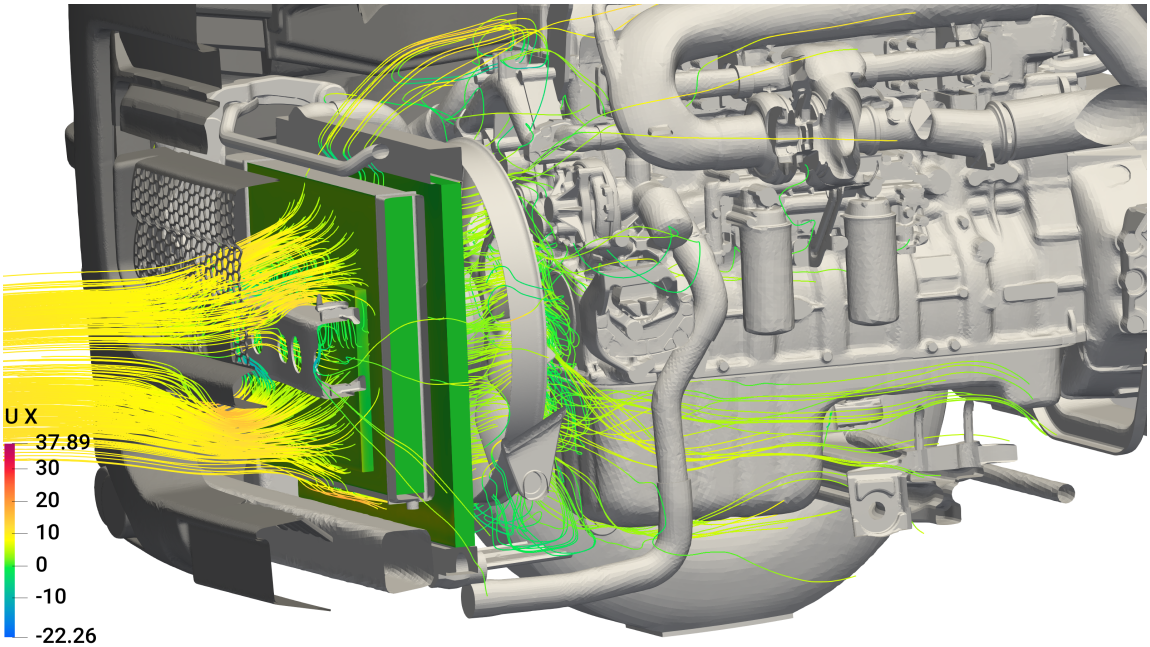

Figure 5.2.6: Ford Otosan truck cold flow, underhood streamlines: axial velocity.

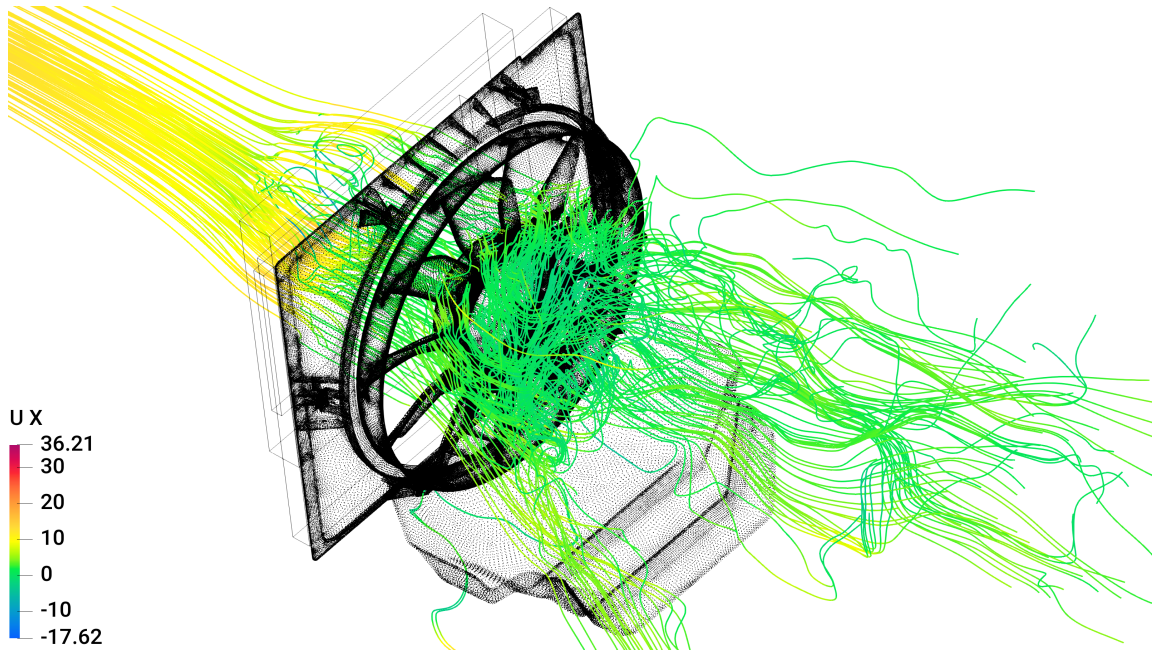

Figure 5.2.7: Ford Otosan truck cold flow, fan streamlines: axial velocity.

Fig. 5.2.8 reveal the increased flow rate through the lower part of the radiator as well as chassis influence on lowering the air velocity through vortex in front of the condenser as seen in Fig. 5.2.7.

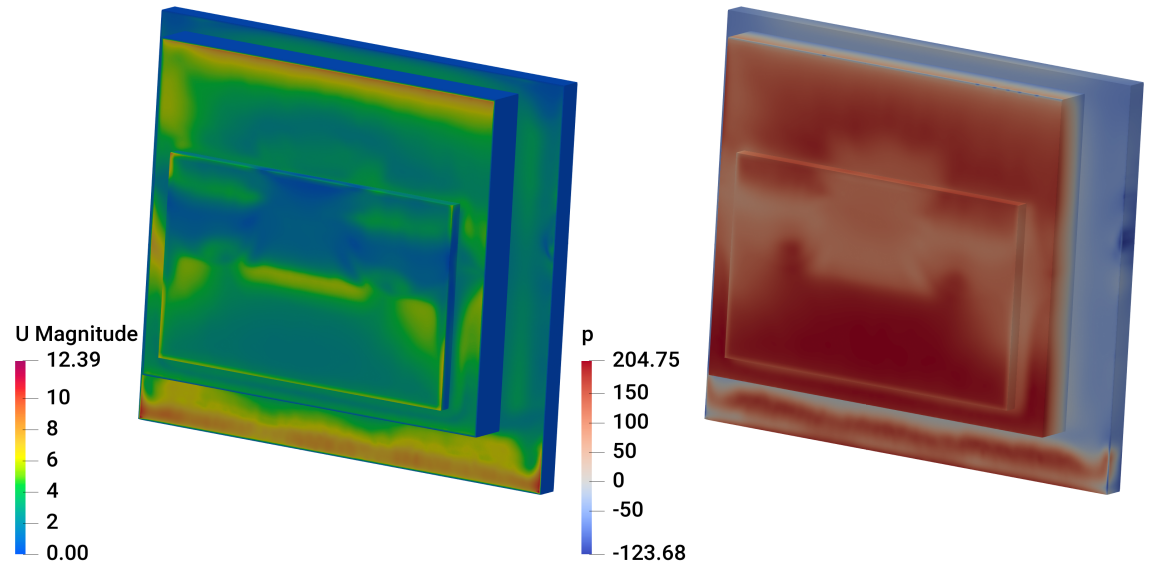

Figure 5.2.8: Ford Otosan truck cold flow: heat exchangers.

Figs. 5.2.9 and 5.2.10 show the chassis influence on lowering axial velocity and thus lowering the air mass flow through the middle part of heat exchangers.

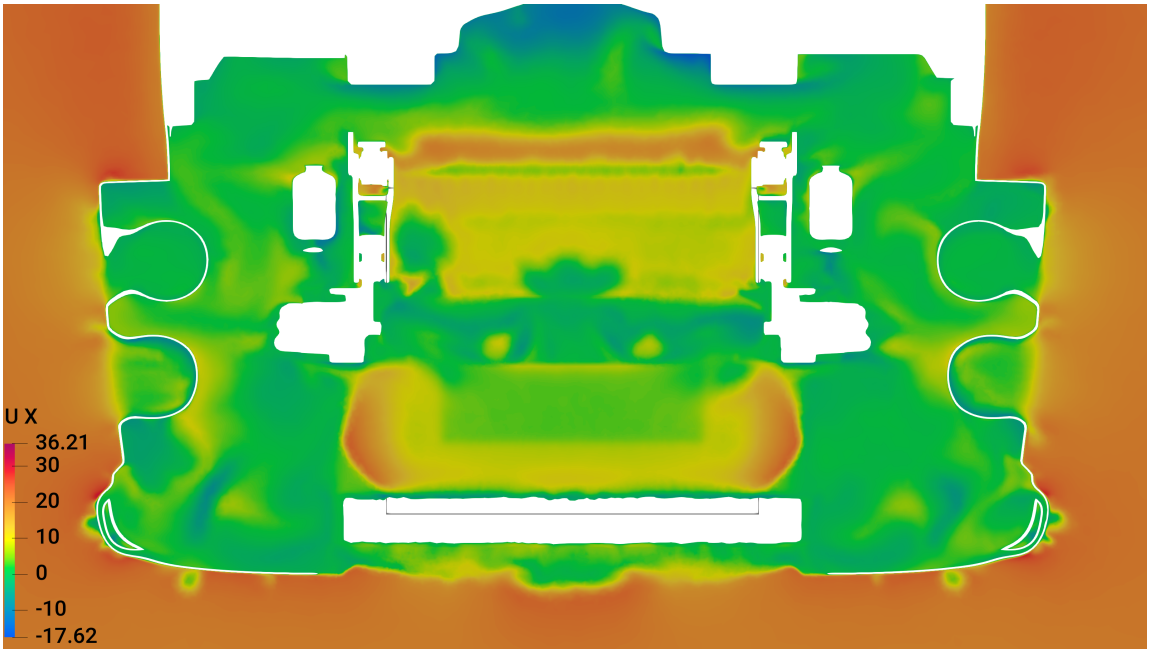

Figure 5.2.9: Ford Otosan truck cold flow, cross section in front of HXs: axial velocity.

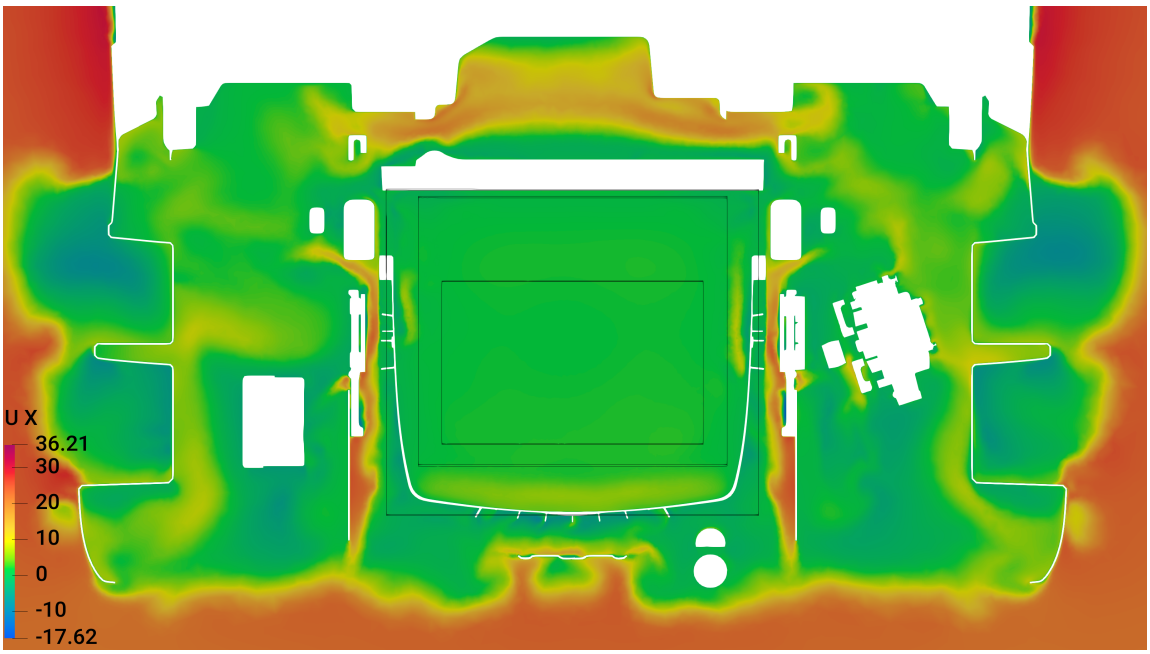

Figure 5.2.10: Ford Otosan truck cold flow, cross section in back of HXs: axial velocity.

From Figs. 5.2.11 and 5.2.12 it is visible that the overall air temperature depends on radiator, but the local temperature of the intercooler cannot be neglected.

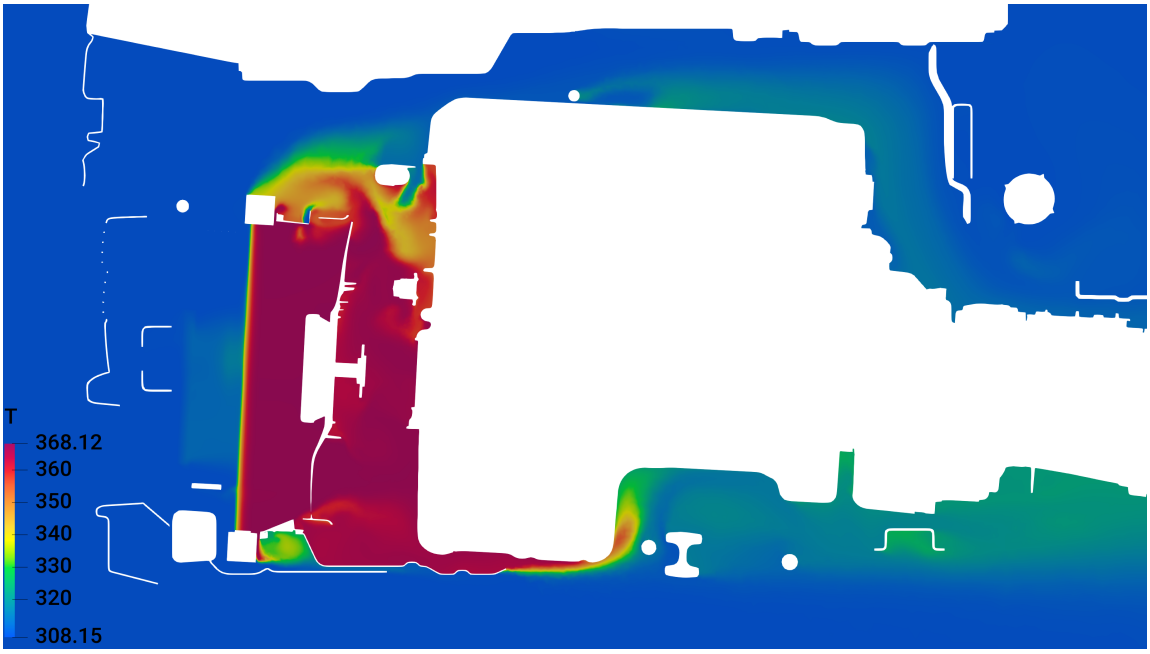

Figure 5.2.11: Ford Otosan truck temperature result, vertical CS: air temperature.

Figure 5.2.12: Ford Otosan truck temperature result, horizontal CS: air temperature.

Figs. 5.2.13 and 5.2.14 show a detail of the flow through intercooler's inlet. High temperature air is being redirected around the radiator.

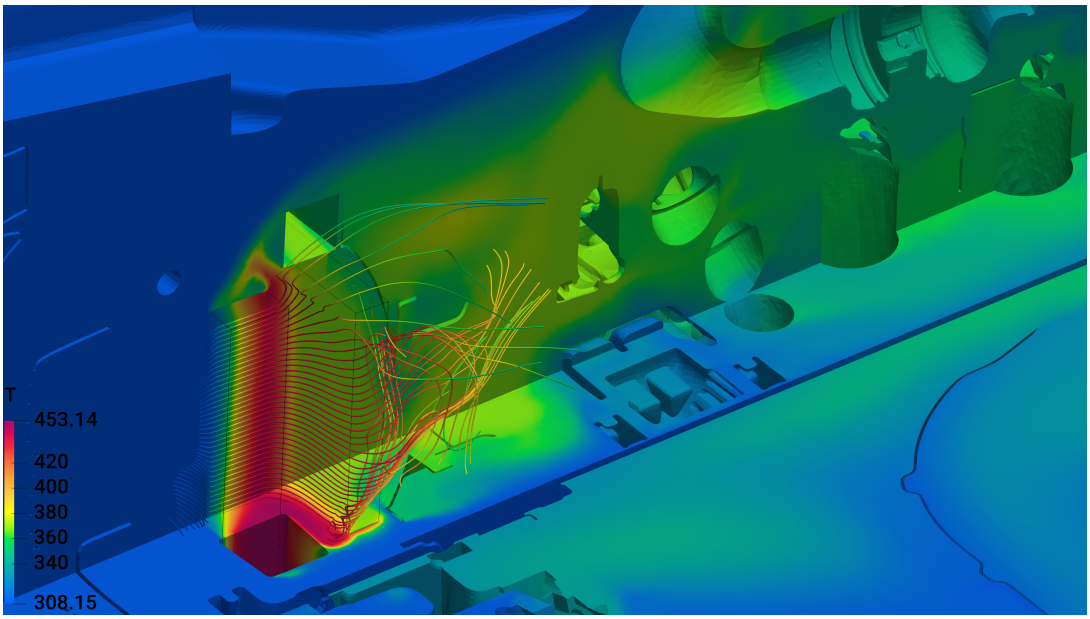

Figure 5.2.13: Ford Otosan truck temperature result, intercooler inlet detail streamlines: air temperature.

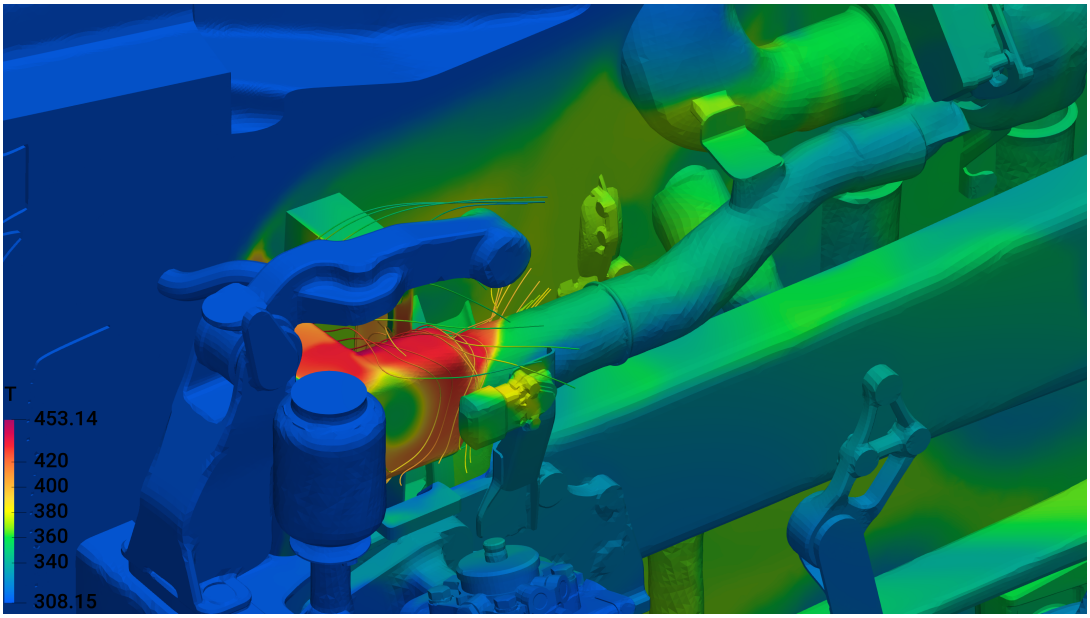

Figure 5.2.14: Ford Otosan truck temperature result, intercooler inlet detail surfaces: air temperature.

The radiator's high heat rejection and intercooler's local high temperature influence are both seen through surface temperature in Figs. 5.2.15 and 5.2.16.

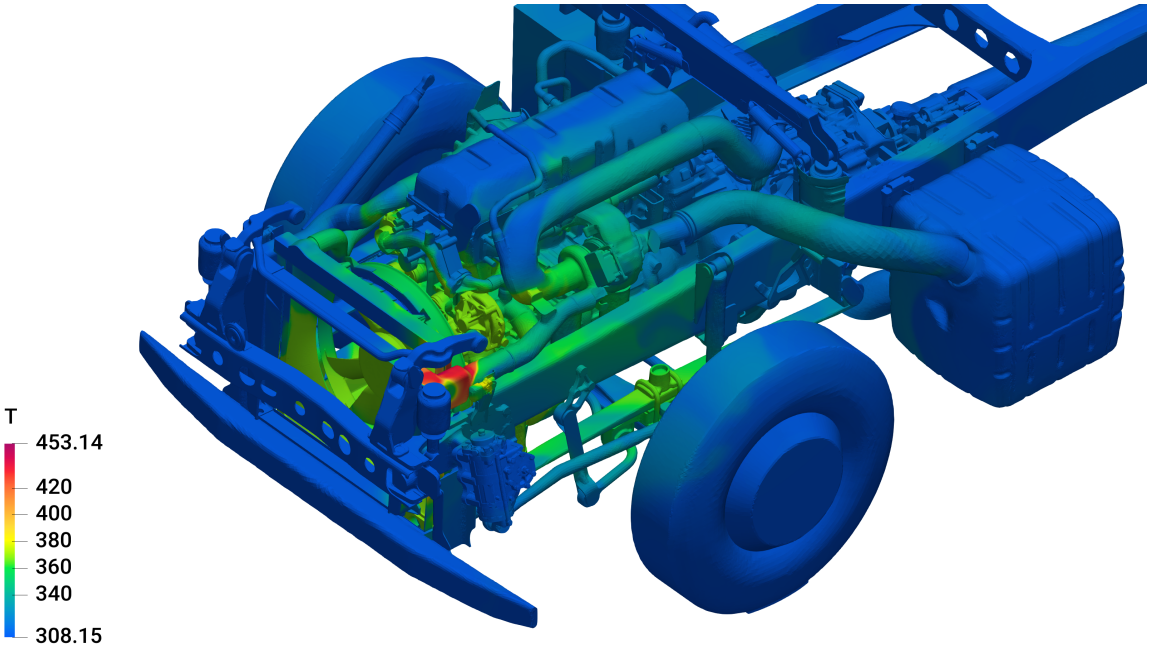

Figure 5.2.15: Ford Otosan truck temperature result, surfaces: air temperature.

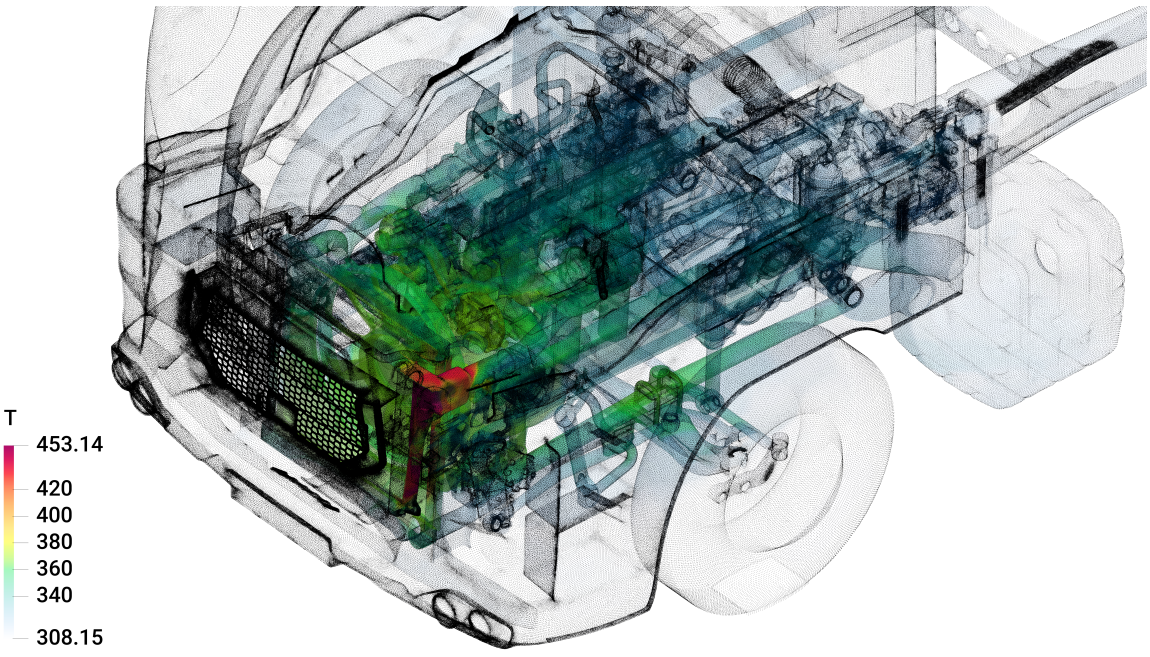

Figure 5.2.16: Ford Otosan truck temperature result, opacity surfaces: air temperature.

Chapter 6

Conclusion

This study presented a possible outcome of modelling heat exchangers for underhood thermal management. The compact heat exchanger found in the automotive industry has a very complex geometry, requiring a lot of computer resources to be analysed. Modelling of heat exchangers greatly reduces the time and resources.

The validation of the implemented heat exchanger model was performed successfully. Both individual and simultaneous operation confirmed its integral form preserved.

Time needed to produce a valid volume mesh is reduced through advanced automated meshing algorithms. Additional engineer's intervention via manual corrections is needed. Pre-processing is a skill that grows in time with more training.

The purpose of a CFD simulation is to obtain a temperature field that presents the heat exchanger's influence on thermal stress that is used later for part designing. The Dual Stream heat exchanger model confirmed to be an applicable method for performing thermal underhood CFD simulations. Experimental data is needed for accurate modelling of the porosity and effectiveness of the exchanger.

Solvers showed stable convergence, with heat exchangers temperature field under-relaxed to stabilise its non linear behaviour. Results presented possible hot spots that need attention and further investigation.

For future work, the heat exchanger model can be further advanced through the modelling of heat effectiveness dependency on the Number of Transfer Units (NTU). Thermal radiation is an important part of underhood thermal management; Thus, it should be modelled. Due to the limited time abailable for this study, it was neglected.

Bibliography

[1] H. Jasak, "The OpenFOAM Extend Project (Community-driven Releases of OpenFOAM)." `https://foam-extend.fsb.hr/about-us`. Accessed: 30-6-2019.

[2] BETA CAE Systems, "ANSA, the advanced CAE pre-processing software for complete model build up." `https://www.beta-cae.com/about_us.htm`. Accessed: 30-6-2019.

[3] R. Shah and D. Sekulić, *Fundamentals of Heat Exchanger Design.* John Wiley & Sons, 2003.

[4] D. Zrnić, "Thermal Management Analysis in the Engine Compartment of a Light Aircraft using Computational Fluid Dynamics," Master's thesis, Faculty of Mechanical Engineering and Naval Architecture, 2018.

[5] OpenCFD Ltd, "OpenFOAM." `https://www.openfoam.com/about`. Accessed: 30-6-2019.

[6] E. Ljungskog and U. Nilsson, "CFD for Underhood Modeling: Development of an Efficient Method," Master's thesis, Chalmers University of Technology, 2014.

[7] J. Nordin, "CFD Study of Optimal Under-hood Flow for Thermal Management of Electric Vehicles," Master's thesis, Chalmers University of Technology, 2017.

[8] J. Ferziger and M. Perić, *Computational Methods for Fluid Dynamics.* Springer-Verlag, 2002.

[9] F. Moukalled, L. Mangani, and M. Darwish, *The Finite Volume Method in Computational Fluid dynamics: An Advanced Introduction with OpenFOAM and Matlab.* Springer, 2016.

[10] H. Jasak, *Error Analysis and Estimation for the Finite Volume Method with Applications to Fluid Flows*. PhD thesis, Imperial College of Science, Technology and Medicine, 1996.

[11] I. D. Dominicis, G. Cvijetić, M. Willetts, and H. Jasak, *OpenFOAM: Selected Papers of the 11th Workshop*. Springer International Publishing, 2019.

[12] H. Hafsteinsson, "Porous Media in OpenFOAM." `http://www.tfd.chalmers.se/~hani/kurser/OS_CFD_2008/HaukurElvarHafsteinsson/haukurReport.pdf`. Accessed: 30-6-2019.

[13] F. R. Menter, M. Kuntz, and R. Langtry, "Ten years of industrial experience with the SSTturbulence model," *Heat and Mass Transfer*, vol. 4, pp. 625–632, 20033.